

**AEDC-TR-74-78
AFATL-TR-74-118**



**EXPERIMENTAL MAGNUS CHARACTERISTICS OF SEVERAL
BALLISTIC PROJECTILES WITH VARIOUS
BOATTAIL ANGLES AND LENGTHS AT
MACH NUMBERS 1.5, 2.0, AND 2.5**

**Leroy M. Jenke
ARO, Inc.**

**VON KÁRMÁN GAS DYNAMICS FACILITY
ARNOLD ENGINEERING DEVELOPMENT CENTER
AIR FORCE SYSTEMS COMMAND
ARNOLD AIR FORCE STATION, TENNESSEE 37389**

September 1974

Final Report for Period March 22-26, 1974

Approved for public release; distribution unlimited.

Prepared for

**AIR FORCE ARMAMENT LABORATORY (DLDL)
EGLIN AFB, FLORIDA 32542**

NOTICES

When U. S. Government drawings specifications, or other data are used for any purpose other than a definitely related Government procurement operation, the Government thereby incurs no responsibility nor any obligation whatsoever, and the fact that the Government may have formulated, furnished, or in any way supplied the said drawings, specifications, or other data, is not to be regarded by implication or otherwise, or in any manner licensing the holder or any other person or corporation, or conveying any rights or permission to manufacture, use, or sell any patented invention that may in any way be related thereto.

Qualified users may obtain copies of this report from the Defense Documentation Center.

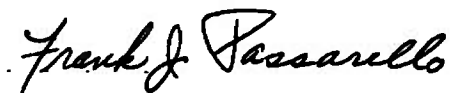
References to named commercial products in this report are not to be considered in any sense as an endorsement of the product by the United States Air Force or the Government.

APPROVAL STATEMENT

This technical report has been reviewed and is approved.



JIMMY W. MULLINS
Lt Colonel, USAF
Chief Air Force Test Director, VKF
Directorate of Test



FRANK J. PASSARELLO
Colonel, USAF
Director of Test

UNCLASSIFIED

SECURITY CLASSIFICATION OF THIS PAGE (When Data Entered)

REPORT DOCUMENTATION PAGE		READ INSTRUCTIONS BEFORE COMPLETING FORM	
1 REPORT NUMBER AEDC-TR-74-78 AFATL-TR-74-118	2. GOVT ACCESSION NO.	3 RECIPIENT'S CATALOG NUMBER	
4 TITLE (and Subtitle) EXPERIMENTAL MAGNUS CHARACTERISTICS OF SEVERAL BALLISTIC PROJECTILES WITH VARIOUS BOATTAIL ANGLES AND LENGTHS AT MACH NUMBERS 1.5, 2.0, AND 2.5		5 TYPE OF REPORT & PERIOD COVERED Final Report-March 22- 26, 1974	
		6 PERFORMING ORG. REPORT NUMBER	
7 AUTHOR(s) Leroy M. Jenke, ARO, Inc.		8 CONTRACT OR GRANT NUMBER(s)	
9 PERFORMING ORGANIZATION NAME AND ADDRESS Arnold Engineering Development Center (DYFS) Arnold Air Force Station, Tennessee 37389		10 PROGRAM ELEMENT, PROJECT, TASK AREA & WORK UNIT NUMBERS Program Element 62602F Project 2547	
11. CONTROLLING OFFICE NAME AND ADDRESS Air Force Armament Laboratory (DLDL) Eglin AFB, Florida 32542		12. REPORT DATE September 1974	
		13 NUMBER OF PAGES 81	
14 MONITORING AGENCY NAME & ADDRESS (if different from Controlling Office)		15. SECURITY CLASS. (of this report) UNCLASSIFIED	
		15a. DECLASSIFICATION/DOWNGRADING SCHEDULE N/A	
16 DISTRIBUTION STATEMENT (of this Report) Approved for public release; distribution unlimited.			
17. DISTRIBUTION STATEMENT (of the abstract entered in Block 20, if different from Report)			
18 SUPPLEMENTARY NOTES Available in DDC			
19 KEY WORDS (Continue on reverse side if necessary and identify by block number) Magnus effect conical bodies models tail assemblies ballistics Mach numbers projectiles Reynolds numbers			
20 ABSTRACT (Continue on reverse side if necessary and identify by block number) An experimental investigation was conducted to determine the effects of boattail angle, the boattail length, and the base diameter on the Magnus-force and moment characteristics of spin-stabilized projectiles. The models were tested at Mach numbers 1.5, 2.0, and 2.5 over an angle-of-attack range from -2 to 8 deg. Data were obtained at length Reynolds numbers of 2.44×10^6 , 9.60×10^6 , and 17.53×10^6 , and for spin parameter $(pd/2V_\infty)$ values			

20. ABSTRACT (Continued)

of 0.024 to about 0.270 radians. Results are presented showing the effects of spin, Mach number, angle of attack, boattail geometry, and Reynolds number. The results show that increasing the boattail length or angle decreased $C_{N\alpha}$ and increased the magnitude of $C_{m\alpha}$, $C_{Yp\alpha}$, and $C_{np\alpha}$.

PREFACE

The work reported herein was conducted by the Arnold Engineering Development Center (AEDC), Air Force Systems Command (AFSC), for the Naval Weapons Laboratory (NWL) under sponsorship of the Air Force Armament Laboratory (AFATL), AFSC, under Program Element 62602F, Project 2547. AFATL project monitor was Mr. E. Sears. The results presented herein were obtained by ARO, Inc. (a subsidiary of Sverdrup & Parcel and Associates, Inc.), contract operator of AEDC, AFSC, Arnold Air Force Station, Tennessee. The tests were conducted on March 22, 25, and 26, 1974, under ARO Project No. VA427. The final data package was completed on April 26, 1974, and the manuscript (ARO Control No. ARO-VKF-TR-74-48) was submitted for publication on June 17, 1974.

CONTENTS

	<u>Page</u>
1.0 INTRODUCTION	7
2.0 APPARATUS AND PROCEDURE	7
3.0 TEST CONDITIONS AND DATA PRECISION	9
4.0 RESULTS AND DISCUSSION	10
5.0 CONCLUDING REMARKS	12
REFERENCES	12

ILLUSTRATIONS

Figure

1. Model Photographs	
a. Tunnel A Installation (Configuration 3)	13
b. Boattail Configurations	14
2. Model Details	16
3. Magnus-Force Test Mechanism	17
4. Balance Details	18
5. Variation of C_N and C_m with Angle of Attack, $Re_\ell = 9.6 \times 10^6$	
a. Configuration 0	19
b. Configuration 1	20
c. Configuration 2	21
d. Configuration 3	22
e. Configuration 4	23
f. Configuration 5	24
g. Configuration 6	25
h. Configuration 7	26
i. Configuration 8	27
j. Configuration 9	28
6. Effect of Reynolds Number Variation on C_N and C_m at $M_\infty = 2$, Configuration 3	29
7. Variation of C_{N_α} and C_{m_α} with Mach No., $Re_\ell = 9.6 \times 10^6$	
a. Effect of Boattail Angle with a Constant Boattail Length	30

<u>Figure</u>	<u>Page</u>
7. Continued	
b. Effect of Boattail Length with a Constant Boattail Angle	31
c. Effect of Boattail Length with a Constant Base Diameter	32
8. Typical Variation of C_Y and C_N with $pd/2V_\infty$, Configuration 3, $M_\infty = 1.5$, $Re_\ell = 9.6 \times 10^6$	33
9. Variation of C_Y and C_N with $pd/2V_\infty$ for Configuration 0, $Re_\ell = 9.6 \times 10^6$	
a. $M_\infty = 1.5$	34
b. $M_\infty = 2.0$	35
c. $M_\infty = 2.5$	36
10. Variation of C_Y and C_N with $pd/2V_\infty$ for Configuration 1, $Re_\ell = 9.6 \times 10^6$	
a. $M_\infty = 1.5$	37
b. $M_\infty = 2.0$	38
c. $M_\infty = 2.5$	39
11. Variation of C_Y and C_N with $pd/2V_\infty$ for Configuration 2, $Re_\ell = 9.6 \times 10^6$	
a. $M_\infty = 1.5$	40
b. $M_\infty = 2.0$	41
c. $M_\infty = 2.5$	42
12. Variation of C_Y and C_N with $pd/2V_\infty$ for Configuration 3, $Re_\ell = 9.6 \times 10^6$	
a. $M_\infty = 1.5$	43
b. $M_\infty = 2.0$	44
c. $M_\infty = 2.5$	45
13. Variation of C_Y and C_N with $pd/2V_\infty$ for Configuration 4, $Re_\ell = 9.6 \times 10^6$	
a. $M_\infty = 1.5$	46
b. $M_\infty = 2.0$	47
c. $M_\infty = 2.5$	48
14. Variation of C_Y and C_N with $pd/2V_\infty$ for Configuration 5, $Re_\ell = 9.6 \times 10^6$	
a. $M_\infty = 1.5$	49
b. $M_\infty = 2.0$	50
c. $M_\infty = 2.5$	51

<u>Figure</u>	<u>Page</u>
15. Variation of C_Y and C_N with $pd/2V_\infty$ for Configuration 6, $Re_\ell = 9.6 \times 10^6$	
a. $M_\infty = 1.5$	52
b. $M_\infty = 2.0$	53
c. $M_\infty = 2.5$	54
16. Variation of C_Y and C_N with $pd/2V_\infty$ for Configuration 7, $Re_\ell = 9.6 \times 10^6$	
a. $M_\infty = 1.5$	55
b. $M_\infty = 2.0$	56
c. $M_\infty = 2.5$	57
17. Variation of C_Y and C_N with $pd/2V_\infty$ for Configuration 8, $Re_\ell = 9.6 \times 10^6$	
a. $M_\infty = 1.5$	58
b. $M_\infty = 2.0$	59
c. $M_\infty = 2.5$	60
18. Variation of C_Y and C_N with $pd/2V_\infty$ for Configuration 9, $Re_\ell = 9.6 \times 10^6$	
a. $M_\infty = 1.5$	61
b. $M_\infty = 2.0$	62
c. $M_\infty = 2.5$	63
19. Variation of C_{Y_p} and C_{N_p} with Angle of Attack, $Re_\ell = 9.6 \times 10^6$	
a. Configuration 0	64
b. Configuration 1	65
c. Configuration 2	66
d. Configuration 3	67
e. Configuration 4	68
f. Configuration 5	69
g. Configuration 6	70
h. Configuration 7	71
i. Configuration 8	72
j. Configuration 9	73
20. Effect of Reynolds Number Variation on C_{Y_p} and C_{N_p} at $M_\infty = 2$, Configuration 3	74
21. Variation of $C_{Y_{p\alpha}}$ and $C_{N_{p\alpha}}$ with Mach No., $Re_\ell = 9.6 \times 10^6$	
a. Effect of Boattail Angle with a Constant Boattail Length	75

<u>Figure</u>	<u>Page</u>
21. Continued	
b. Effect of Boattail Length with a Constant Boattail Angle	76
c. Effect of Boattail Length with a Constant Base Diameter	77

TABLES

1. Balance Uncertainty	78
2. Test Summary	78
3. Wind Tunnel Test Parameters	78
4. Wind Tunnel Parameter Precision	79
5. Coefficient Precision	79
6. Derivative Coefficient Precision	79
 NOMENCLATURE	 80

1.0 INTRODUCTION

This test was conducted as part of a continuing investigation (Refs. 1 and 2) by the Naval Weapons Laboratory (NWL) on development work of ballistic shells. Since these projectiles are statically unstable, they must be spin-stabilized. The spin velocity required to stabilize the projectiles tends to induce Magnus effects, which can lead to dynamic instabilities. Both of these factors will influence the flight path. This test was initiated to determine the effects of boattail angle, boattail length, and base diameter on the Magnus-force and moment characteristics of projectiles. Data were obtained at Mach numbers 1.5, 2.0, and 2.5 at a Reynolds number (based on a model length of 28.662 in.) of 9.6×10^6 . Some additional data were obtained at $M_\infty = 2$ for Reynolds numbers of 2.4×10^6 and 17.5×10^6 . The angle of attack was varied from -2 to 8 deg., and values of the spin parameter ($\rho d/2V_\infty$) ranged from 0.02 to about 0.27 radians.

2.0 APPARATUS AND PROCEDURE

2.1 TEST ARTICLES AND TEST MECHANISM

The aluminum models (Figs. 1 and 2) were supplied by NWL and were similar to the ones tested in Ref. 2. The models consisted of one common nose section and ten afterbody sections with various boattail lengths and angles as well as various base diameters. All of the models were dynamically balanced in roll at VKF so that there would be no vibrational loads on the balance.

The models were mounted on the Magnus-force test mechanism shown in Fig. 3. Basically, the Magnus-force test mechanism has a sting-mounted, water-jacketed, four-component balance with a shell mounted on ball bearings over the water jacket. A two-stage, air-driven turbine is mounted inside the model mounting shell at a fixed axial position near the forward end of the sting. The turbine is used to spin the model to some desired speed and then is disengaged with an air-operated sliding clutch to allow the model to spin freely on the ball bearings. It is estimated that the turbine will produce a starting torque of 50 in.-lb and a developed torque of approximately 100 in.-lb. The mechanism is designed to operate under normal-force loads up to 500 lb and axial-force loads of 125 lb and for a maximum spin rate of approximately 25,000 rpm.

2.2 TEST FACILITY

Supersonic Wind Tunnel (A) is a continuous, closed-circuit, variable density wind tunnel with an automatically driven flexible-plate-type nozzle and a 40- by 40-in. test section. The tunnel can be operated at Mach numbers from 1.5 to 6 at maximum stagnation pressures from 29 to 200 psia, respectively, and stagnation temperatures up to 750°R ($M_\infty = 6$). Minimum operating pressures range from about one-tenth to one-twentieth of the maximum at each Mach number. In most instances, Mach number changes may be made without stopping the tunnel flow. The model can be injected into the tunnel for a test run and then retracted for model changes without stopping the tunnel flow.

2.3 INSTRUMENTATION

Tunnel A stilling chamber pressure is measured with a 150-psid transducer referenced to a near vacuum and having full-scale calibrated ranges of 10, 50, and 150 psi. Based on periodic comparisons with secondary standards, the precision of this transducer (a band which includes 95 percent of the residuals) is estimated to be within ± 0.5 percent of the measured pressure. The stilling chamber temperature is measured with a copper-constantan thermocouple to a precision of $\pm 2^\circ\text{R}$ based on the thermocouple wire manufacturer's specifications.

Model forces and moments were measured with the VKF four-component, moment-type, strain-gage balance shown in Fig. 4. The small outrigger side beams of the balance, with semiconductor strain gages, were used to obtain the sensitivity required to measure small side loads while maintaining adequate balance stiffness for the larger pitch loads. When a yawing moment is imposed on the balance, secondary bending moments are induced in the side beams. Thus, the outrigger beams act as mechanical amplifiers, and a normal-force to side-force capability ratio of 20 was achieved for a 500-lb normal-force loading. Before testing, static loads in each plane and combined static loads were applied to the balance, simulating the range of model loads anticipated for the test. The uncertainties shown in Table 1 represent the bands for 95 percent of the measurement residuals based on differences between the applied loads and the corresponding values calculated from the final data reduction equations.

The transfer distance to the model moment reference was measured with a precision of ± 0.005 in.

The rotational speed of the model was computed from the electrical pulses produced by a ring with reflective surfaces passing an internally mounted infrared-emitting diode and phototransistor. This tachometer system could measure spin rates from 0 to 25,000 rpm.

2.4 TEST PROCEDURE

The model was positioned at the desired attitude with the tunnel pitch mechanism and then spun with the turbine. When the desired spin rate was achieved, the nitrogen to the turbine was shut off, the clutch was disengaged, and data were recorded as the model spin rate decayed. Model spin rates were monitored using the internally mounted tachometer described in Section 2.3.

3.0 TEST CONDITIONS AND DATA PRECISION

3.1 TEST CONDITIONS

A summary of the configurations tested is presented in Table 2, and the nominal wind tunnel test parameters at which the data were obtained are presented in Table 3. The "x" in Table 2 indicates that Magnus data were obtained for $\alpha = -2$ to 8 deg.

3.2 DATA PRECISION

Uncertainties (bands which include 95 percent of the calibration data) in the basic tunnel parameters, p_o , T_o , and M_∞ , were estimated from repeat calibrations of the instrumentation and from the repeatability and uniformity of the test section flow during tunnel calibrations. These uncertainties were then used to estimate uncertainties in other free-stream properties, using the Taylor series method of error propagation. Listed in Table 4 are the uncertainties in the basic wind tunnel parameters at which most of the data were obtained.

Measurements of the model attitude in pitch including the model-balance deflection are precise within ± 0.05 deg, based on repeat calibrations. The rpm precision is estimated to be ± 5 rpm.

The basic uncertainties listed in Section 2.3 were combined with uncertainties in the tunnel parameters (Table 4), assuming a Taylor series error propagation, to estimate the precision of the aerodynamic coefficients. The uncertainties shown in Tables 5 and 6 are those that were computed for the test conditions at which most of the data were obtained ($Re \approx 4 \times 10^6/ft$) and are near the maximum aerodynamic loads.

It should be noted that the data repeatability, which is a measure of the random-type errors, was generally within the maximum propagated uncertainties quoted.

4.0 RESULTS AND DISCUSSION

These tests were conducted primarily to determine the effect of varying the boattail geometry of ballistic shell configurations on their Magnus-force and moment characteristics at supersonic Mach numbers. Data were obtained at Mach numbers 1.5, 2.0, and 2.5 for angles of attack from -2 to 8 deg. The spin rate parameter ($pd/2V_\infty$) ranged from 0.024 to 0.270 radians.

The variations of normal force (C_N) and pitching moment (C_m) with angle of attack are presented in Figs. 5 through 7. Since gun-launched projectiles are spin-stabilized, they are all statically unstable, as expected. Both C_N and C_m are essentially linear functions of angle of attack for angles up to 4 deg. For all configurations, C_N increased and C_m decreased with increasing Mach number indicating a rearward shift in the center of pressure. The results presented in Fig. 6 show that varying the Reynolds number at Mach number 2 had no effect on the values of C_N and C_m of Configuration 3. Figure 7 shows the variations of $C_{N\alpha}$ and $C_{m\alpha}$ with Mach number. As was shown in Fig. 5, $C_{N\alpha}$ increases and $C_{m\alpha}$ decreases with increasing Mach number. The results also show that as the boattail length or angle increased, in effect decreasing the projectile planform area aft of the moment reference, $C_{N\alpha}$ decreased and $C_{m\alpha}$ increased as would be expected.

Figure 8 presents the typical variation of side force (C_Y) and yawing moment (C_n) with $pd/2V_\infty$ for Configuration 3 at Mach number 1.5. The data typify the type of data, the amount of scatter, and the number of points that were obtained as the model spin rate changed. The data presented hereafter in this report show a computer fairing through the data

points (a third-degree, least-squares curve fit) instead of a symbol for each data point. The complete C_Y and C_N versus $pd/2V_\infty$ results are presented in Figs. 9 through 18. Generally, the results indicate that both C_Y and C_N are nonlinear with $pd/2V_\infty$ at the higher angles of attack ($\alpha > 4$ deg) and higher spin rates ($pd/2V_\infty > 0.15$). In addition, the usual negative C_Y and positive C_N for positive values of $pd/2V_\infty$ and α were obtained for all configurations.

To examine the effects of angle of attack, the linear portion of the data (slopes of C_Y and C_N versus $pd/2V_\infty$ for $pd/2V_\infty < 0.1$) will be used. Figure 19 presents the variations of C_{Y_p} and C_{N_p} with angle of attack. The results show that the magnitudes of both C_{Y_p} and C_{N_p} generally increase continuously with angle of attack. The only exception to this was Configuration 7 at Mach number 1.5 and $\alpha \approx 6$ deg, where C_{N_p} showed a considerable decrease. In addition, the magnitude of both parameters decreased with increasing Mach number.

The effects of Reynolds number on C_{Y_p} and C_{N_p} for Configuration 3 at Mach number 2.0 are presented in Fig. 20. The results show that for Reynolds numbers of $4.0 \times 10^6/\text{ft}$ and $7.3 \times 10^6/\text{ft}$ there was little difference in the parameters. However, for the low Reynolds number ($1 \times 10^6/\text{ft}$) the magnitude of both parameters increased. This is probably the result of the laminar boundary layer in the boattail region at the low Reynolds number. For the other test conditions the boundary layer was turbulent.

The variations of $C_{Y_{p\alpha}}$ and $C_{N_{p\alpha}}$ with Mach number are presented in Fig. 21. Generally, the magnitude of each parameter is either nearly constant or decreases with increasing Mach number. Increasing the boattail angle and maintaining a constant boattail length (Fig. 21a) increased the magnitude of $C_{Y_{p\alpha}}$ and $C_{N_{p\alpha}}$, except at $M_\infty = 2.5$ where $C_{N_{p\alpha}}$ was not appreciably affected. Increasing the boattail length and maintaining a constant angle (Fig. 21b) produced magnitude increases in both $C_{Y_{p\alpha}}$ and $C_{N_{p\alpha}}$. At $M_\infty = 1.5$ the largest increase in magnitude was produced by increasing the boattail length from 0.5 calibers to 1.0 caliber, while at $M_\infty = 2.0$ and 2.5 the largest increase occurred as the length increased from 1.0 caliber to 1.35 calibers. The effects of increasing the boattail length and maintaining a constant base diameter are shown in Fig. 21c. Generally, the magnitude of $C_{Y_{p\alpha}}$ and $C_{N_{p\alpha}}$ increased as the boattail length increased.

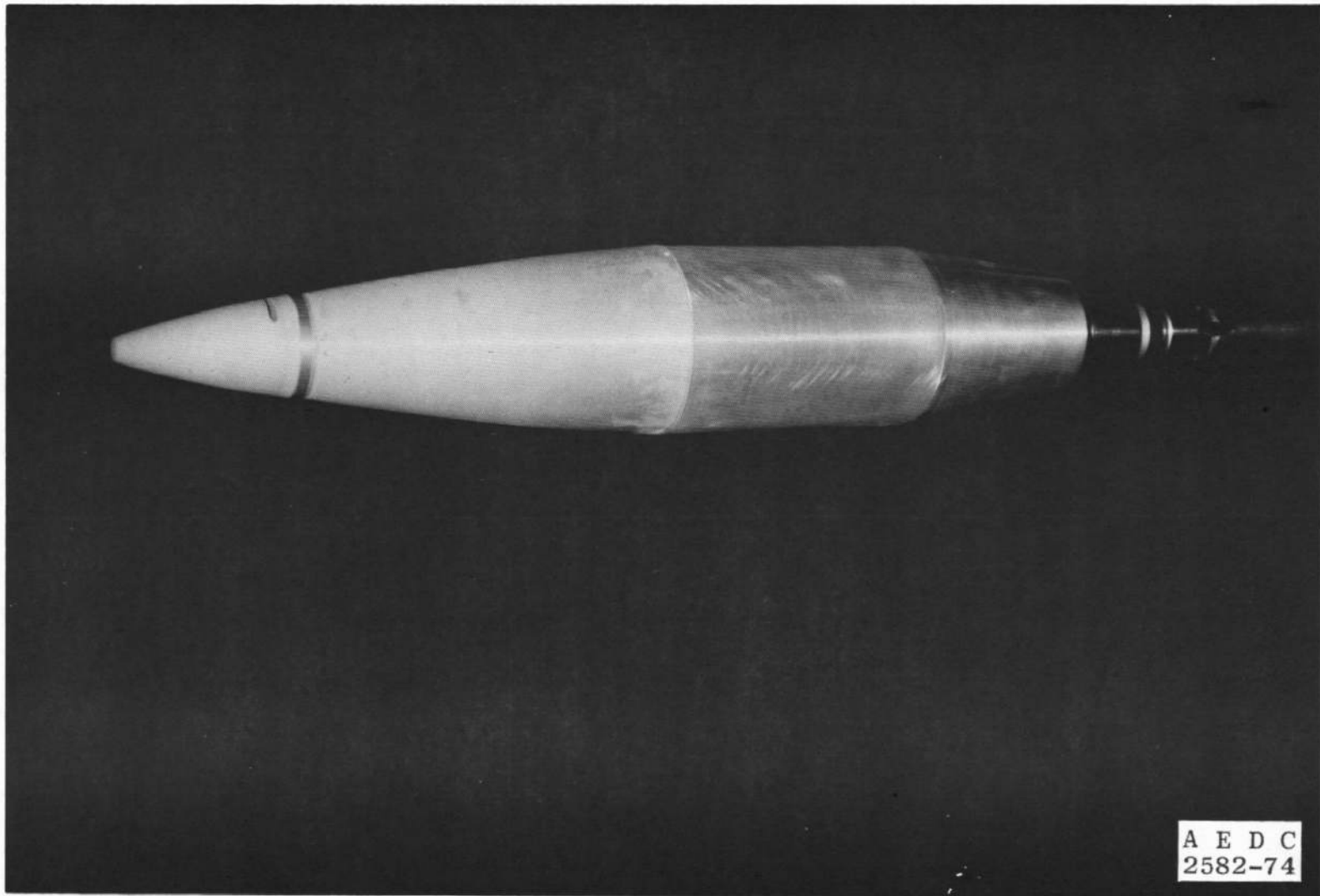
5.0 CONCLUDING REMARKS

An experimental investigation was conducted to determine the effects of boattail geometry changes on the Magnus-force and moment characteristics of ballistic shells at supersonic Mach numbers. The tests were conducted at Mach numbers 1.5, 2.0, and 2.5 for an angle-of-attack range from -2 to 8 deg. Results obtained at spin parameter ($pd/2V_\infty$) values up to 0.270 are summarized as follows:

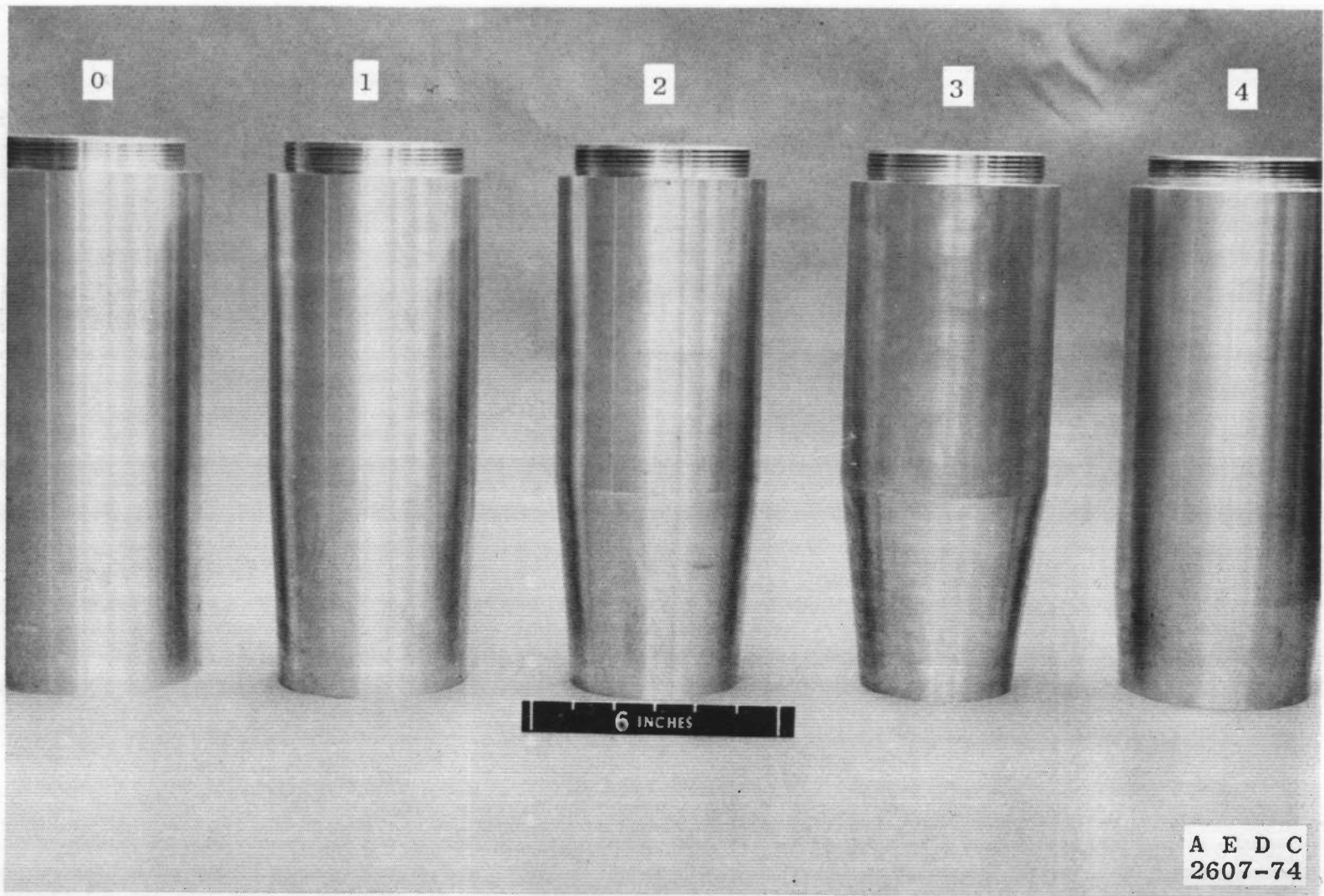
1. All configurations were statically unstable.
2. C_{N_α} increased and C_{m_α} decreased with increasing Mach number.
3. Increasing the boattail length or angle decreased C_{N_α} and increased C_{m_α} .
4. Both C_Y and C_n were nonlinear with $pd/2V_\infty$ at the higher angles of attack ($\alpha > 4$ deg) and higher spin rates ($pd/2V_\infty > 0.15$).
5. C_Y was negative and C_n was positive for positive values of $pd/2V_\infty$ and α .
6. Generally, the magnitude of C_{Y_p} and C_{n_p} increased with α and were linear up to about 2.5 deg.
7. Decreasing the Reynolds number from $4 \times 10^6/\text{ft}$ to $1 \times 10^6/\text{ft}$ increased the magnitude of C_{Y_p} and C_{n_p} .
8. Increasing the boattail length or angle generally increased the magnitude of $C_{Y_{p\alpha}}$ and $C_{n_{p\alpha}}$.

REFERENCES

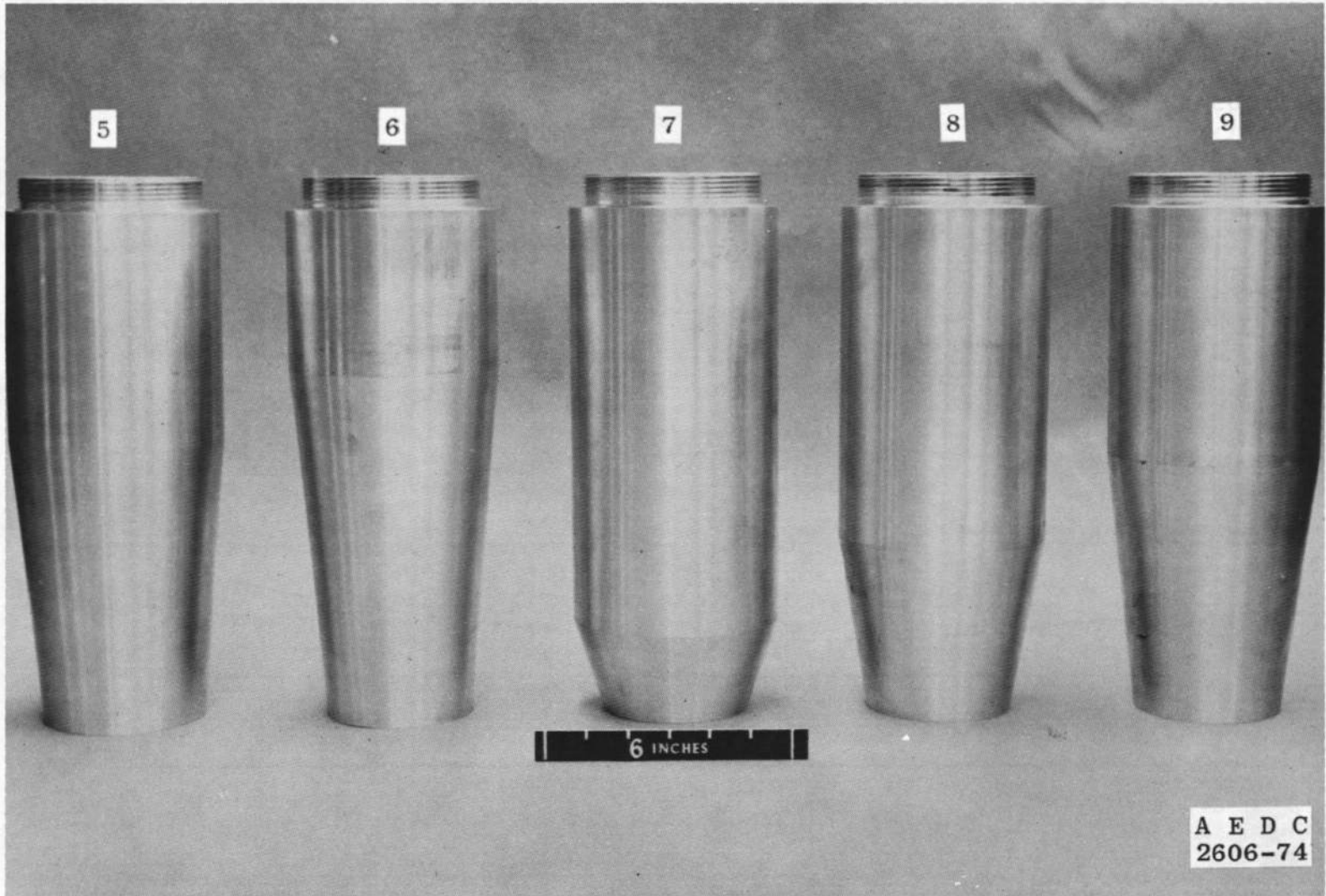
1. Jenke, Leroy M. and Carman, Jack B. "Experimental Magnus Characteristics of Ballistic Projectiles with Anti-Magnus Vanes at Mach Numbers 0.7 through 2.5." AEDC-TR-73-126, AFATL-TR-73-150 (AD773383), December 1973.
2. Jenke, Leroy M. "Experimental Magnus Characteristics of Ballistic Projectiles with and without Anti-Magnus Vanes at Mach Numbers 1.5 through 2.5." AEDC-TR-73-162, AFATL-TR-73-188 (AD771807), December 1973.



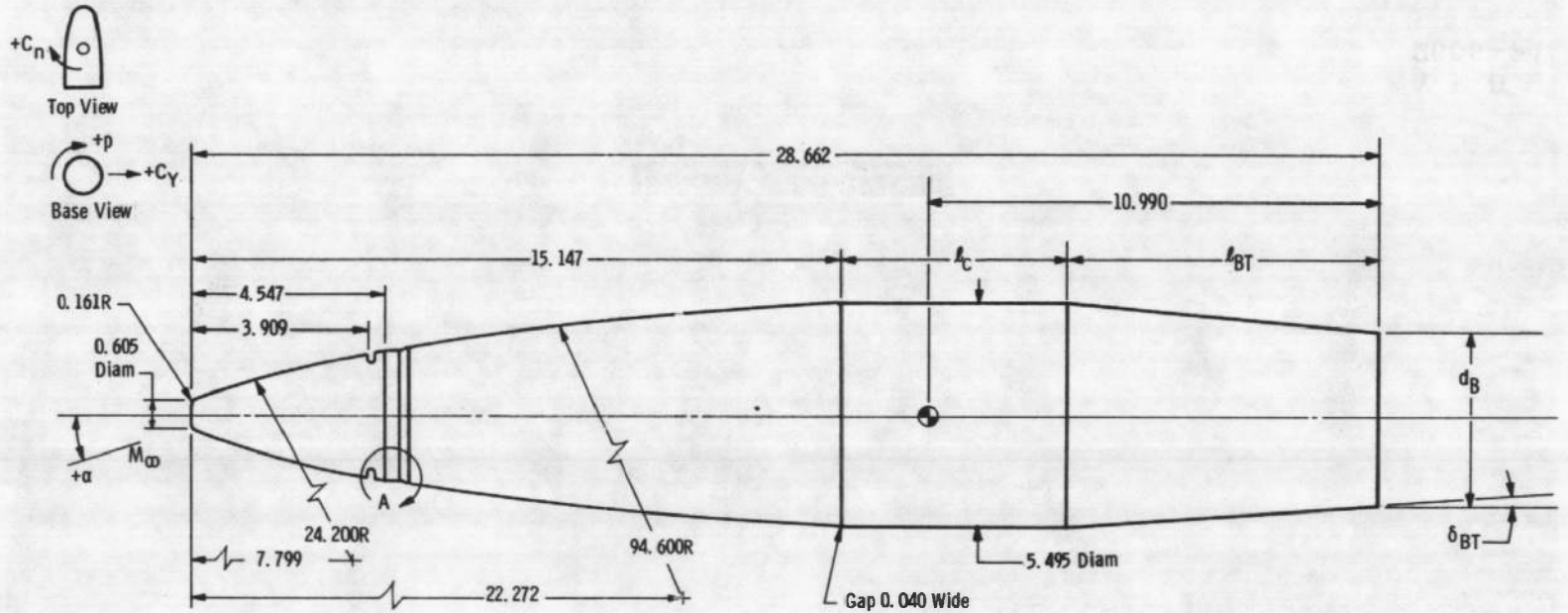
a. Tunnel A installation (configuration 3)
Figure 1. Model photographs.



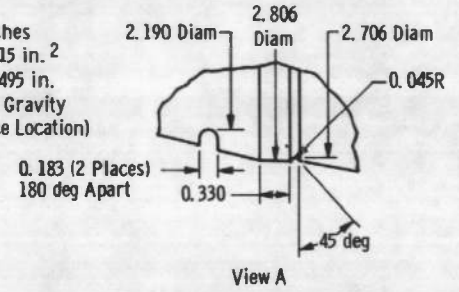
b. Boattail configurations
Figure 1. Continued.



b. Concluded
Figure 1. Concluded.



All Dimensions in Inches
 Reference Area = 23.715 in.²
 Reference Length = 5.495 in.
 ⊙ Denotes Center of Gravity
 (Moment Reference Location)



Configuration	l_{BT} , calibers	δ_{BT} , deg	d_B , calibers	l_c , calibers
0	0	0	1.0000	2.460
1	1.00	2.5	0.9126	1.460
2	1.00	5.0	0.8249	1.460
3	1.00	7.5	0.7366	1.460
4	0.50	5.0	0.9124	1.959
5	1.35	5.0	0.7637	1.110
6	1.70	5.0	0.7024	0.759
7	0.45	18.4	0.7000	2.009
8	0.85	10.0	0.7000	1.609
9	1.25	6.9	0.7000	1.205

Figure 2. Model details.

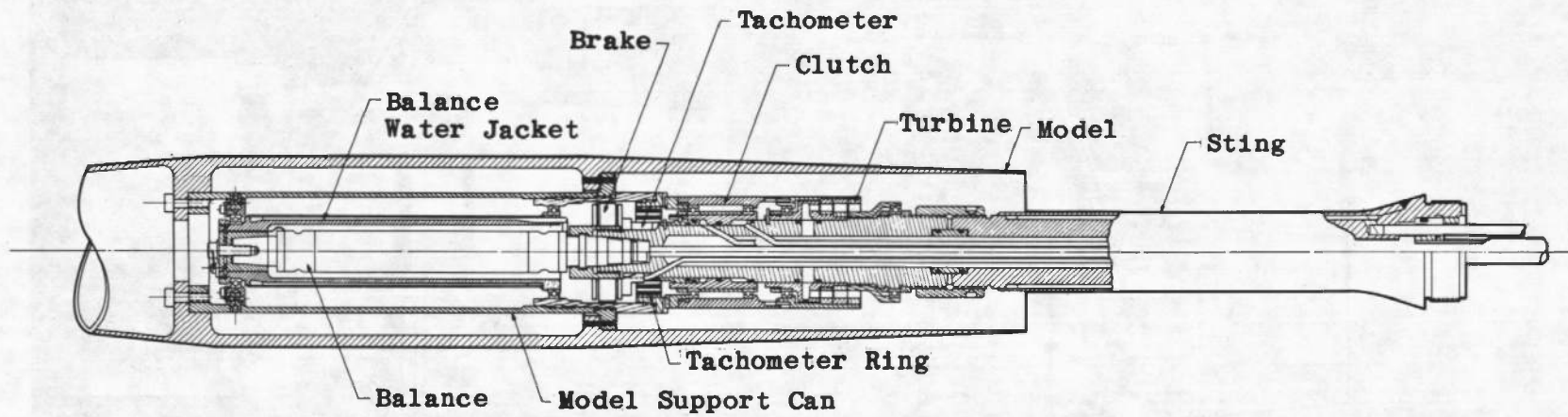


Figure 3. Magnus-force test mechanism.

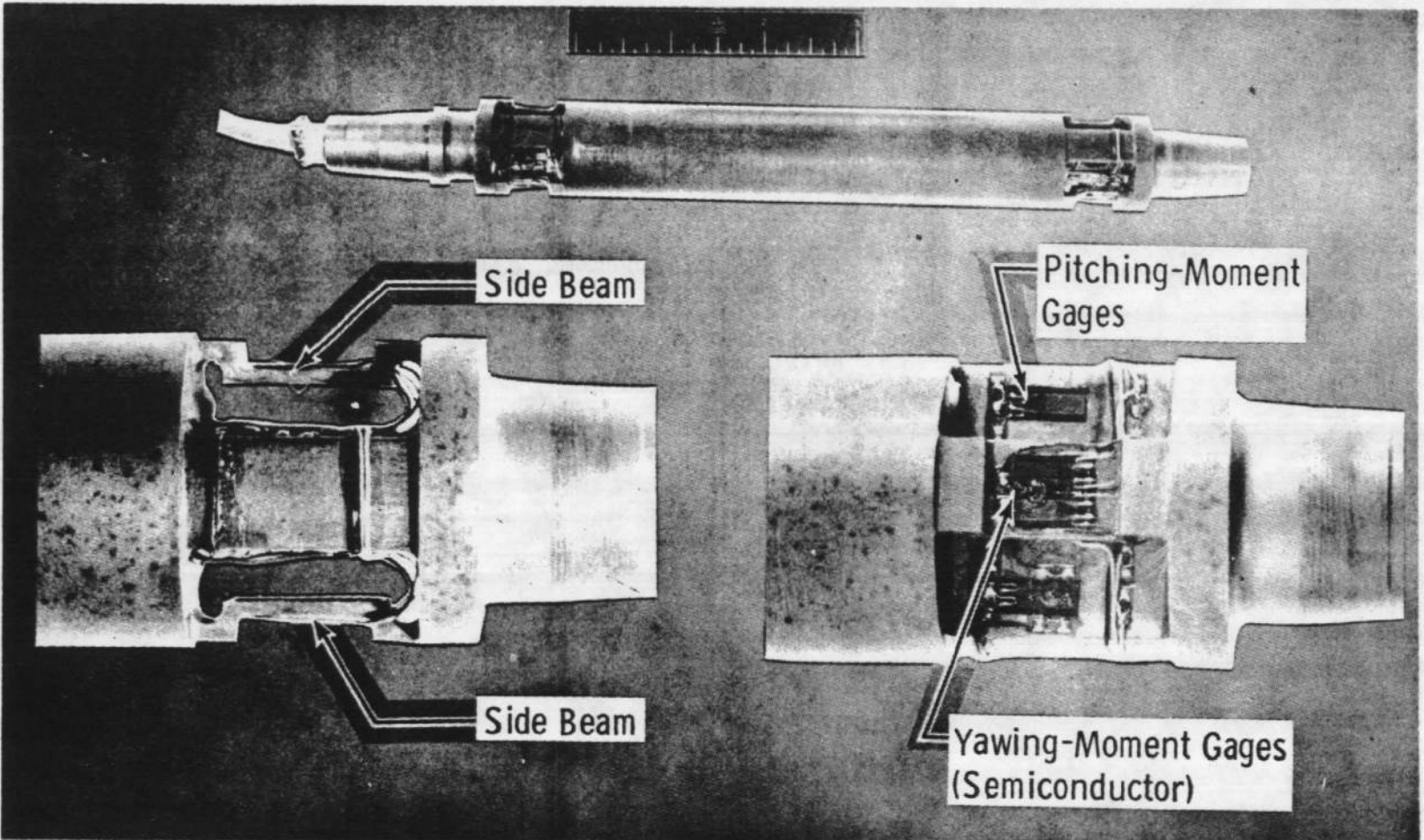
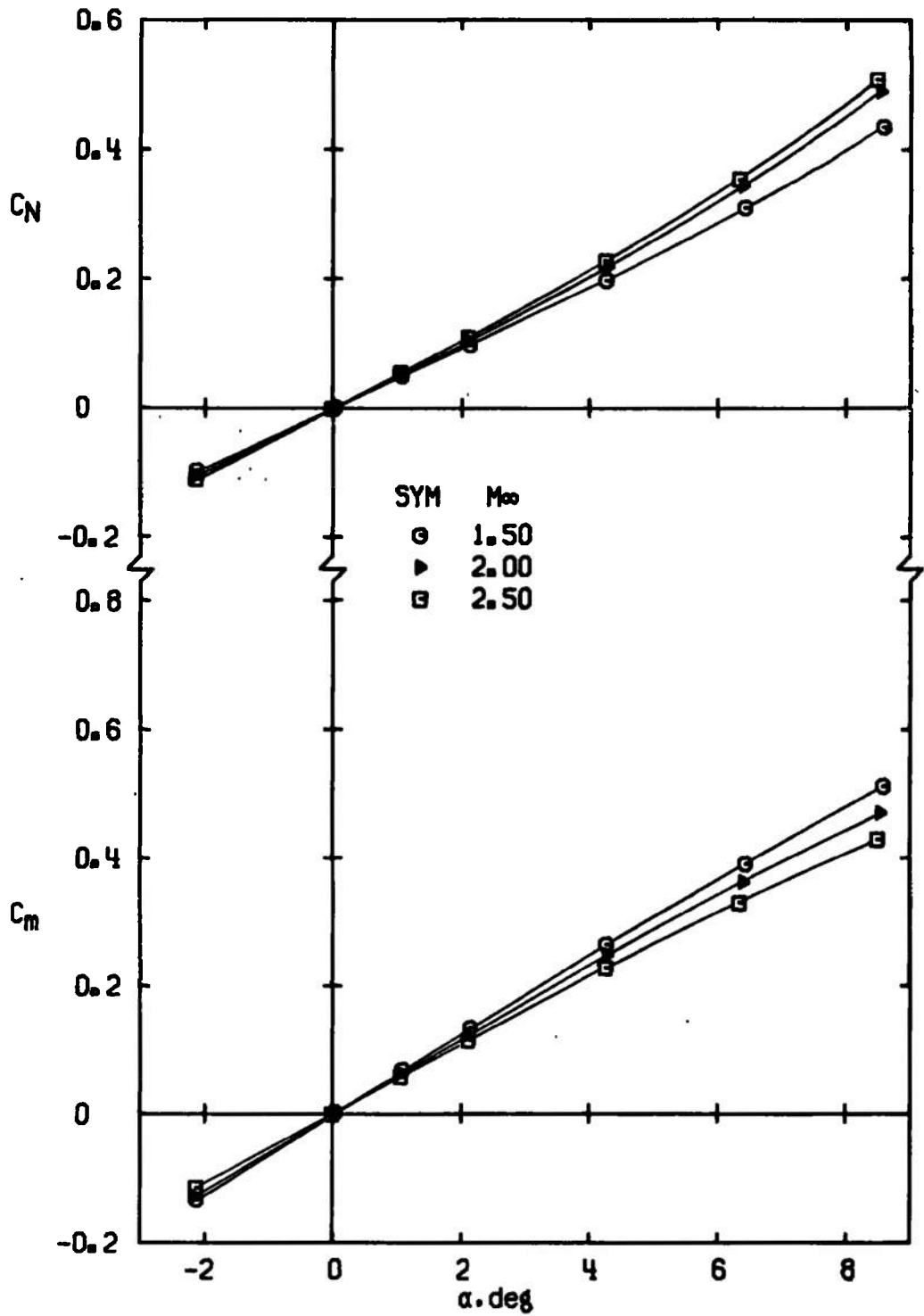
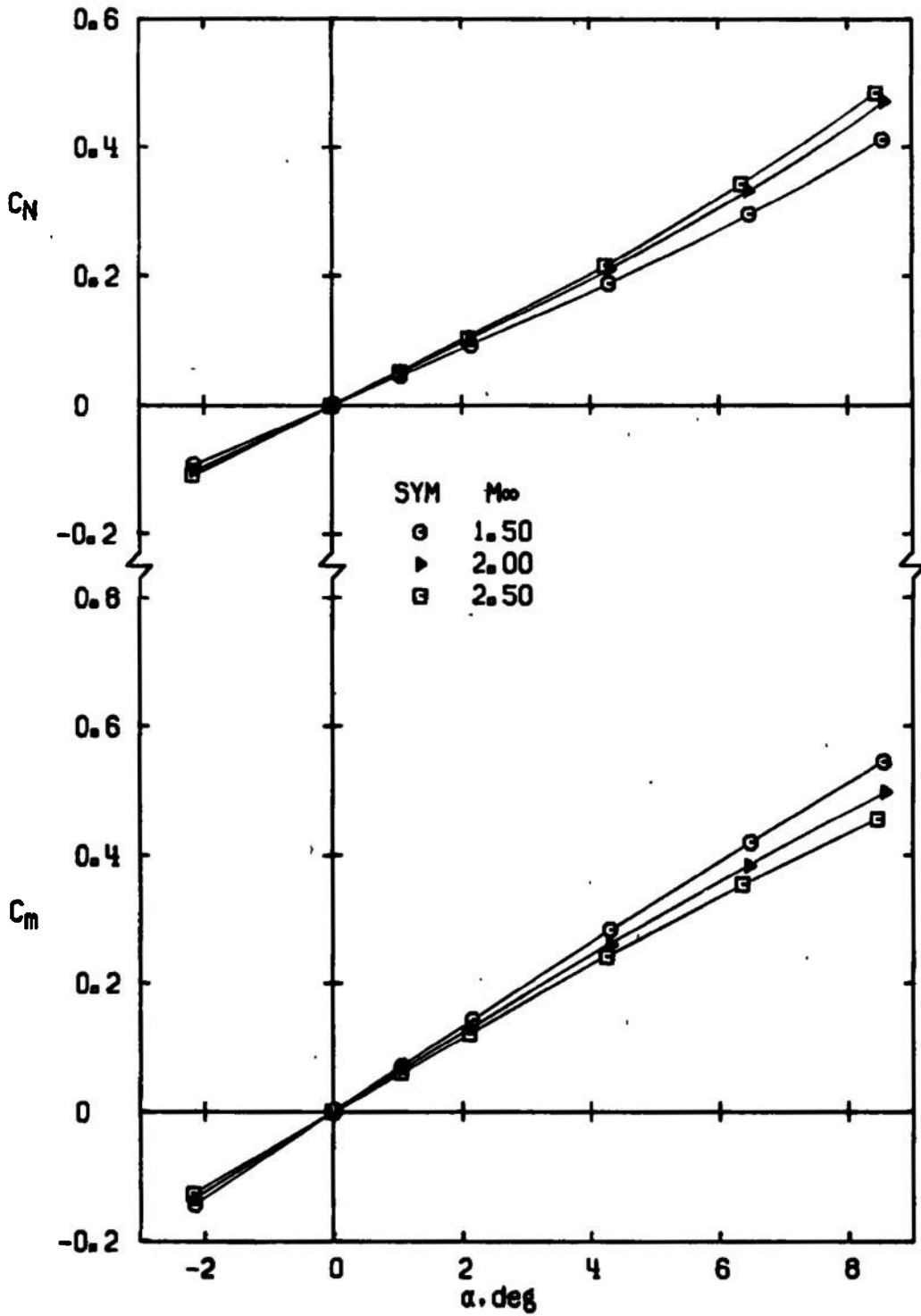


Figure 4. Balance details.

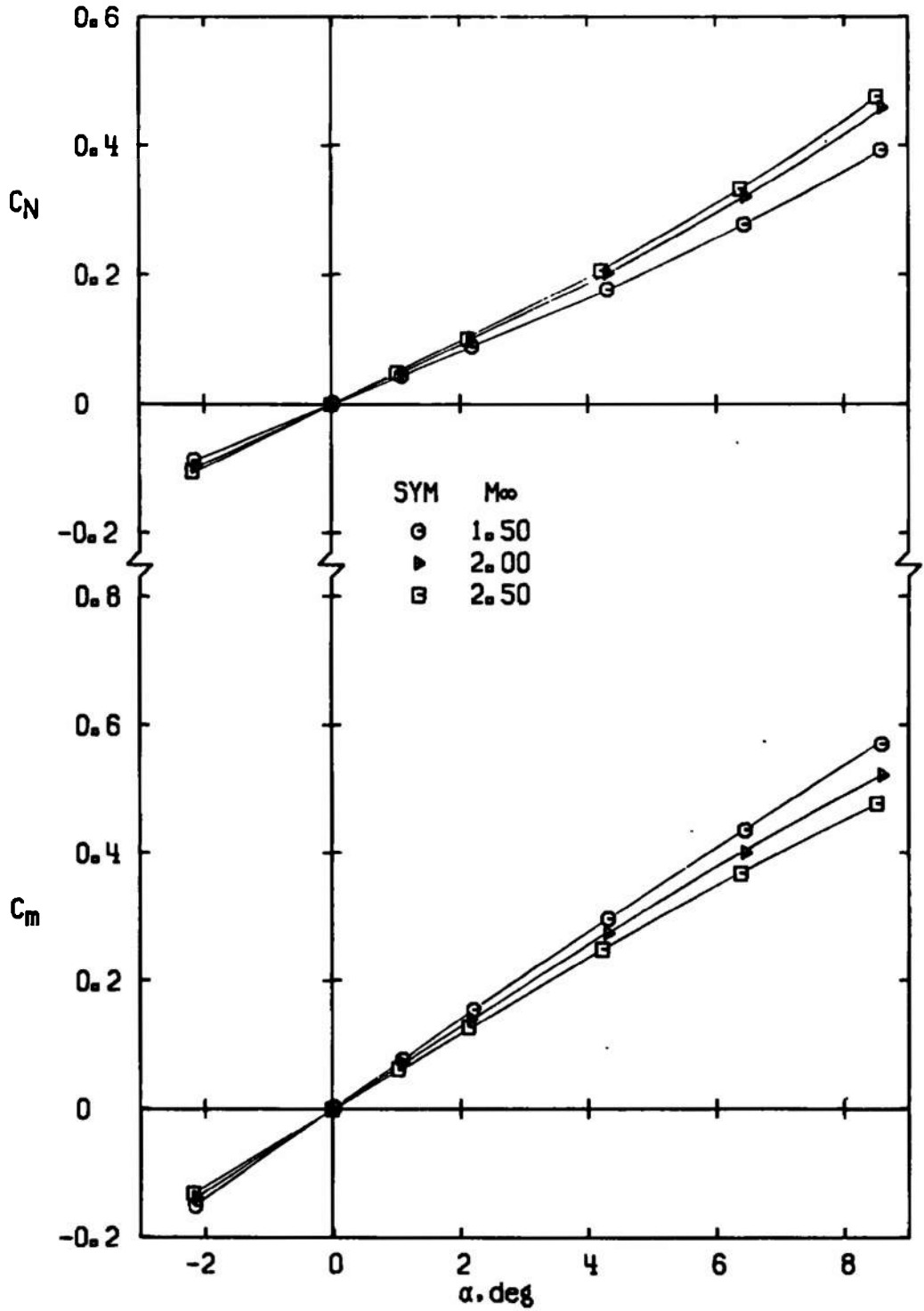


a. Configuration 0

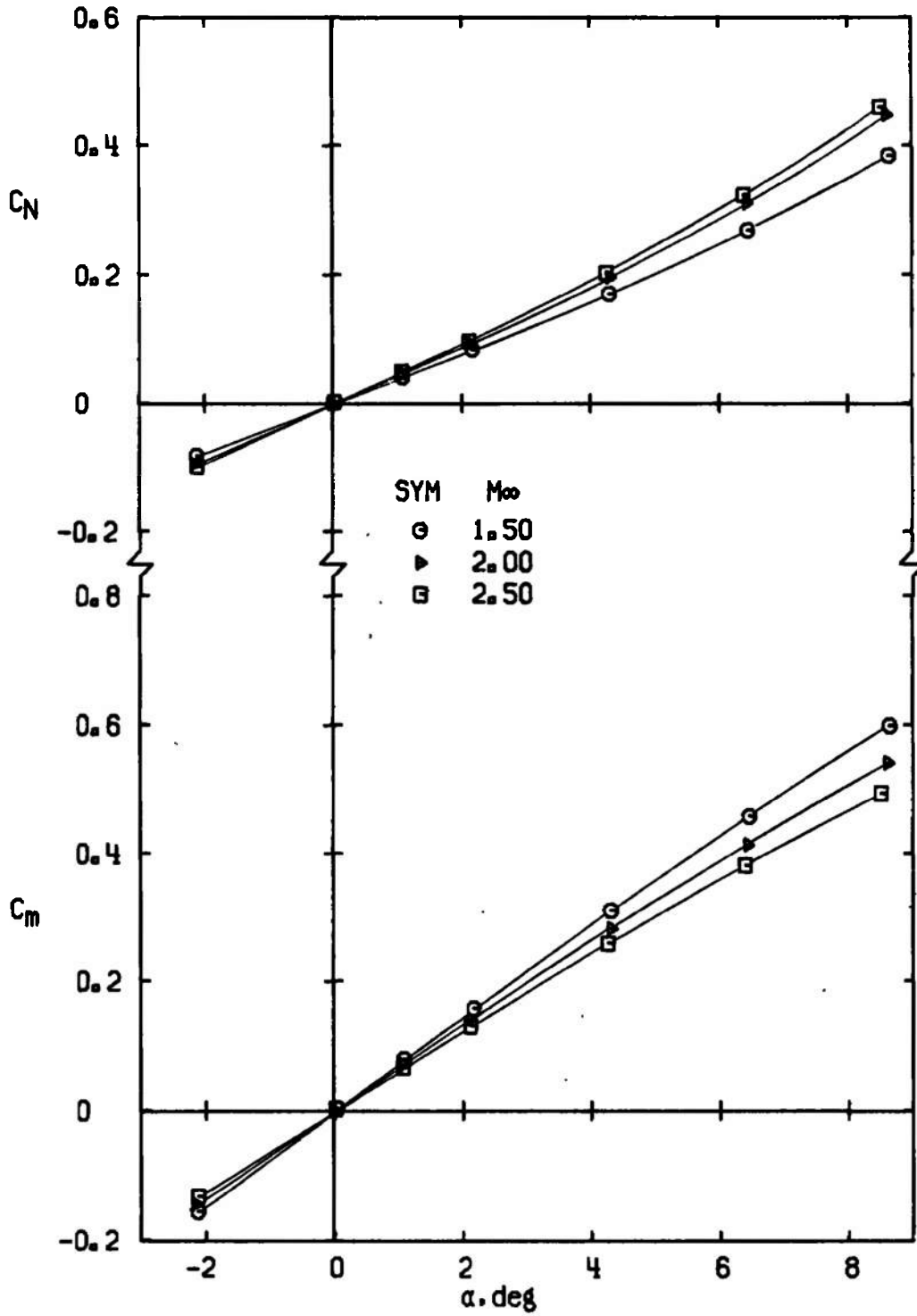
Figure 5. Variation of C_N and C_m with angle of attack, $Re_{\rho} = 9.6 \times 10^6$.



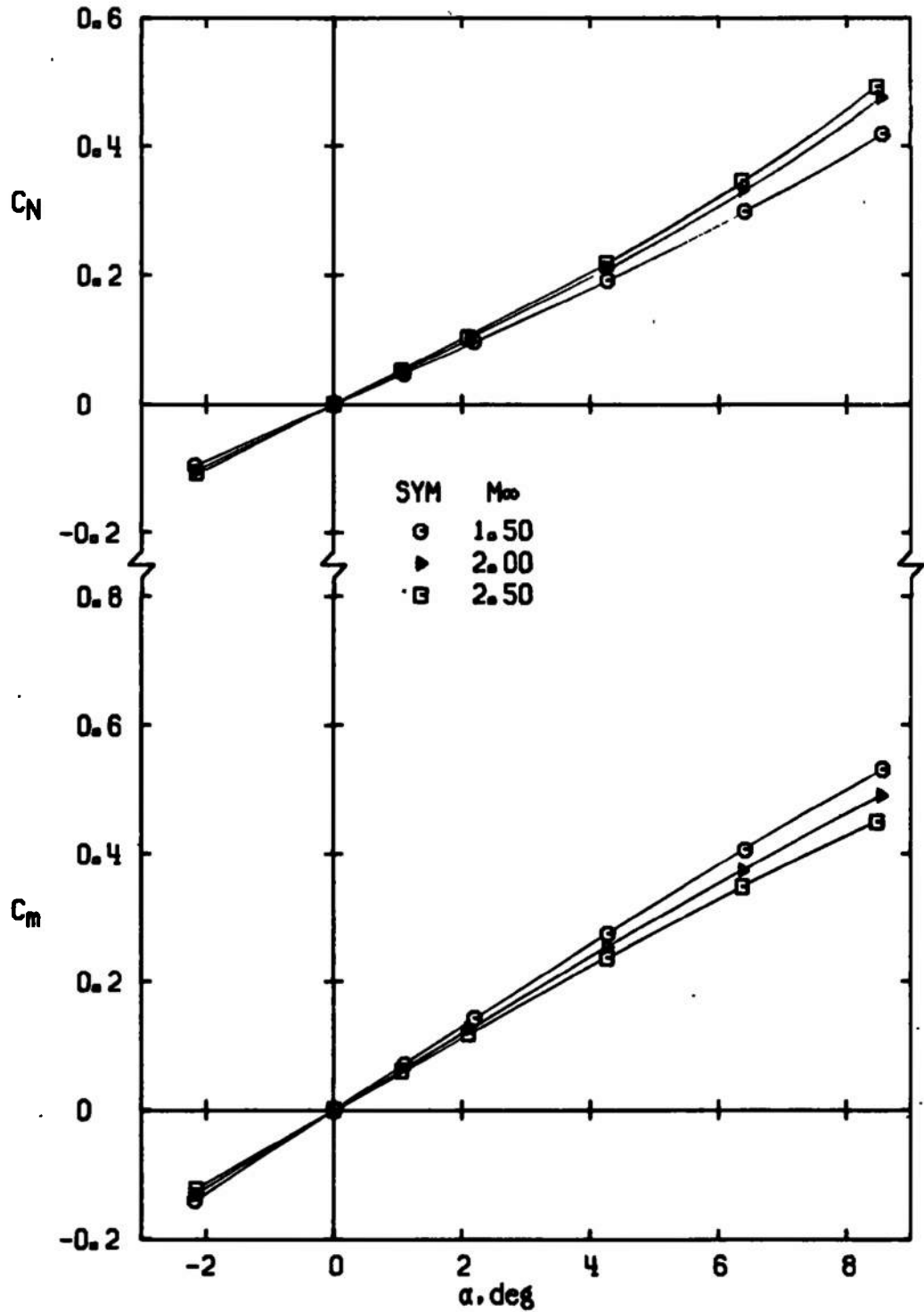
b. Configuration 1
Figure 5. Continued.



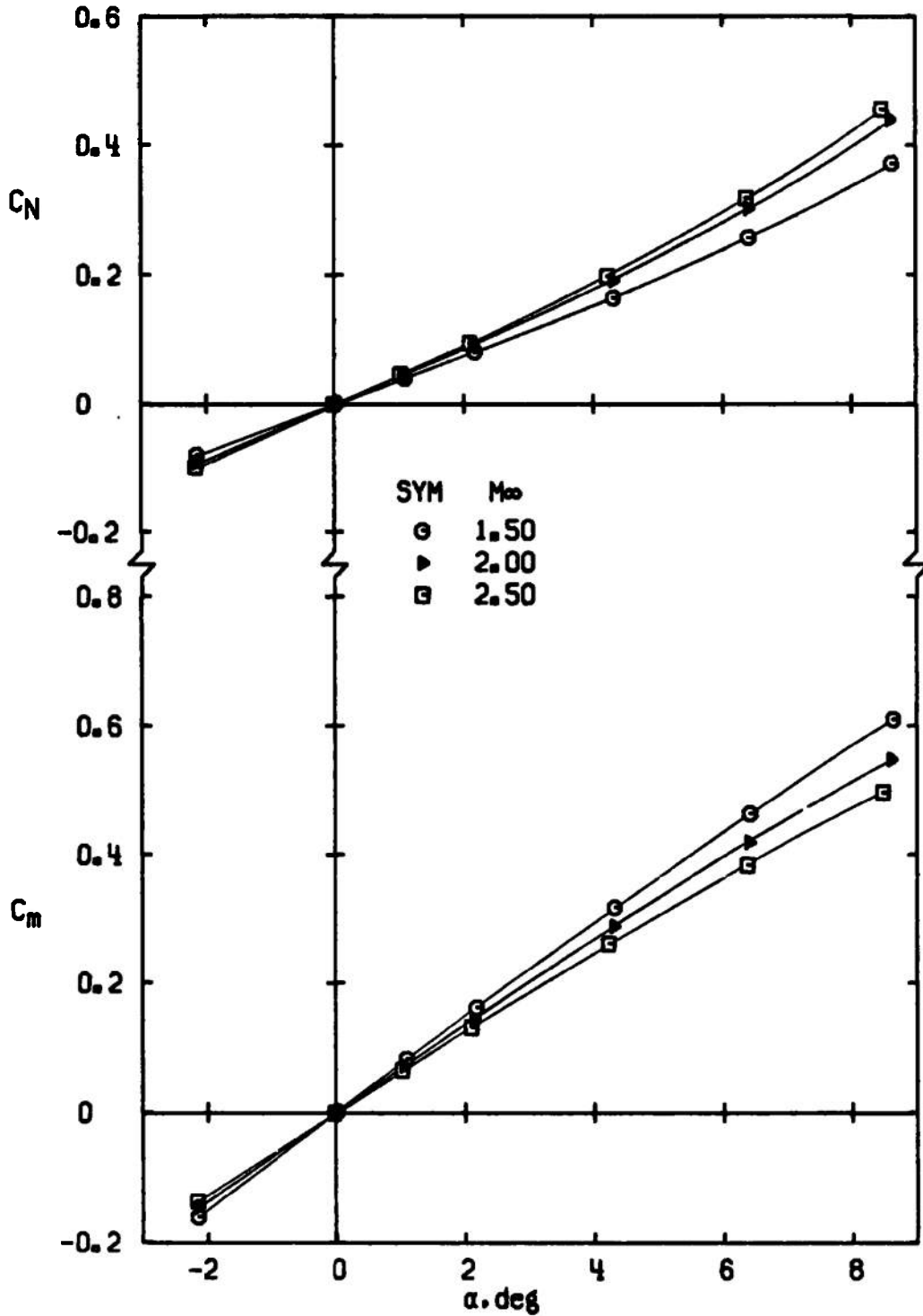
c. Configuration 2
Figure 5. Continued.



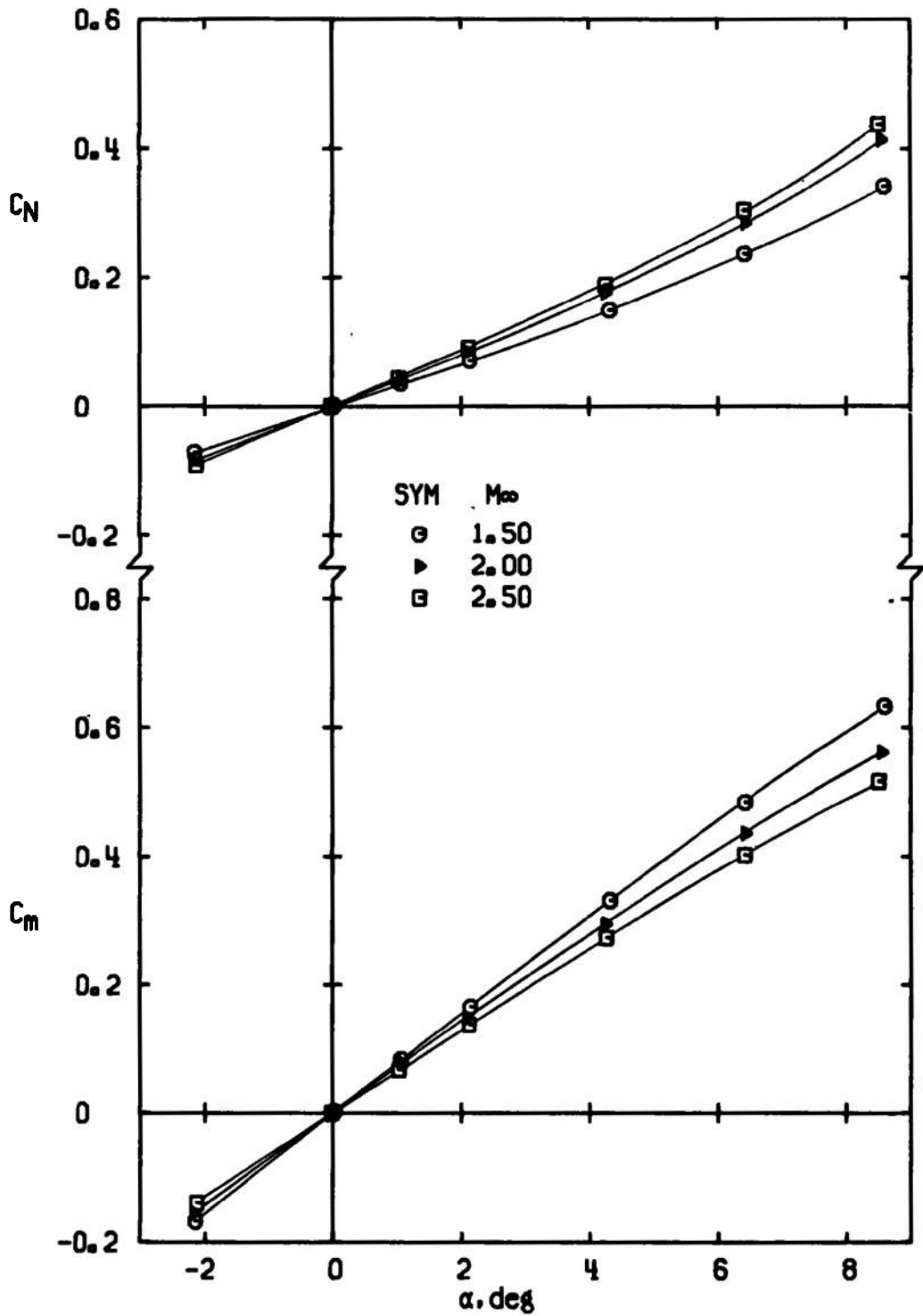
d. Configuration 3
Figure 5. Continued.



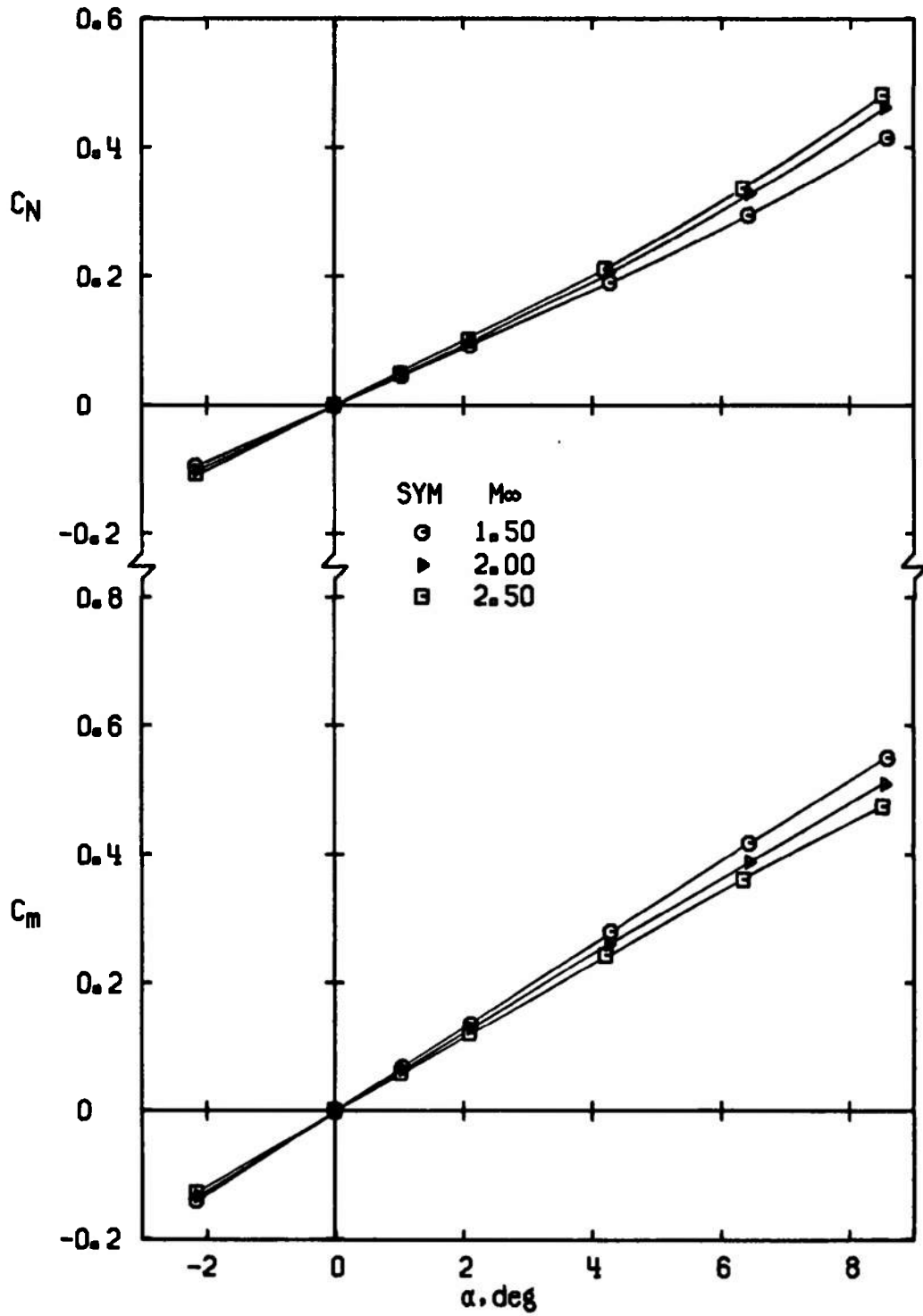
e. Configuration 4
Figure 5. Continued.



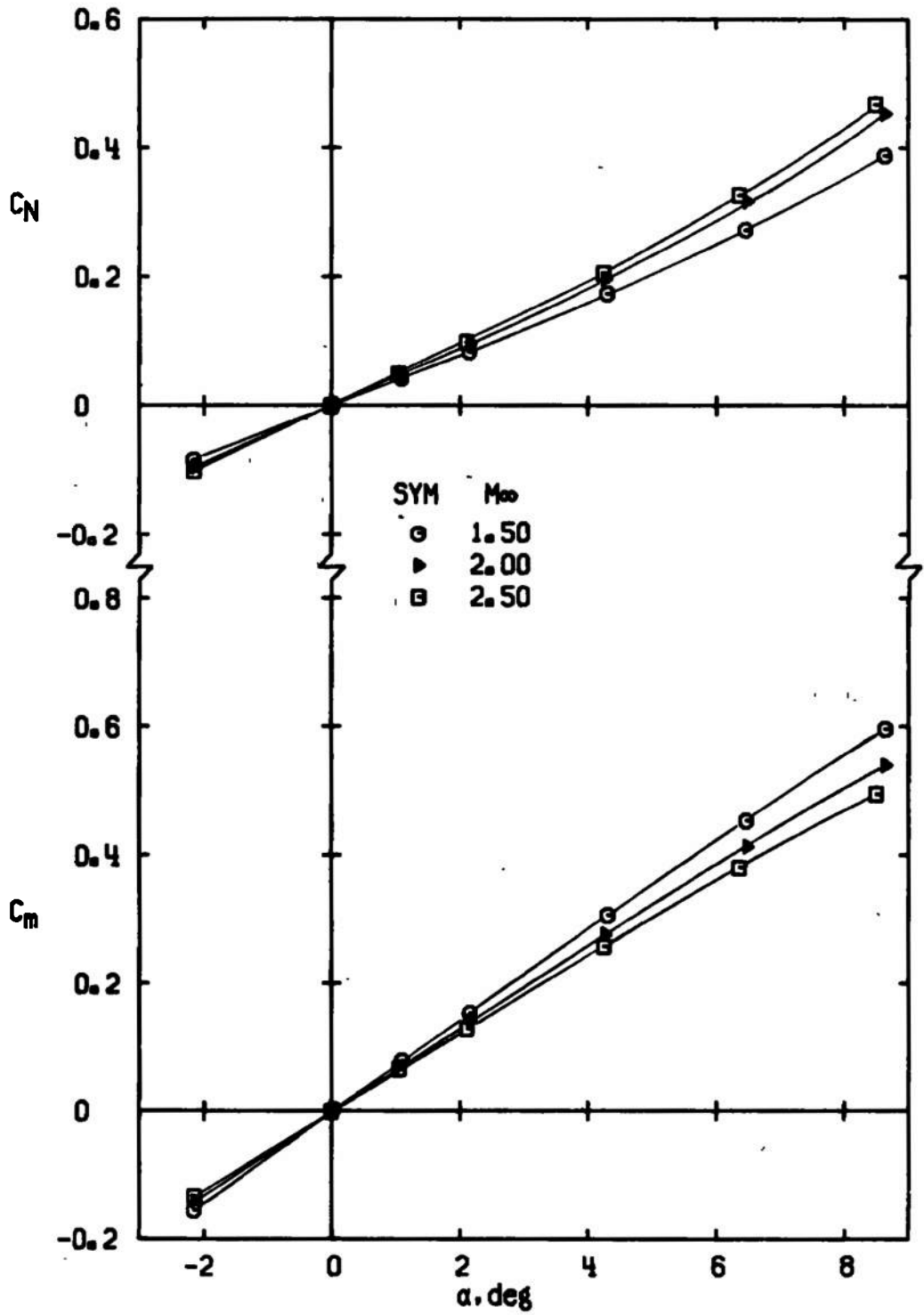
f. Configuration 5
Figure 5. Continued.



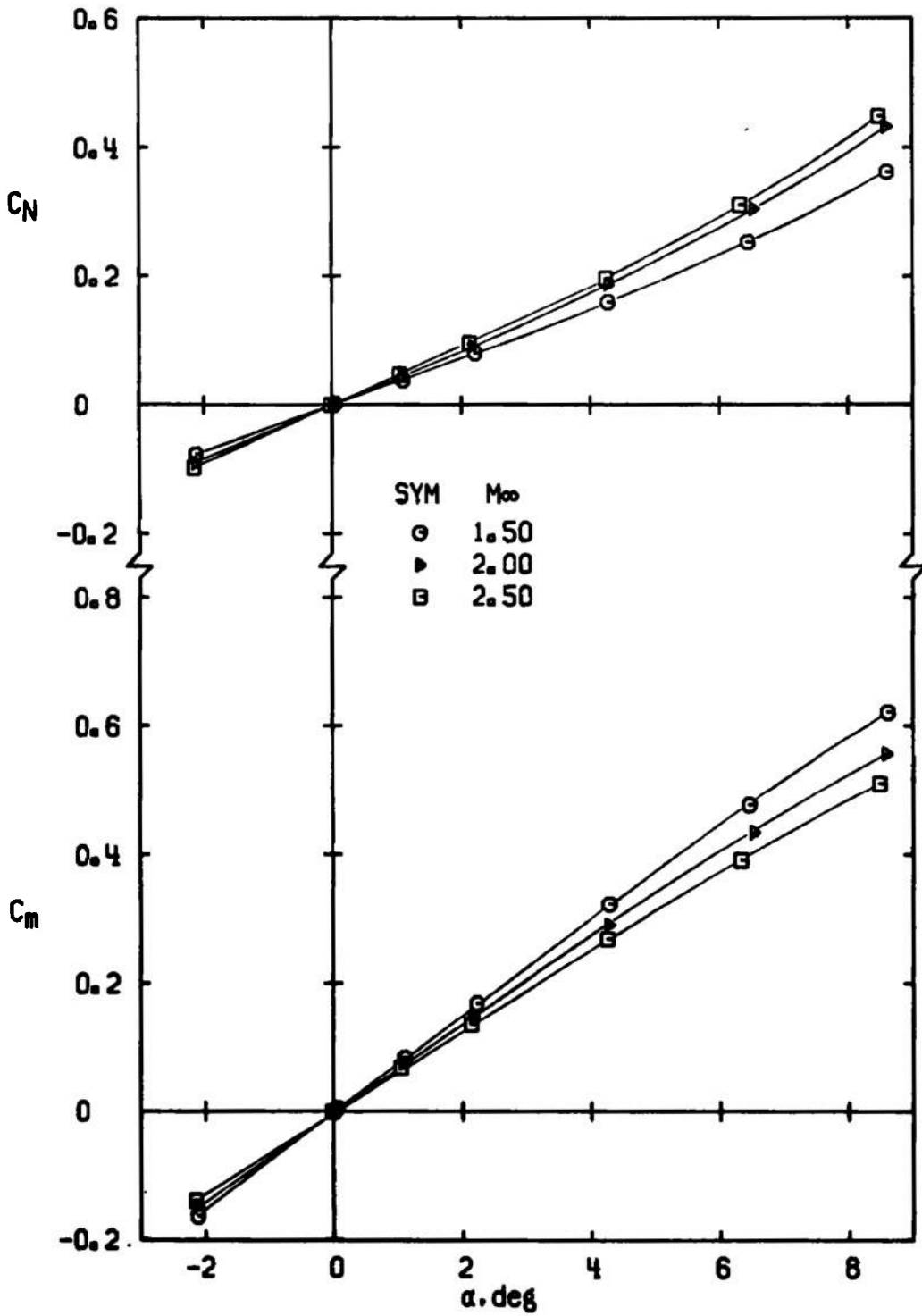
g. Configuration 6
Figure 5. Continued.



h. Configuration 7
Figure 5. Continued.



i. Configuration 8
Figure 5. Continued.



j. Configuration 9
Figure 5. Concluded.

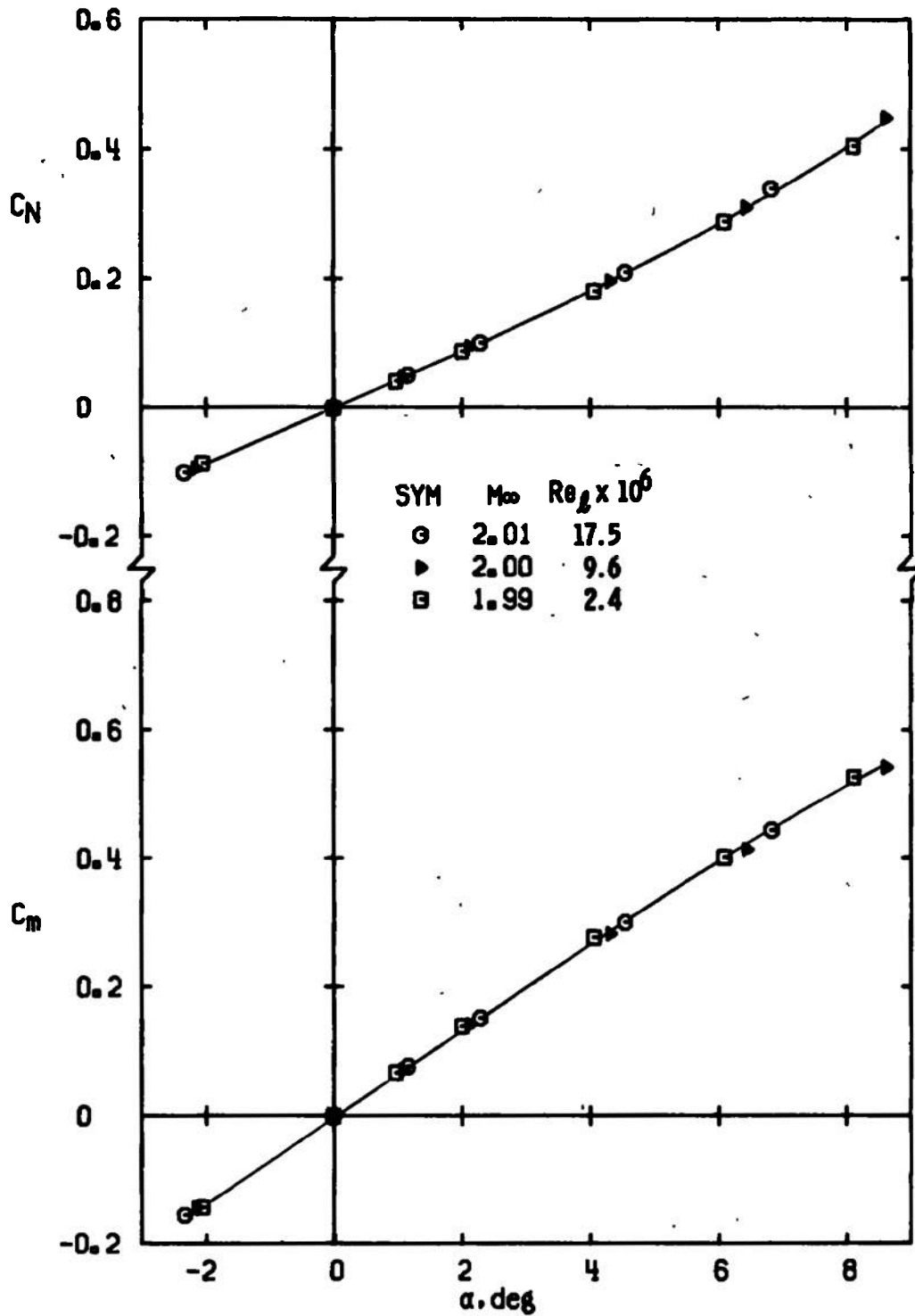
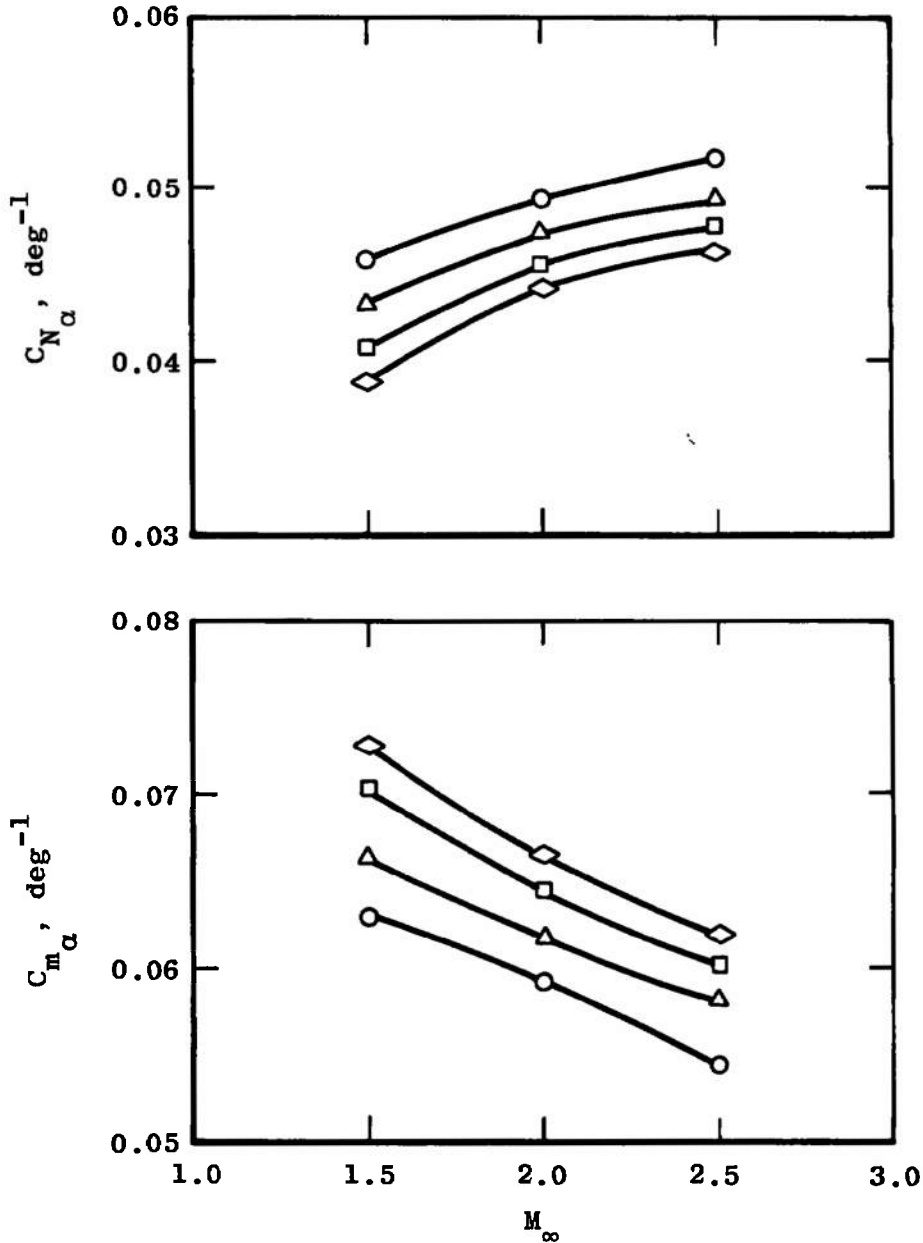


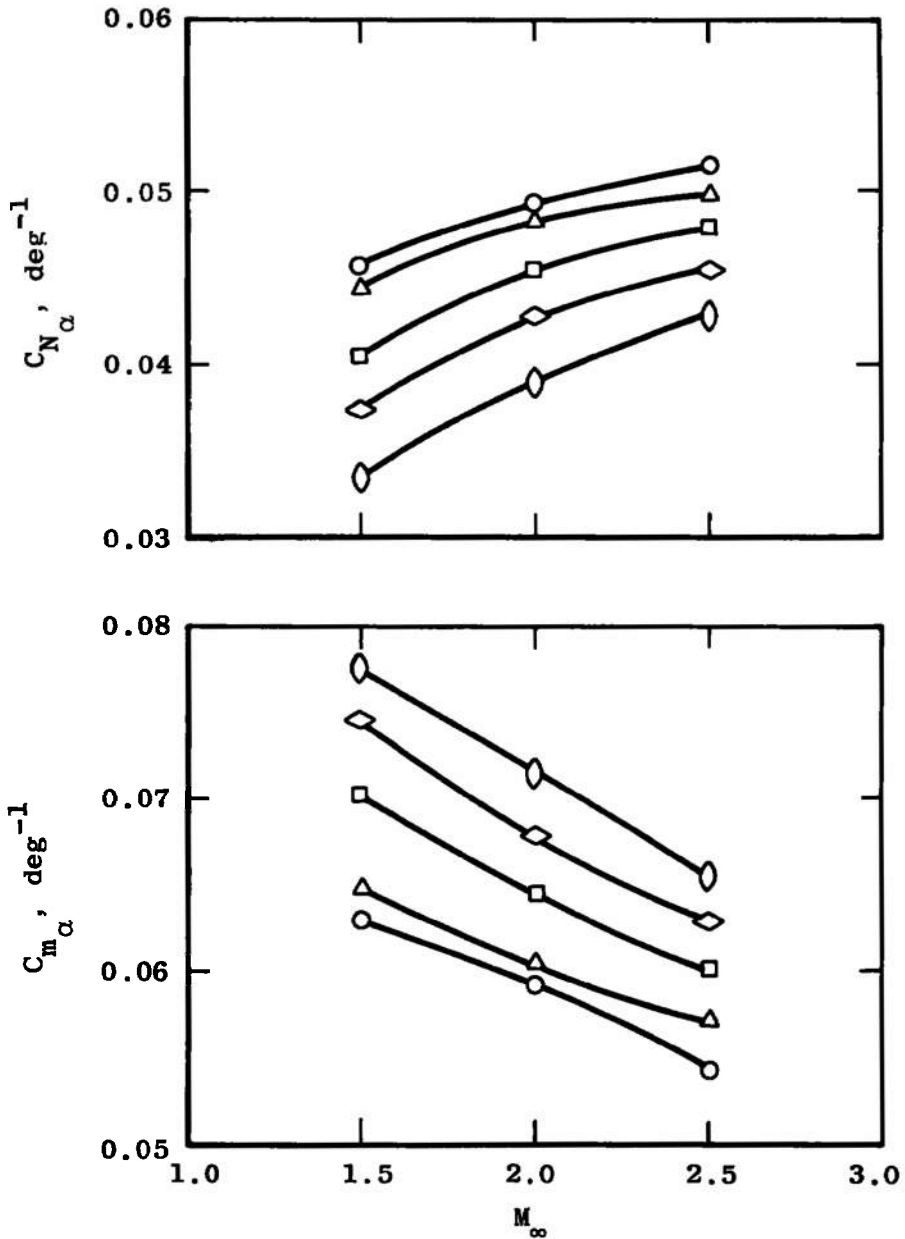
Figure 6. Effect of Reynolds number variation on C_N and C_m at $M_\infty = 2$, configuration 3.

Sym	Configuration	δ_{BT} , deg	l_{BT} , caliber	d_B , caliber
○	0	0	0	1.00
△	1	2.5	1.0	0.91
□	2	5.0	↓	0.83
◇	3	7.5	↓	0.74



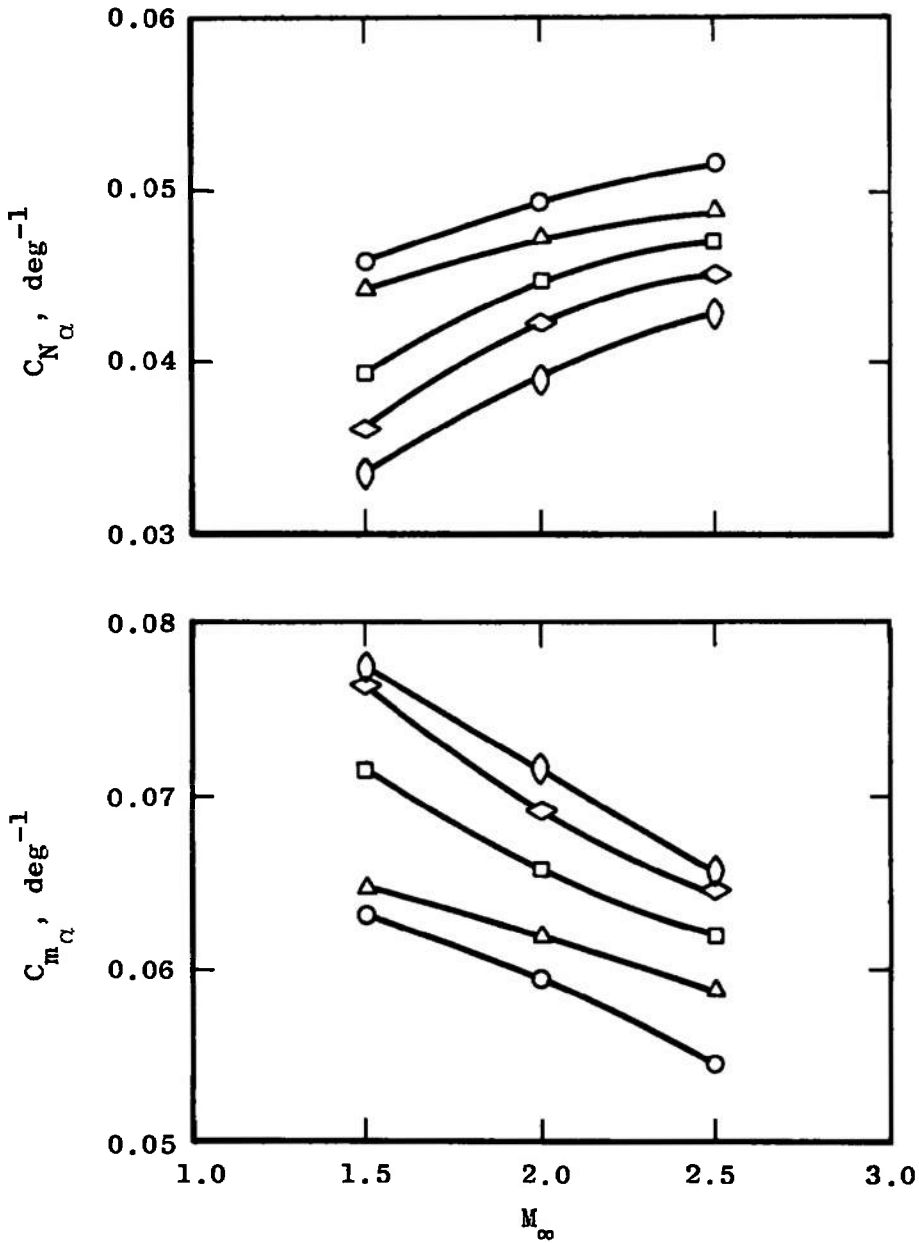
a. Effect of boattail angle with a constant boattail length
 Figure 7. Variation of C_{N_α} and C_{m_α} with Mach number,
 $Re_q = 9.6 \times 10^6$.

Sym	Configuration	l_{BT} , caliber	δ_{BT} , deg	d_B , caliber
○	0	0	0	1.00
△	4	0.50	5	0.91
□	2	1.00	↓	0.83
◇	5	1.35	↓	0.76
◊	6	1.70	↓	0.70



b. Effect of boattail length with a constant boattail angle
Figure 7. Continued.

Sym	Configuration	l_{BT} , caliber	d_B , caliber	δ_{BT} , deg
○	0	0	1.0	0
△	7	0.45	0.7	18.4
□	8	0.85	↓	10.0
◇	9	1.25		6.9
◊	6	1.70		5.0



c. Effect of boattail length with a constant base diameter
 Figure 7. Concluded.

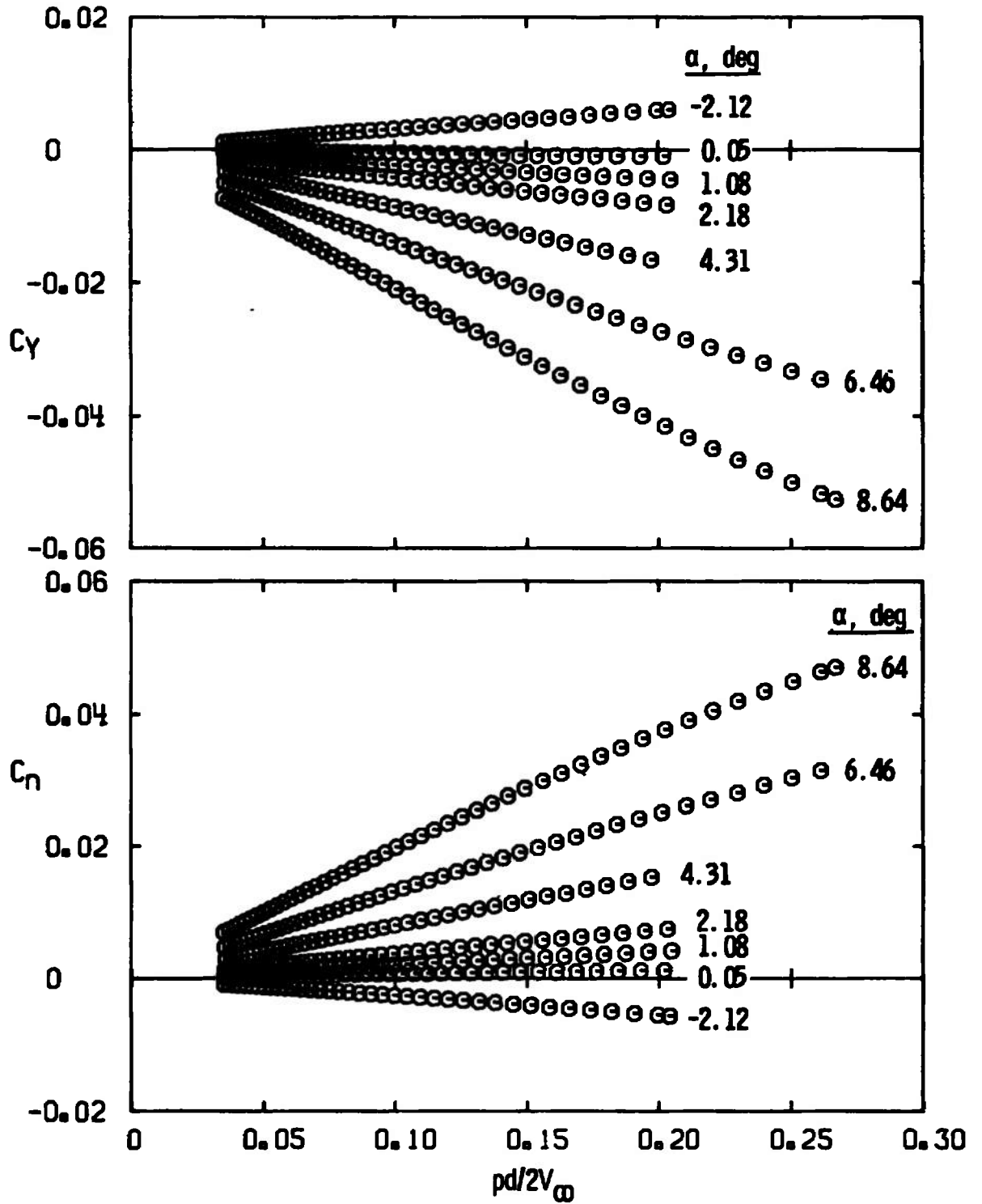
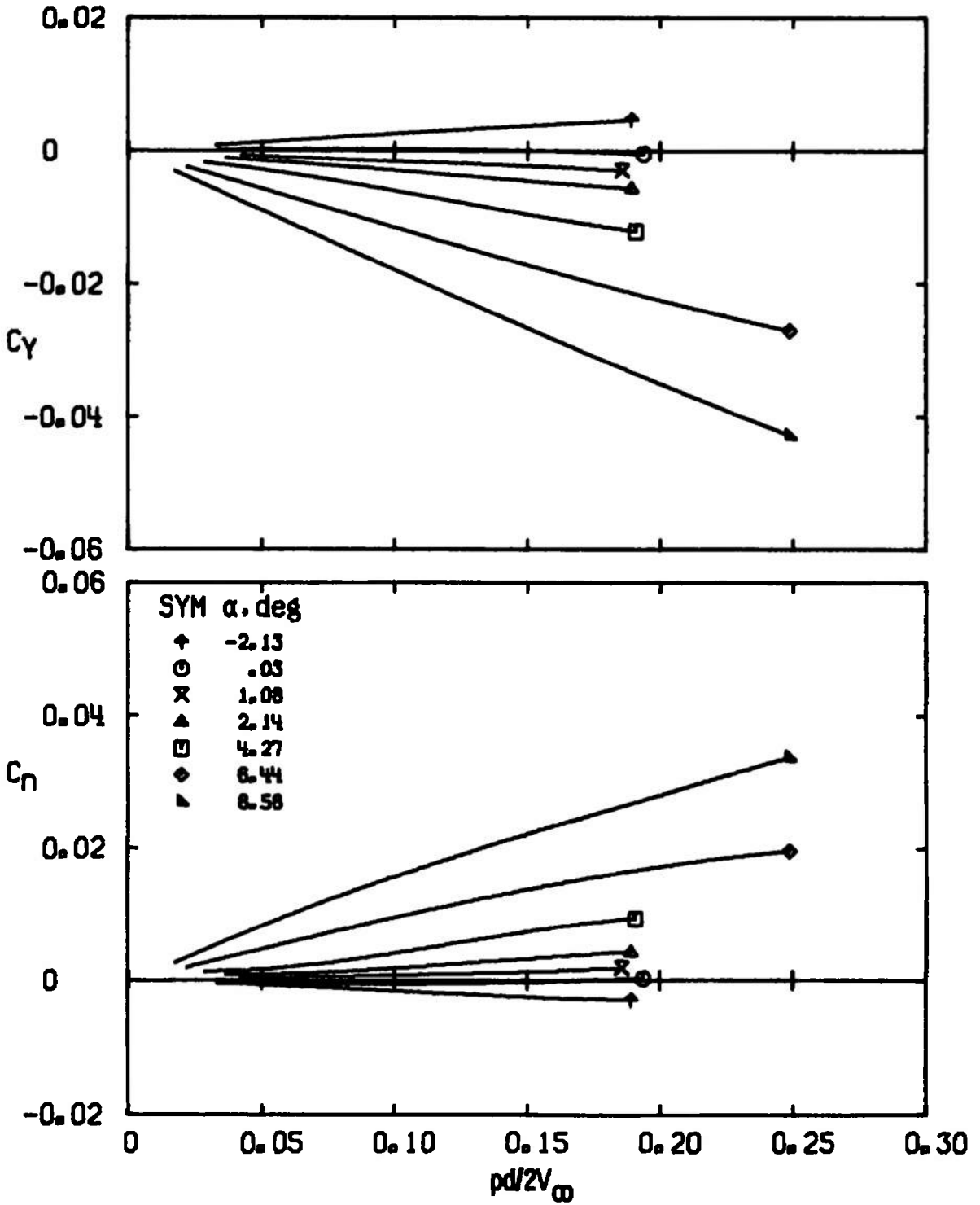
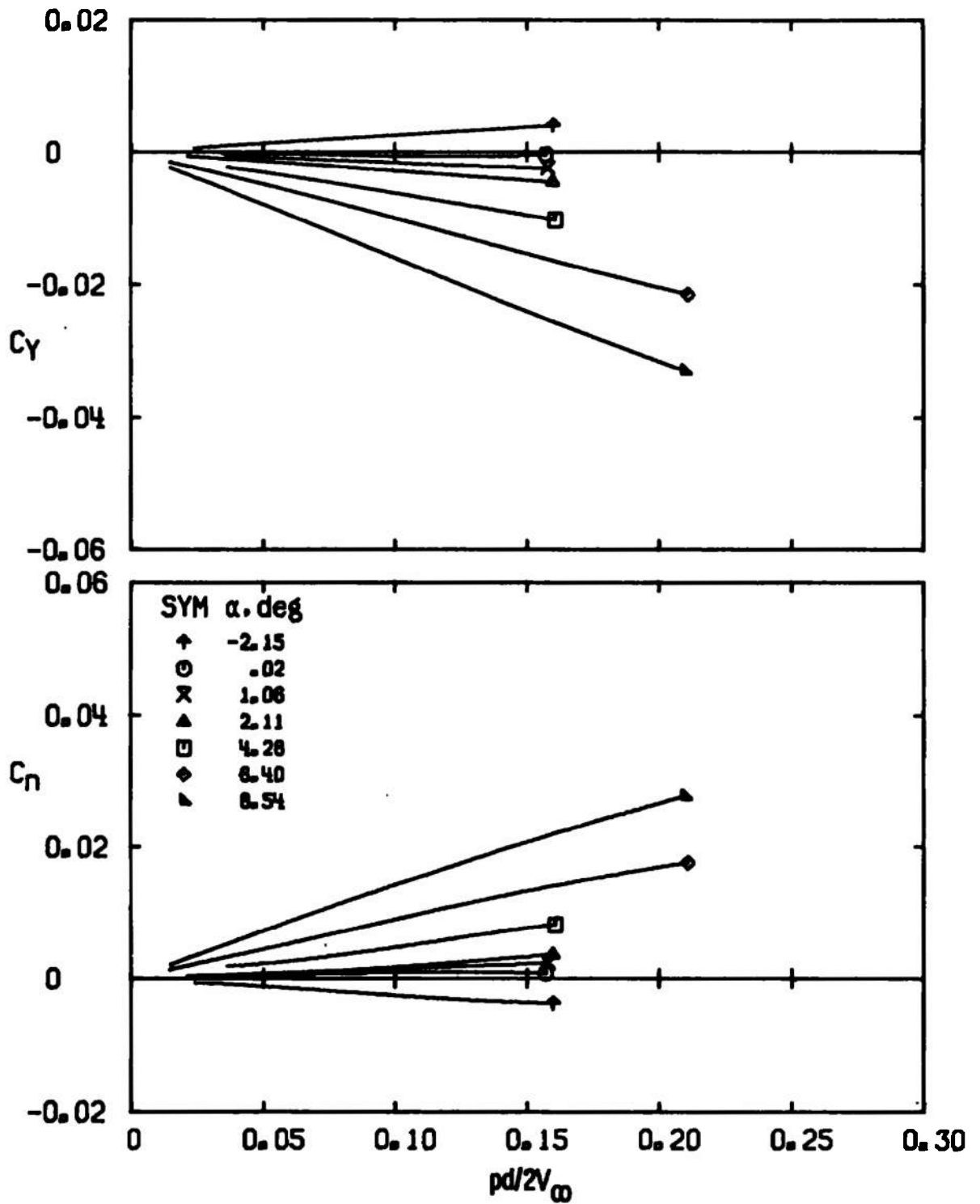


Figure 8. Typical variation of C_y and C_n with $pd/2V_\infty$, configuration 3, $M_\infty = 1.5$, $Re_\ell = 9.6 \times 10^6$.

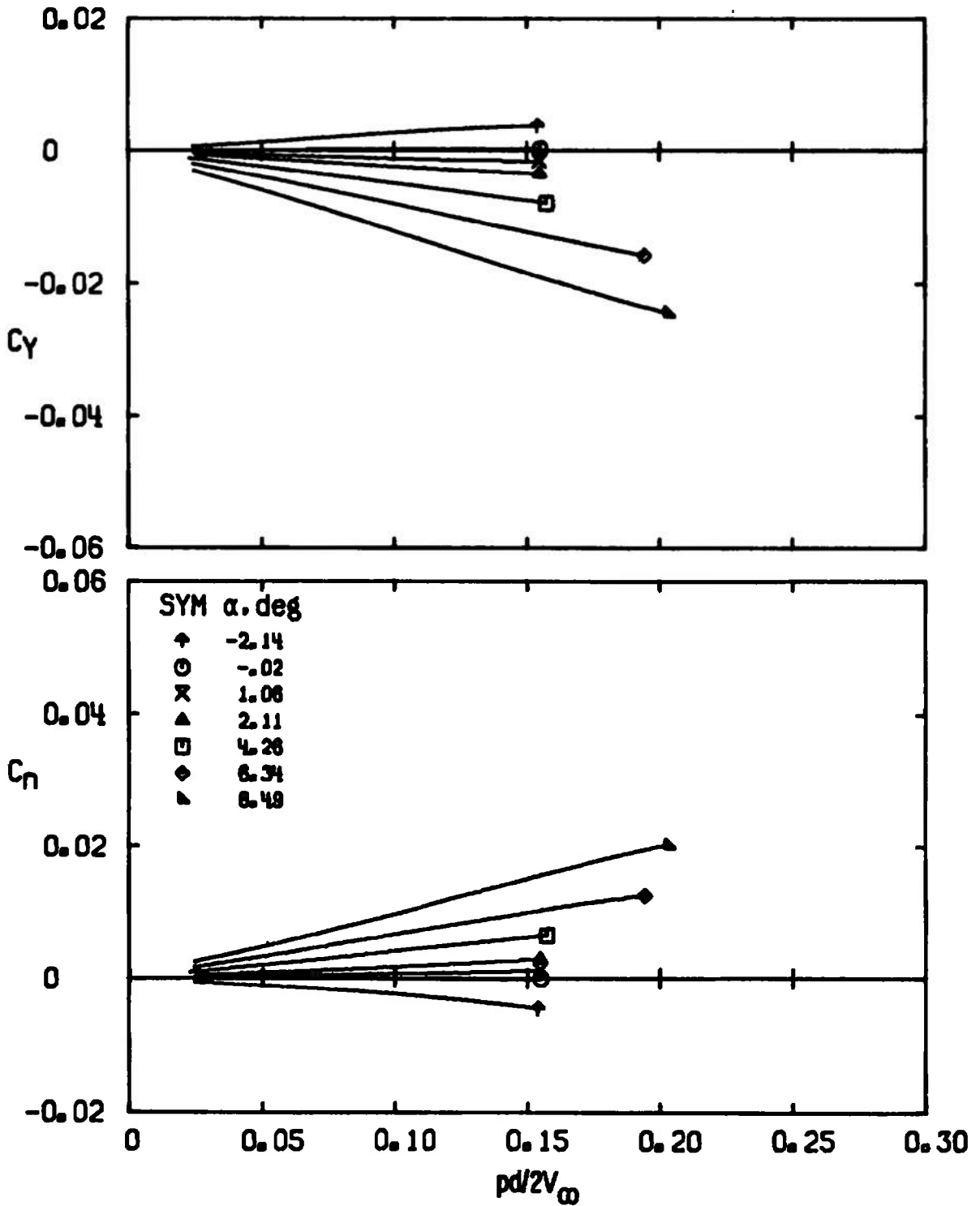


a. $M_\infty = 1.5$

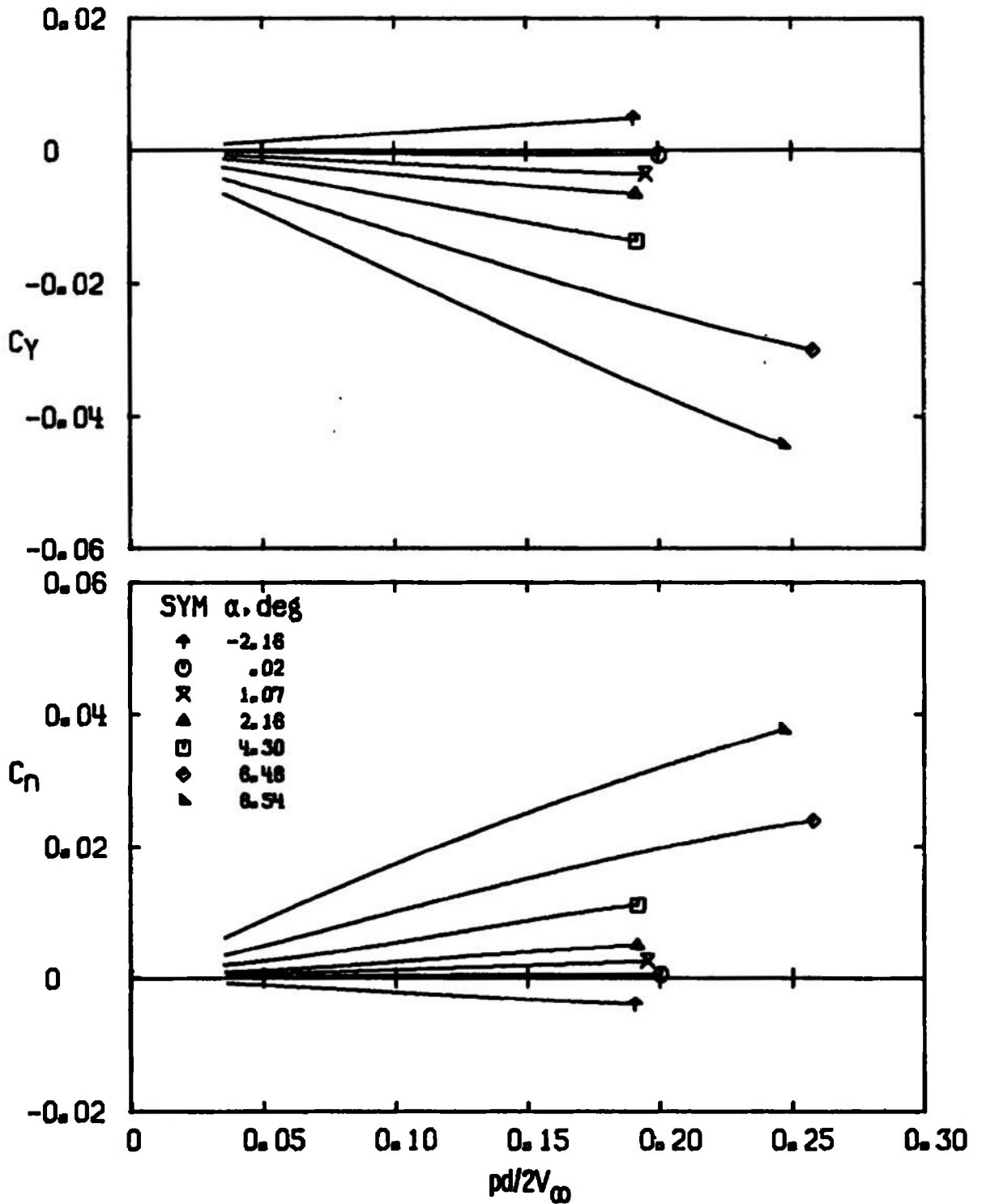
Figure 9. Variation of C_Y and C_n with $pd/2V_\infty$ for configuration 0, $Re_\xi = 9.6 \times 10^6$.



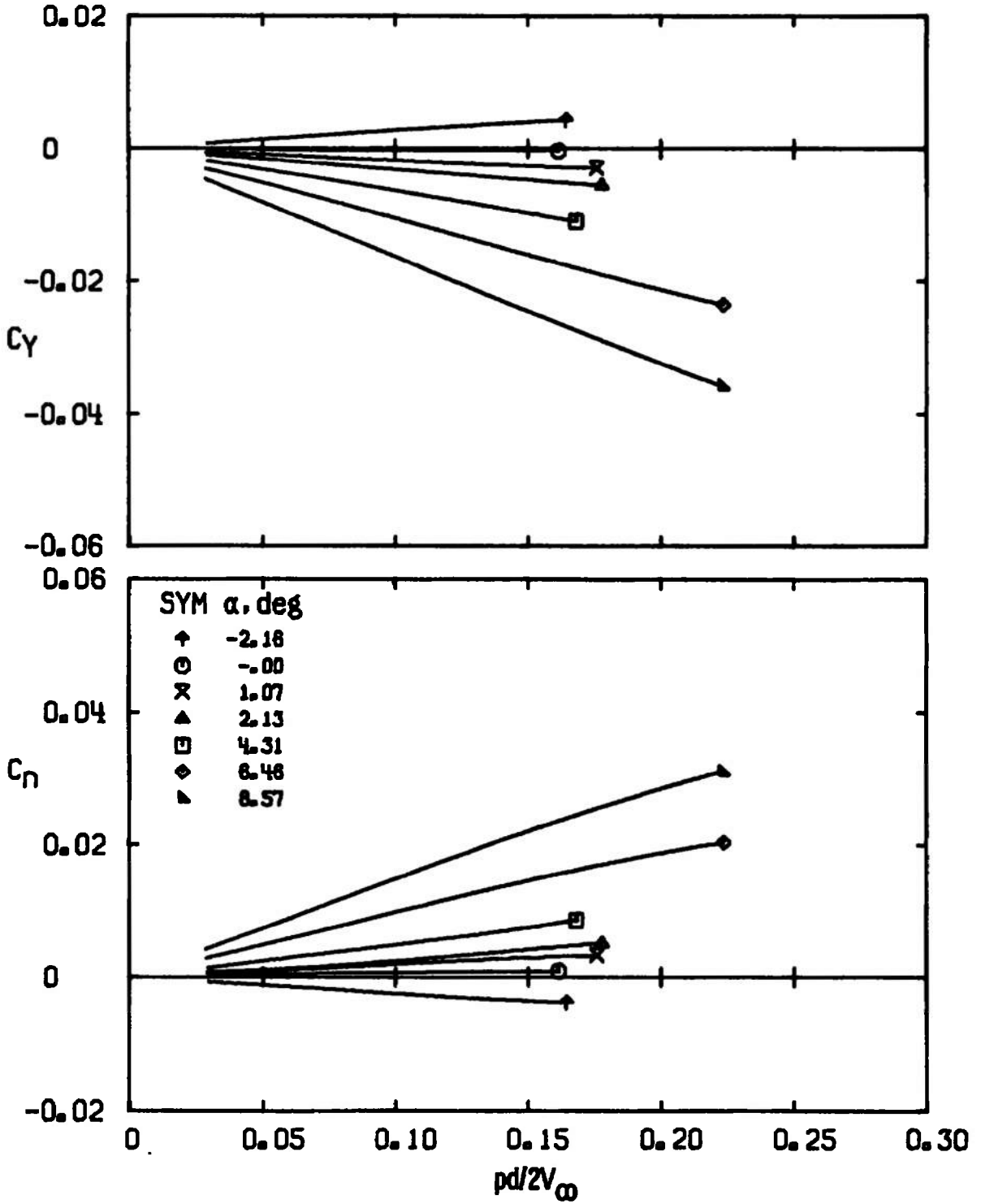
b. $M_\infty = 2.0$
 Figure 9. Continued.



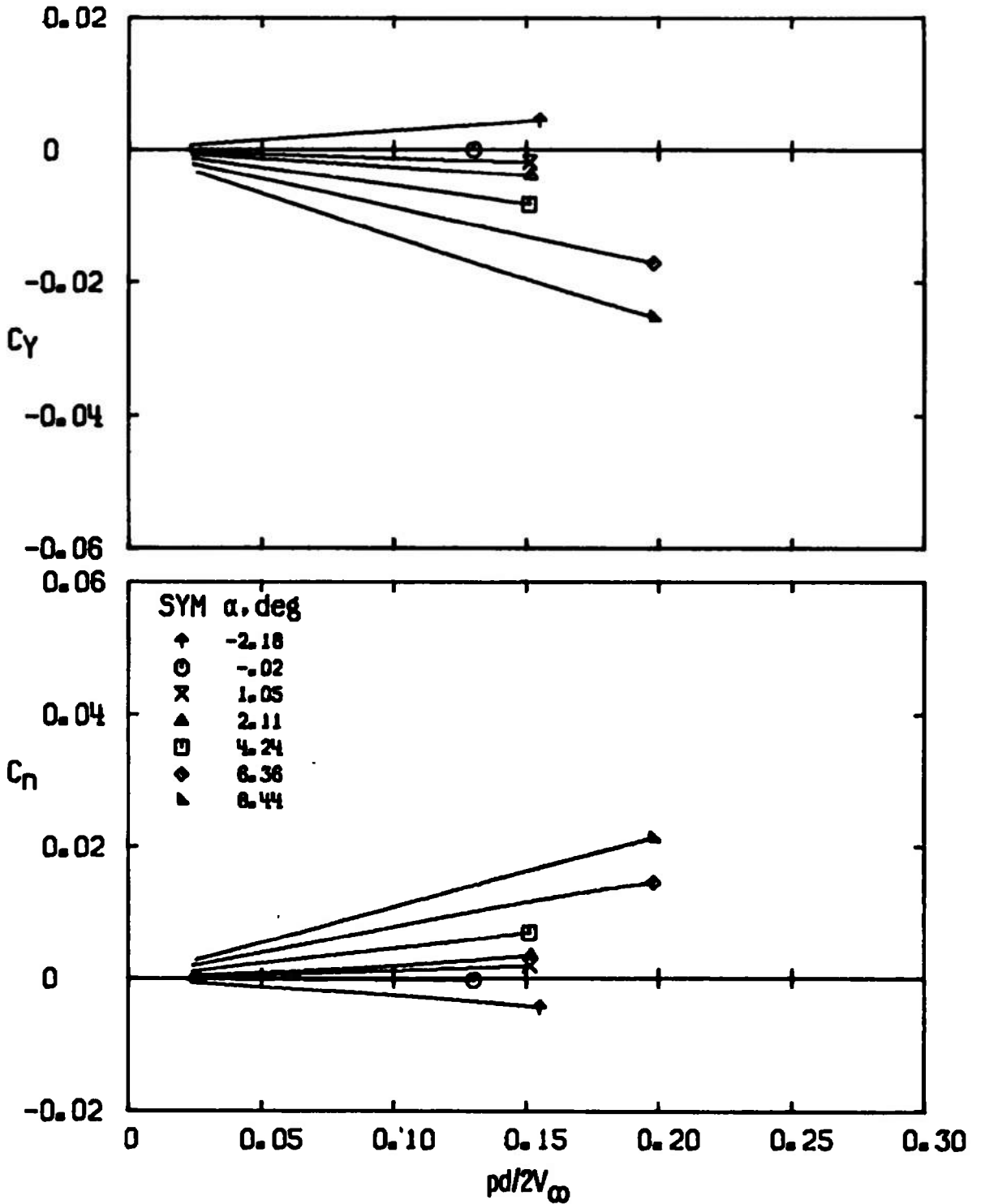
c. $M_{\infty} = 2.5$
 Figure 9. Concluded.



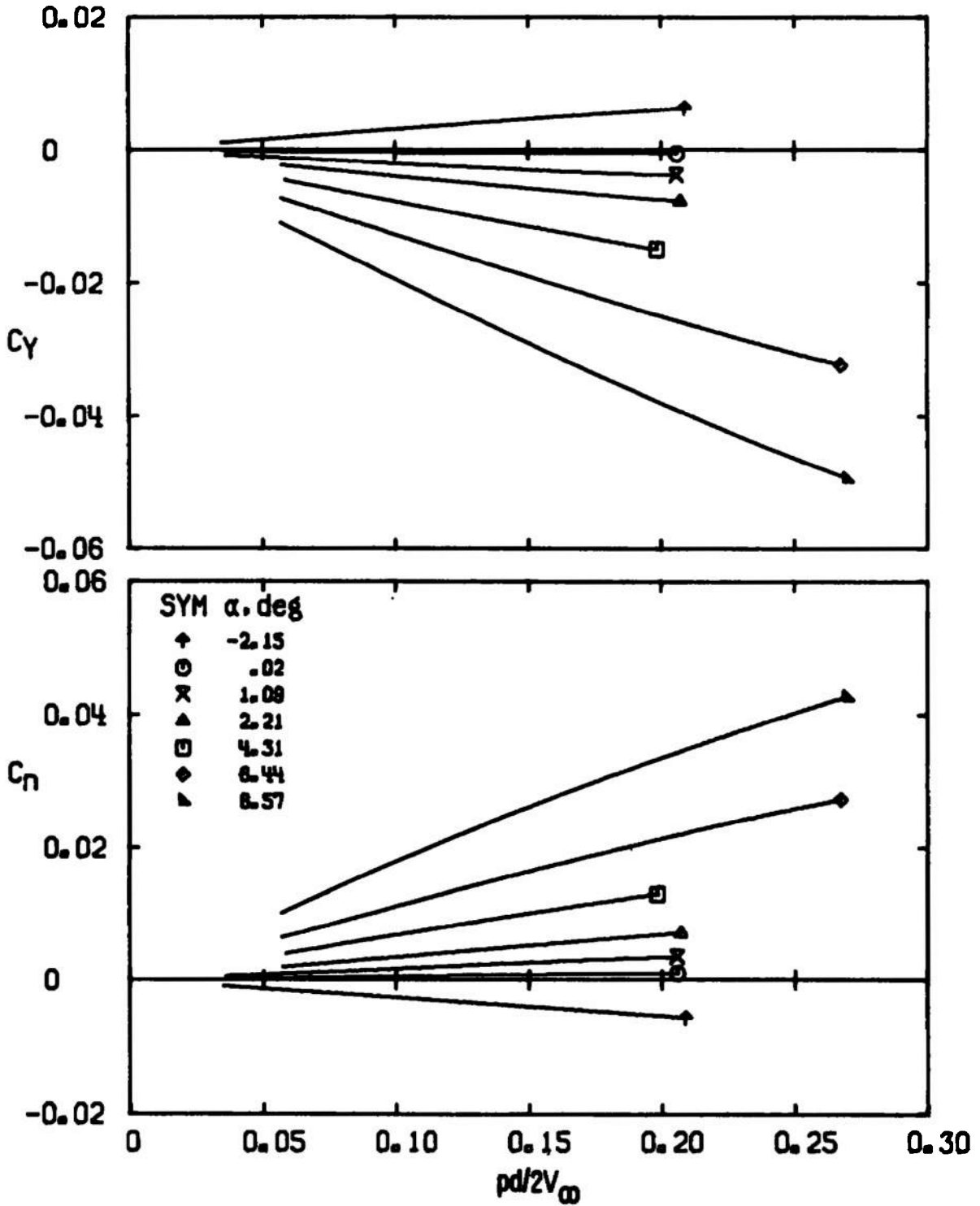
a. $M_\infty = 1.5$
 Figure 10. Variation of C_Y and C_n with $pd/2V_\infty$ for configuration 1,
 $Re_\rho = 9.6 \times 10^6$.



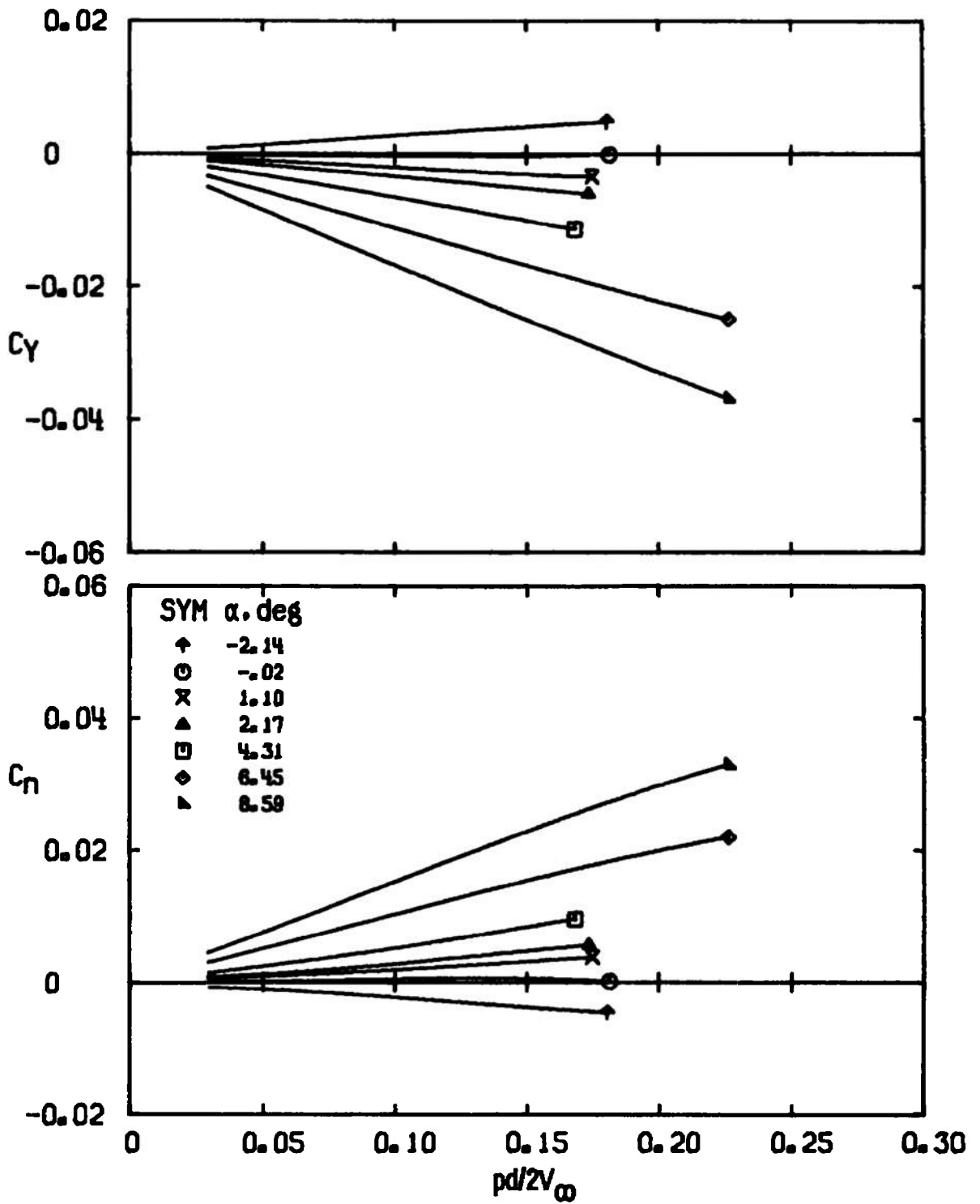
b. $M_\infty = 2.0$
 Figure 10. Continued.



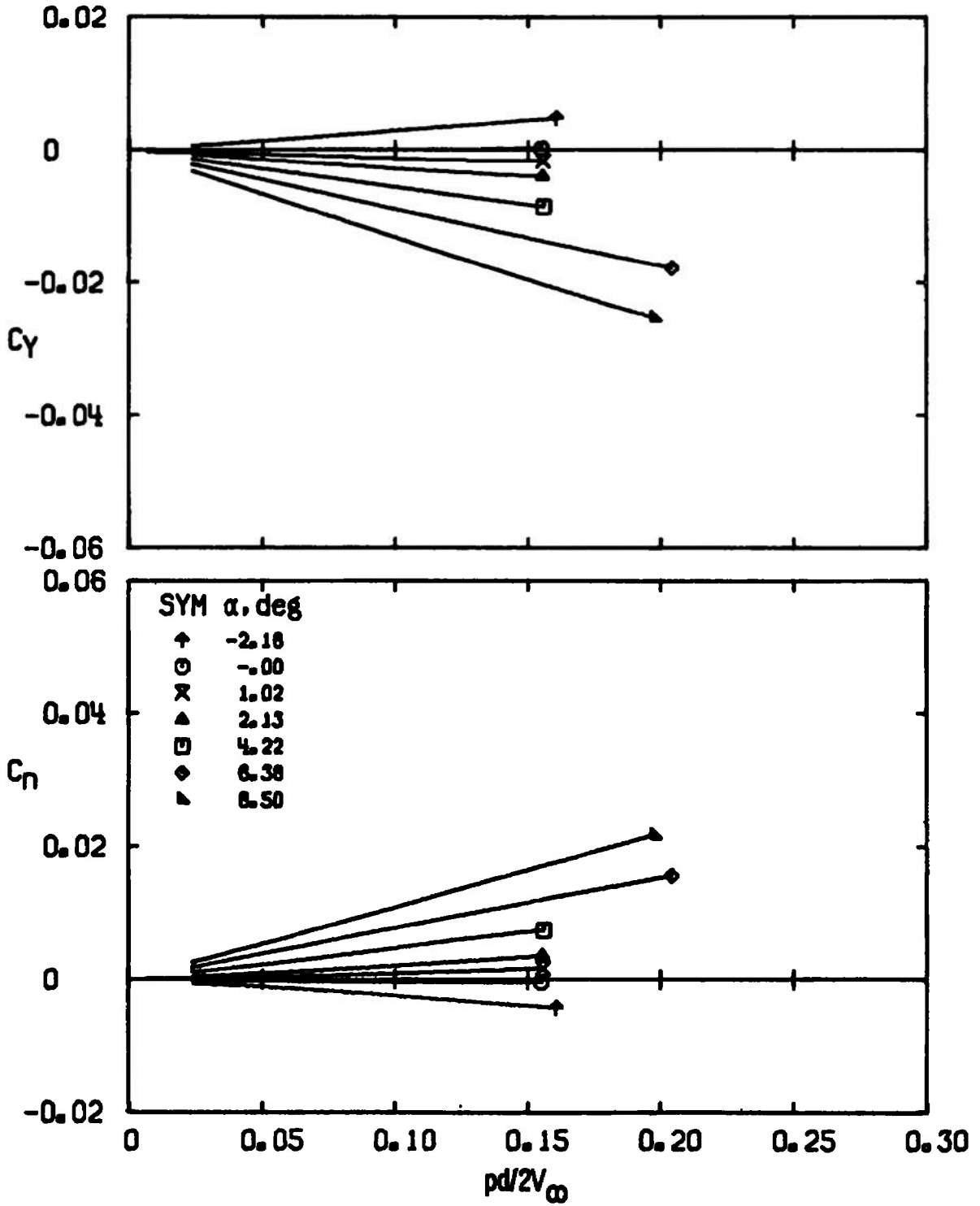
c. $M_\infty = 2.5$
 Figure 10. Concluded.



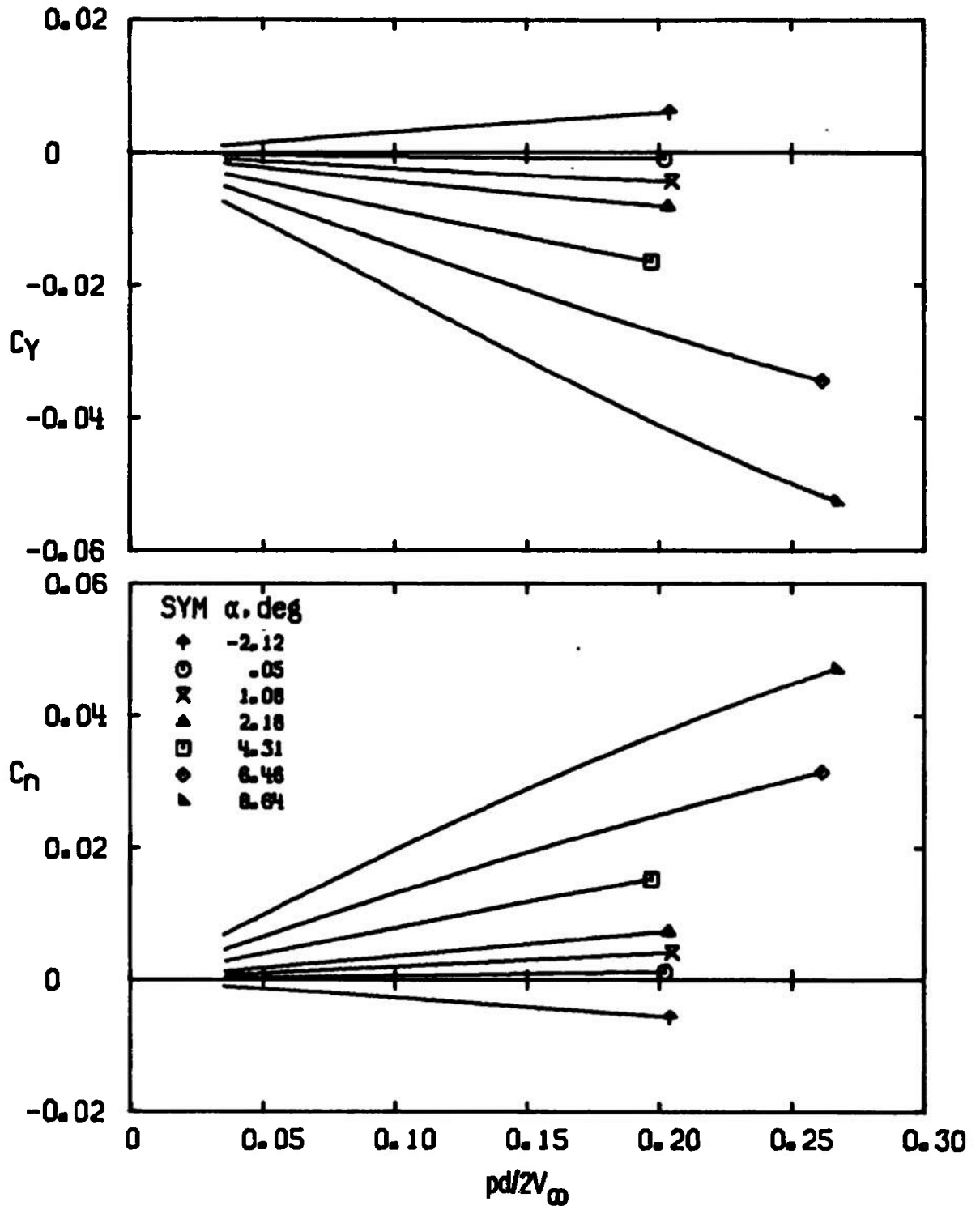
a. $M_\infty = 1.5$
 Figure 11. Variation of C_Y and C_n with $pd/2V_\infty$ for configuration 2, $Re_q = 9.6 \times 10^6$.



b. $M_\infty = 2.0$
 Figure 11. Continued.

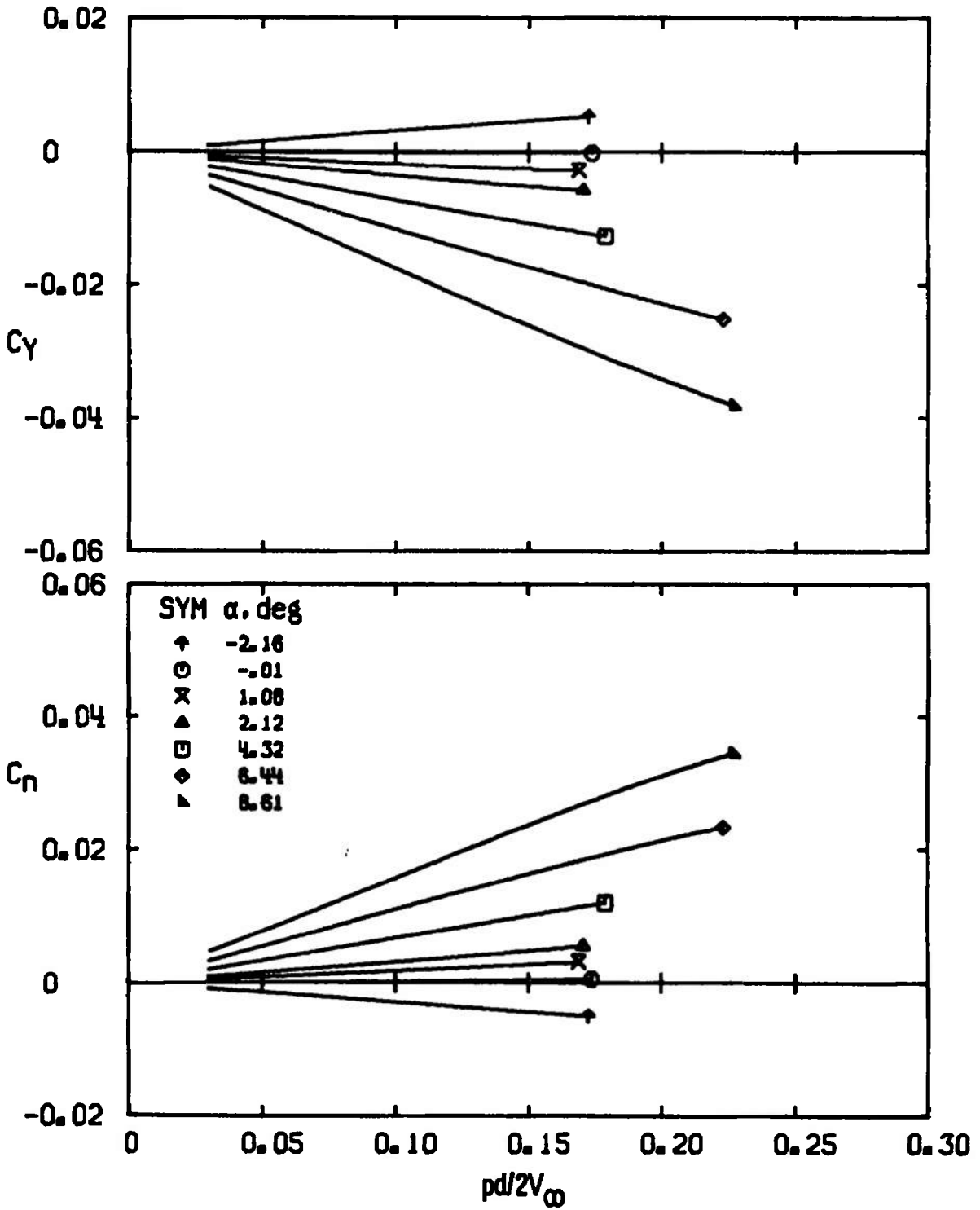


c. $M_\infty = 2.5$
 Figure 11. Concluded.

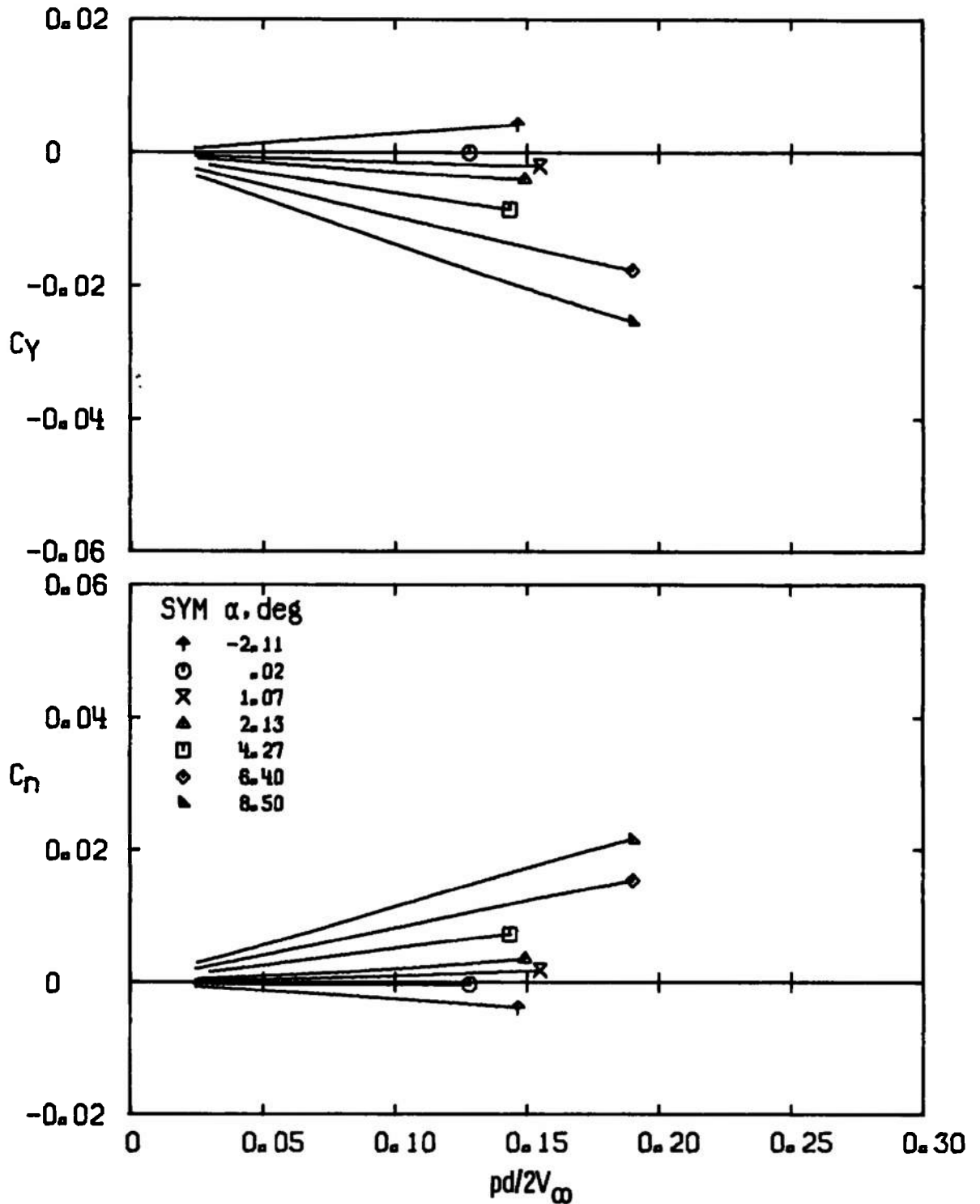


a. $M_\infty = 1.5$

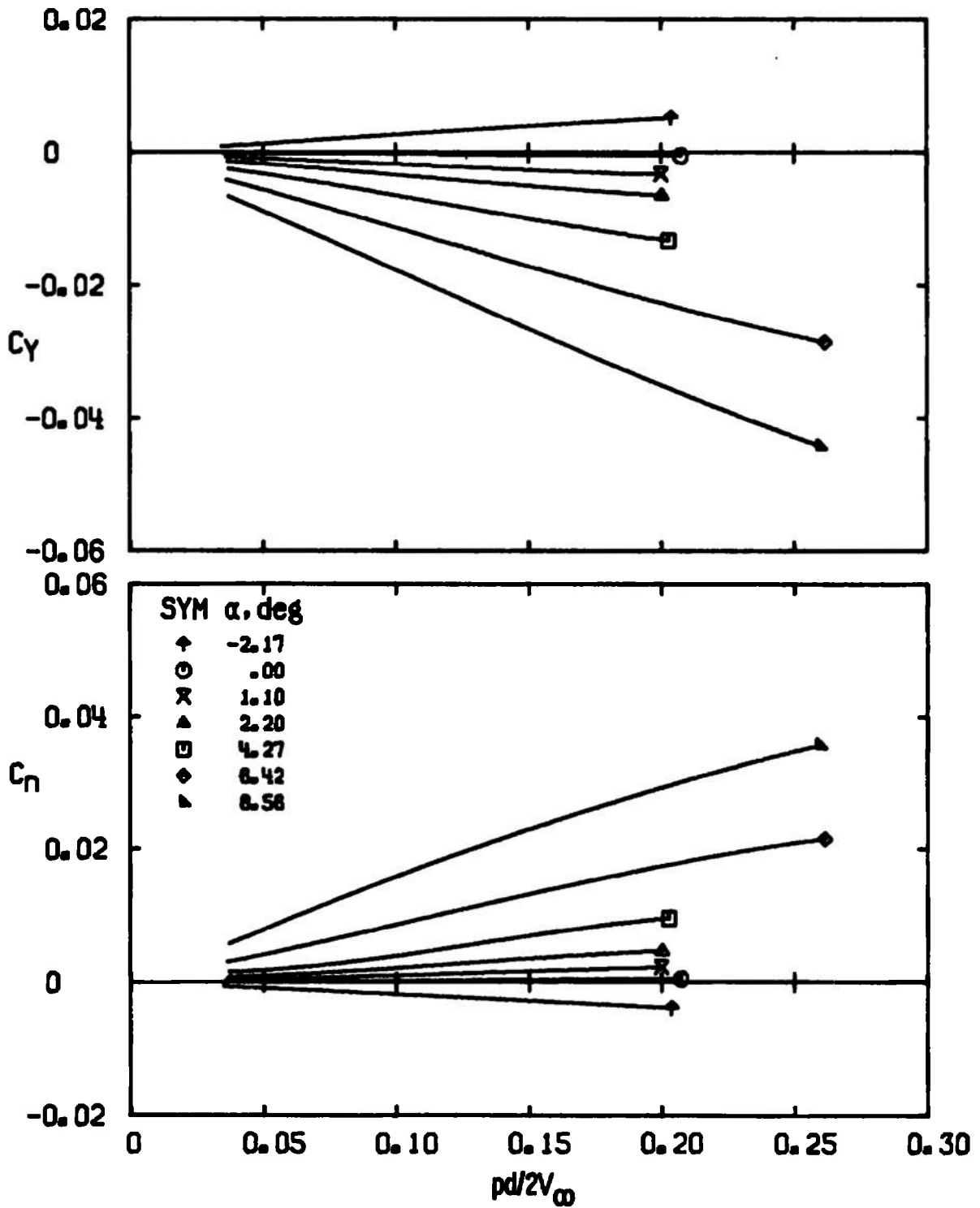
Figure 12. Variation of C_Y and C_n with $pd/2V_\infty$ for configuration 3, $Re_x = 9.6 \times 10^6$.



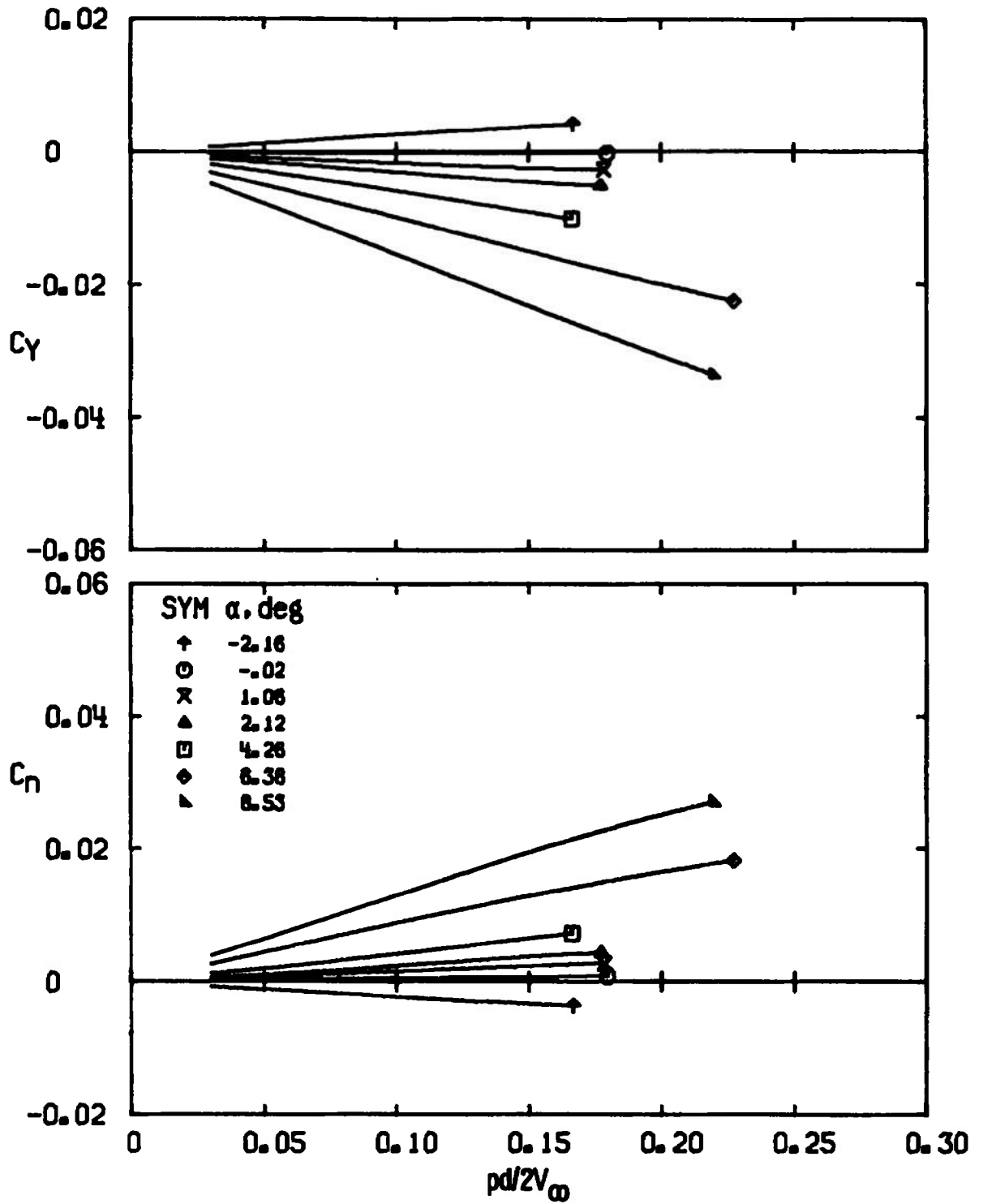
b. $M_\infty = 2.0$
 Figure 12. Continued.



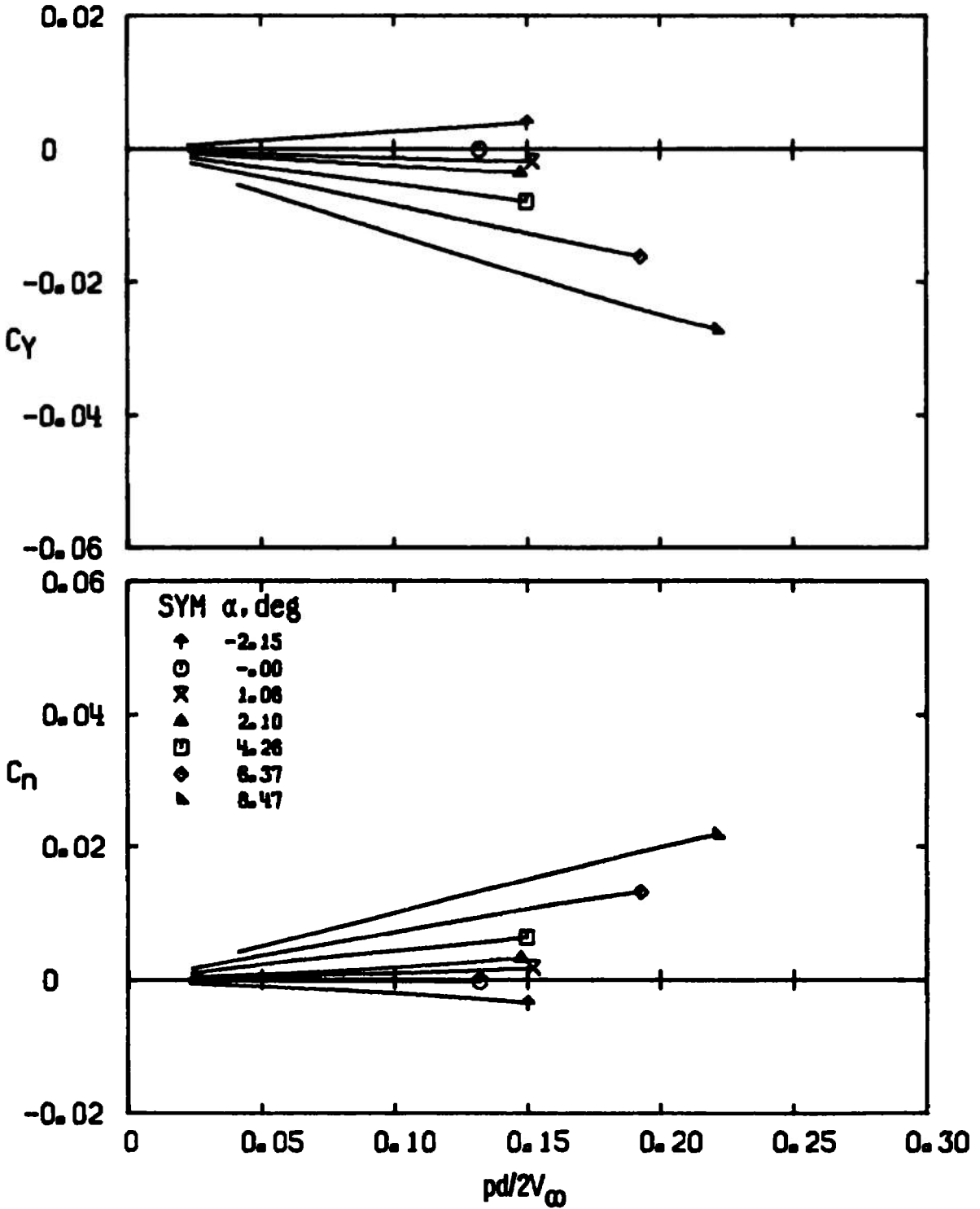
c. $M_\infty = 2.5$
 Figure 12. Concluded.



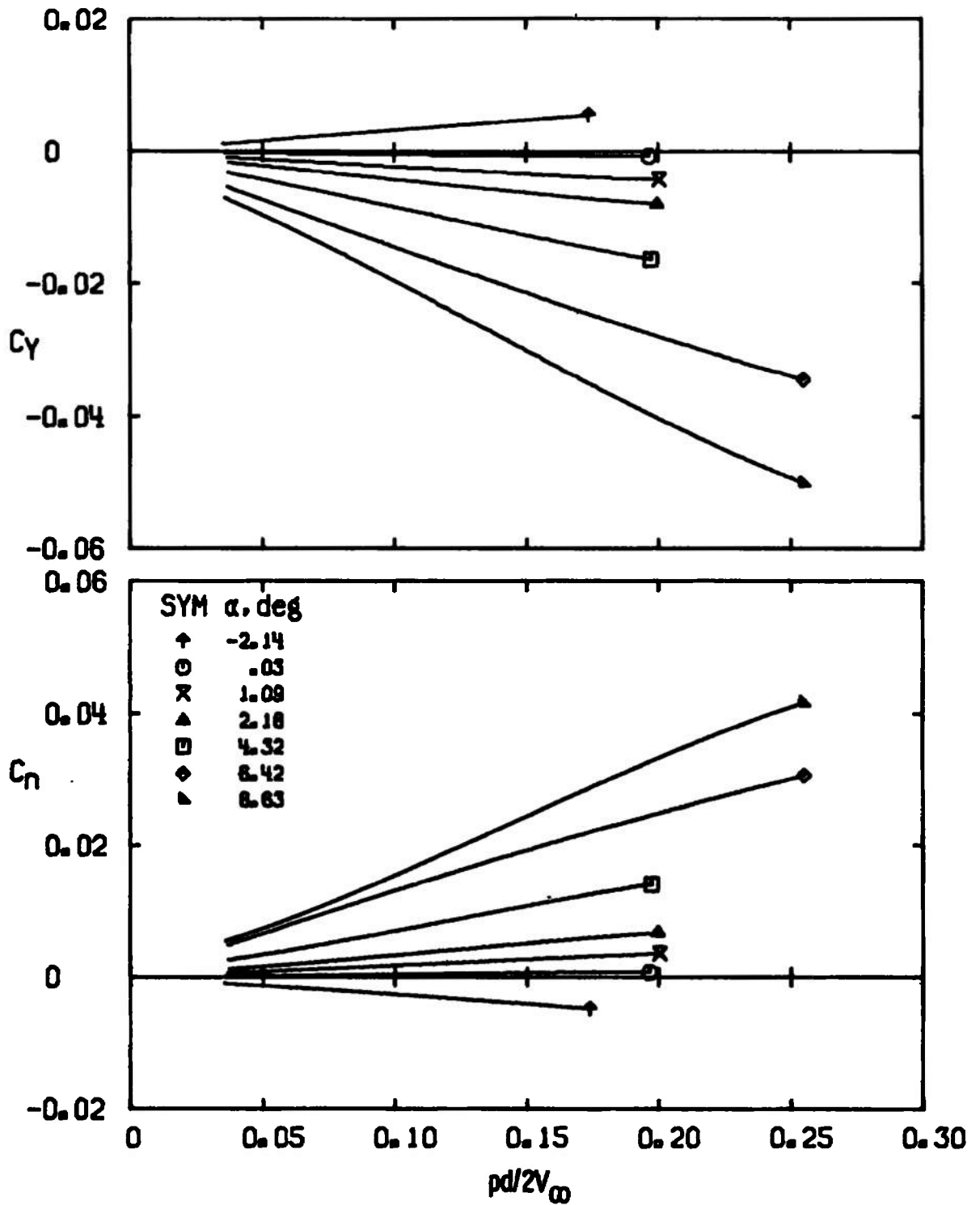
a. $M_\infty = 1.5$
 Figure 13. Variation of C_Y and C_n with $pd/2V_\infty$ for configuration 4,
 $Re_\lambda = 9.6 \times 10^6$.



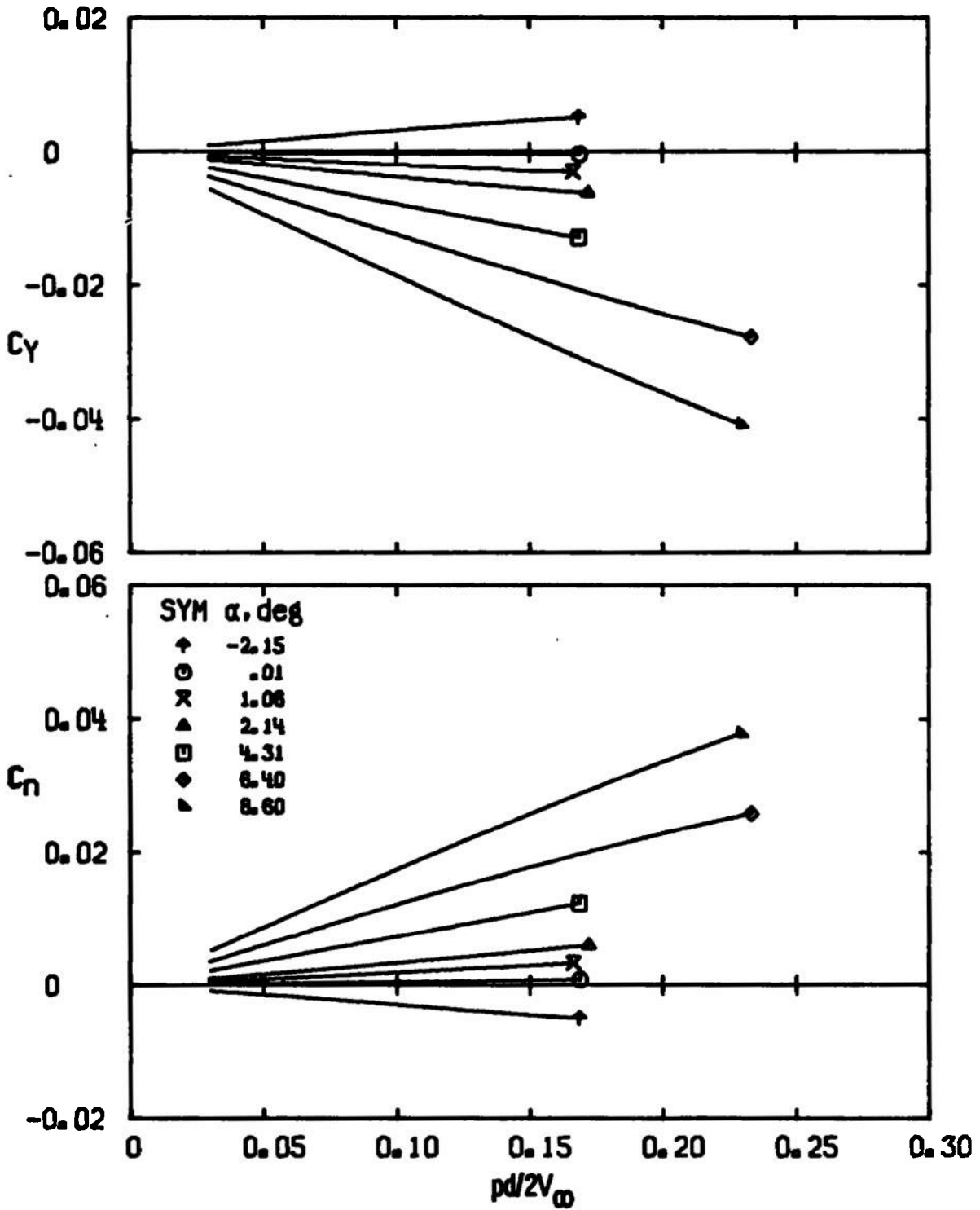
b. $M_{\infty} = 2.0$
 Figure 13. Continued.



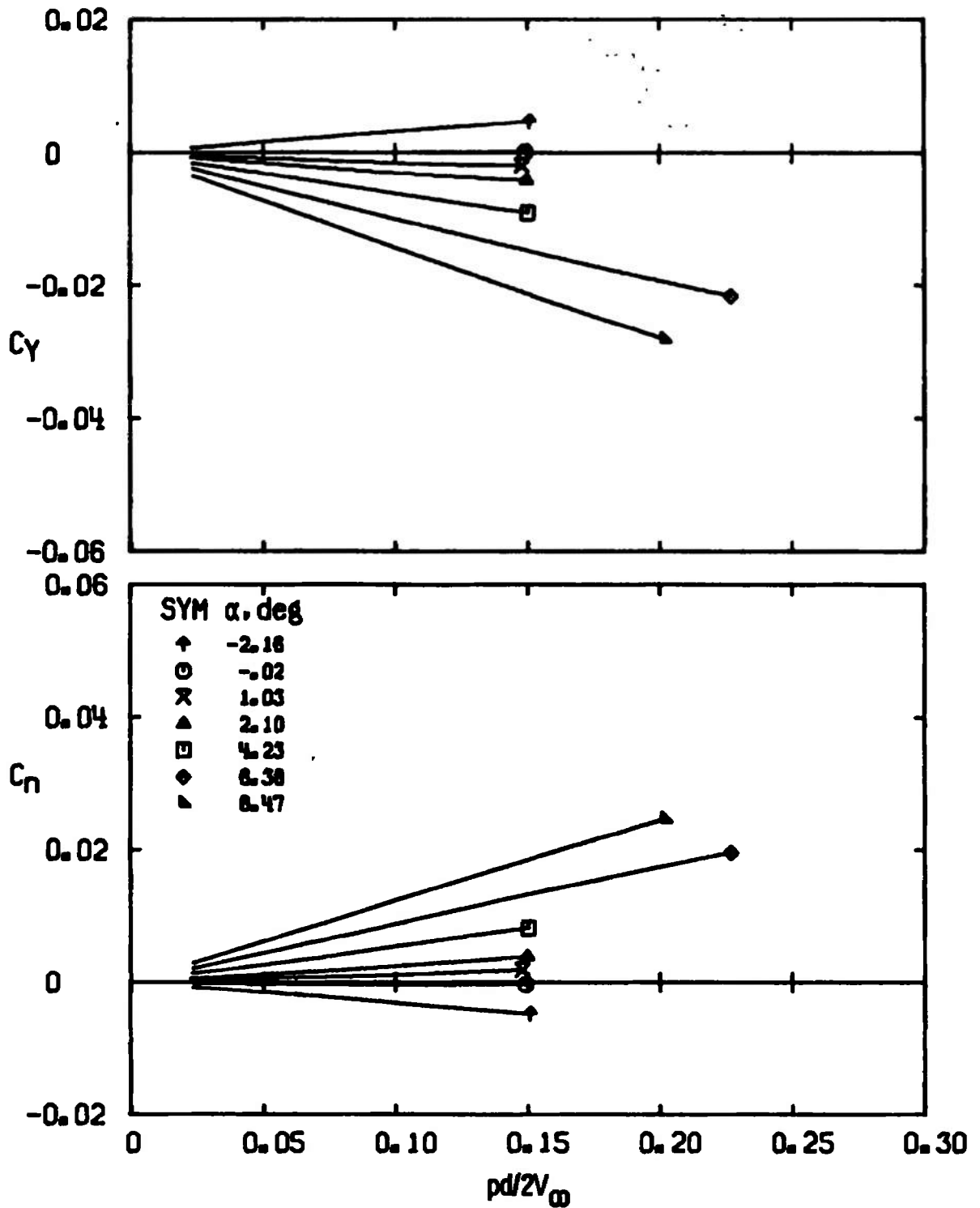
c. $M_\infty = 2.5$
 Figure 13. Concluded.



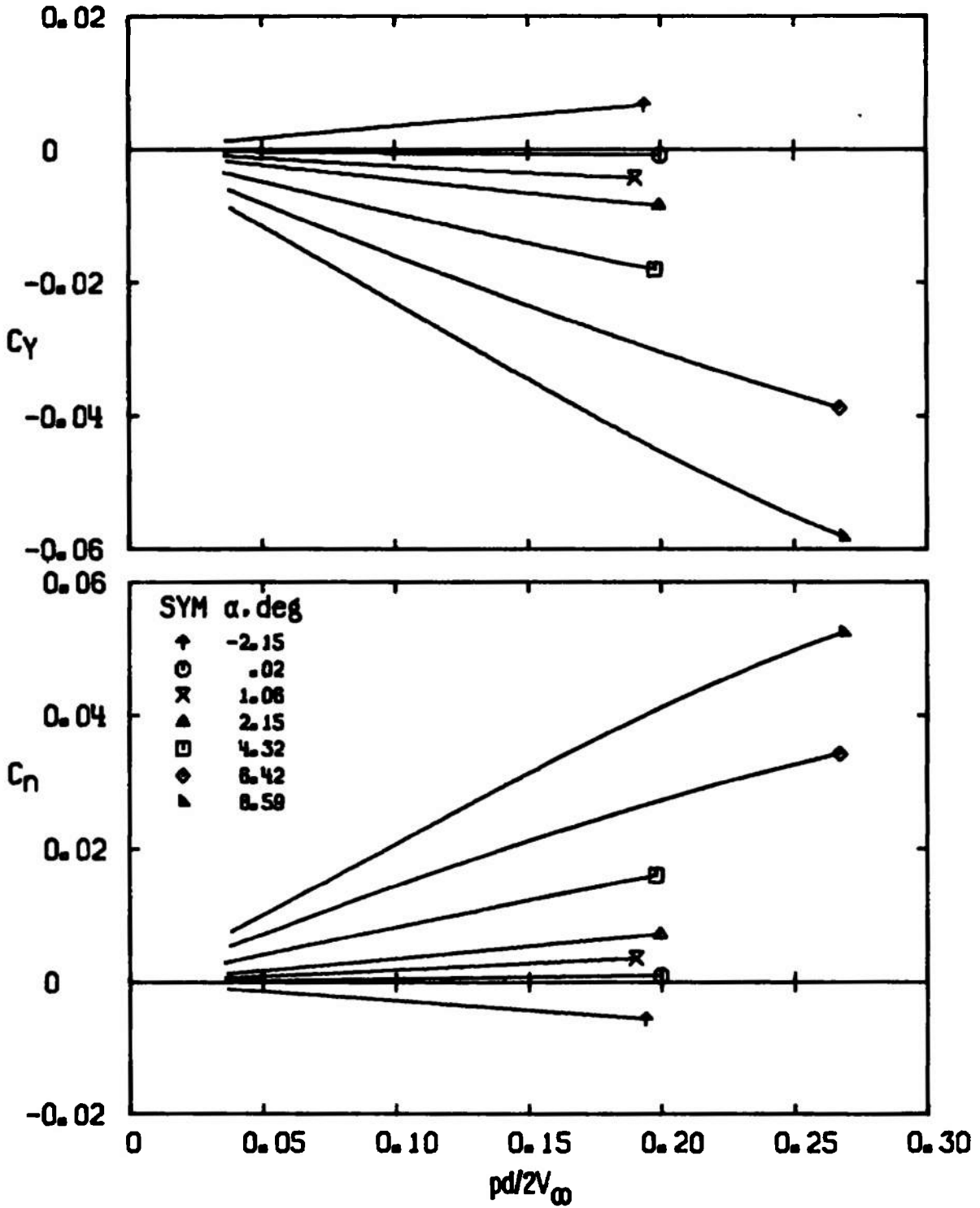
a. $M_\infty = 1.5$
 Figure 14. Variation of C_y and C_n with $pd/2V_\infty$ for configuration 5,
 $Re_\xi = 9.6 \times 10^6$.



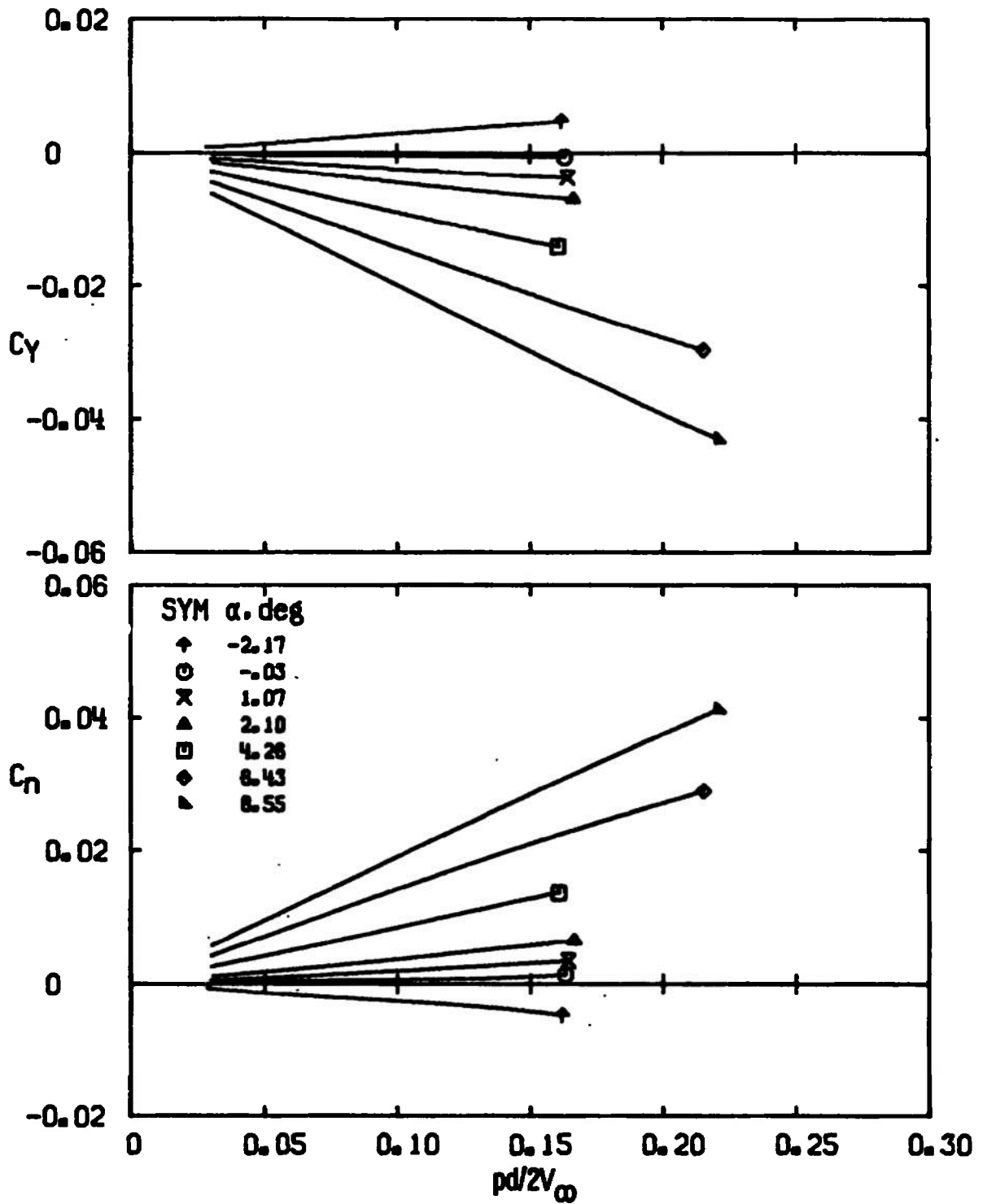
b. $M_\infty = 2.0$
 Figure 14. Continued.



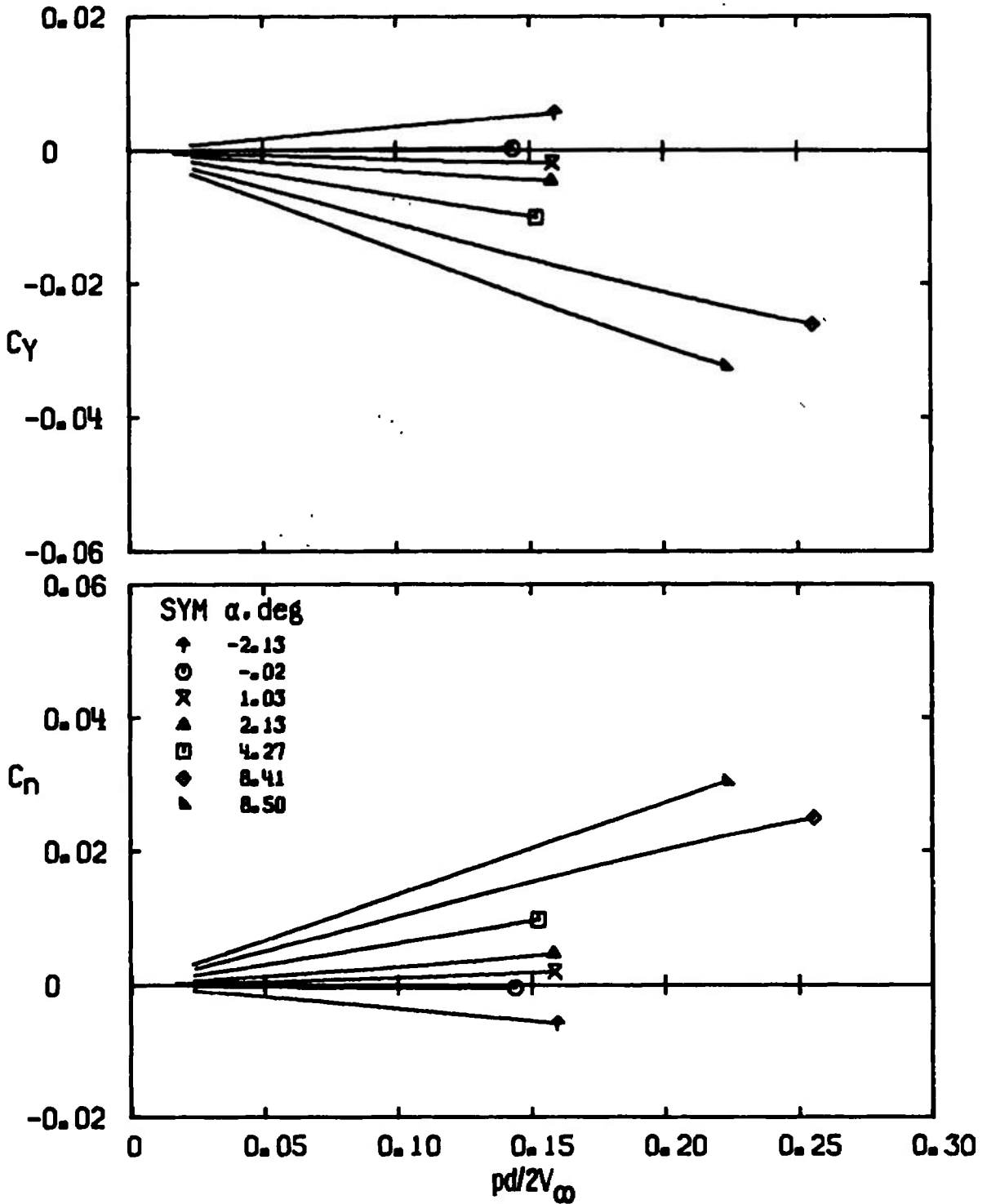
c. $M_{\infty} = 2.5$
 Figure 14. Concluded.



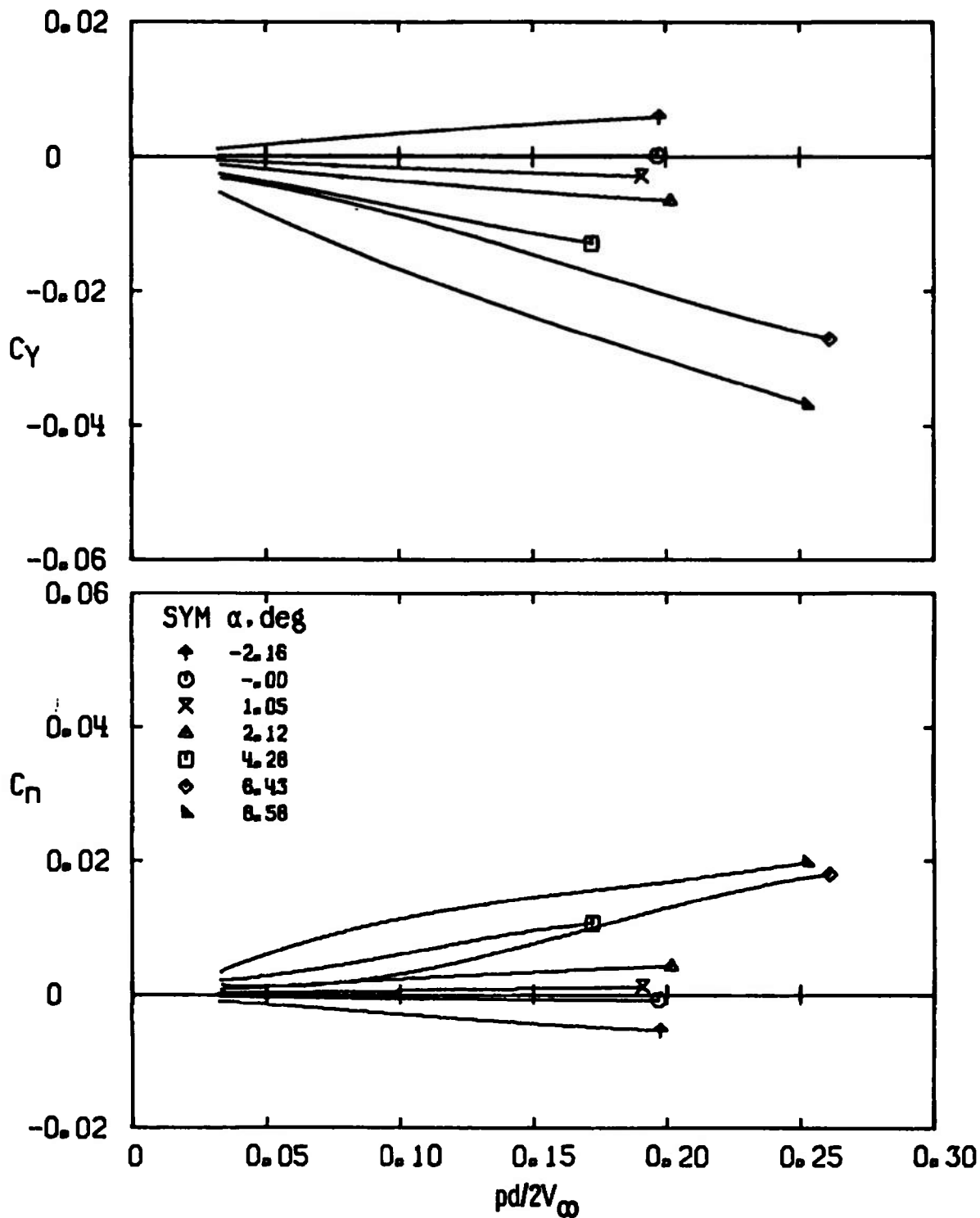
a. $M_\infty = 1.5$
 Figure 15. Variation of C_Y and C_n with $pd/2V_\infty$ for configuration 6,
 $Re_\rho = 9.6 \times 10^6$.



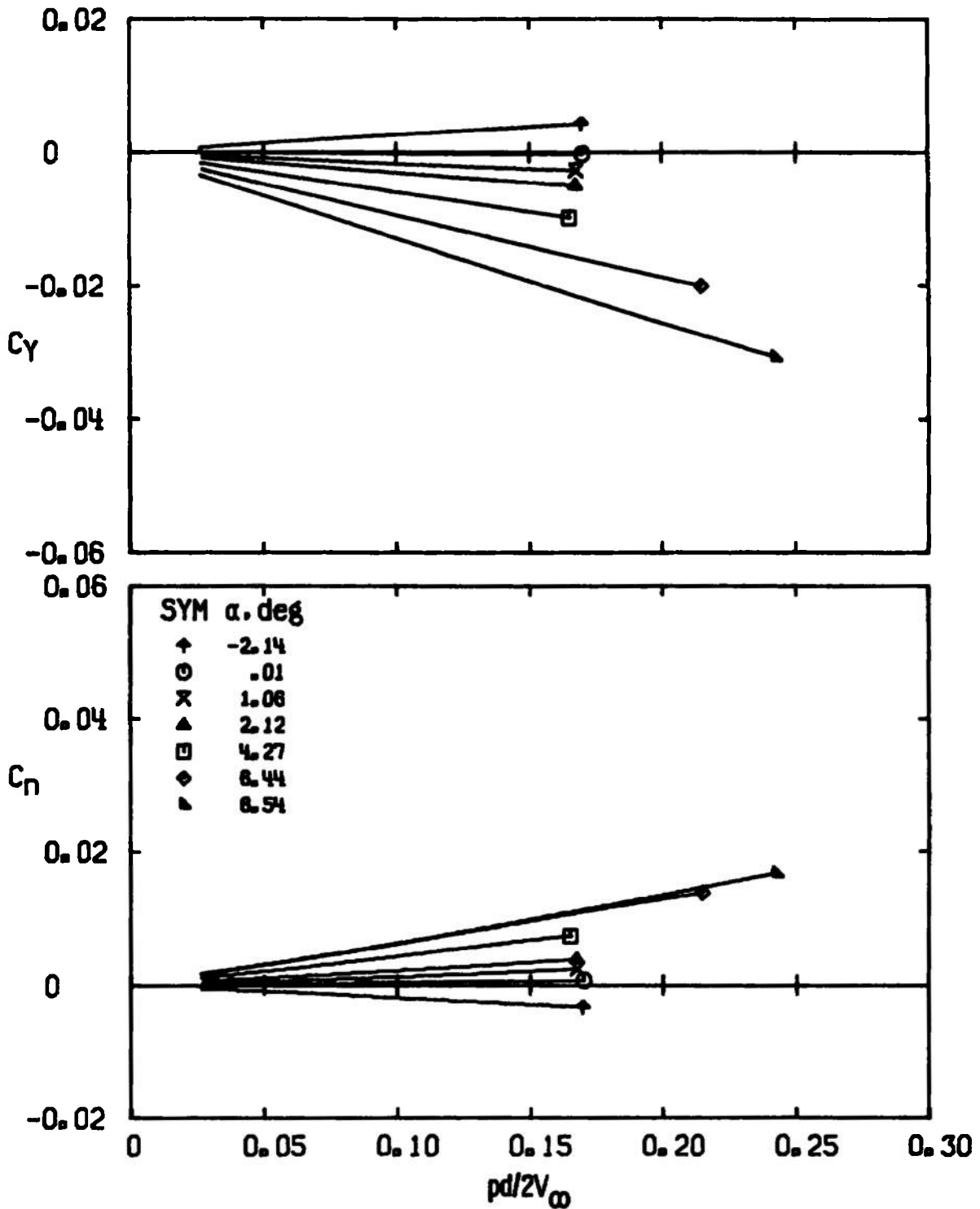
b. $M_{\infty} = 2.0$
 Figure 15. Continued.



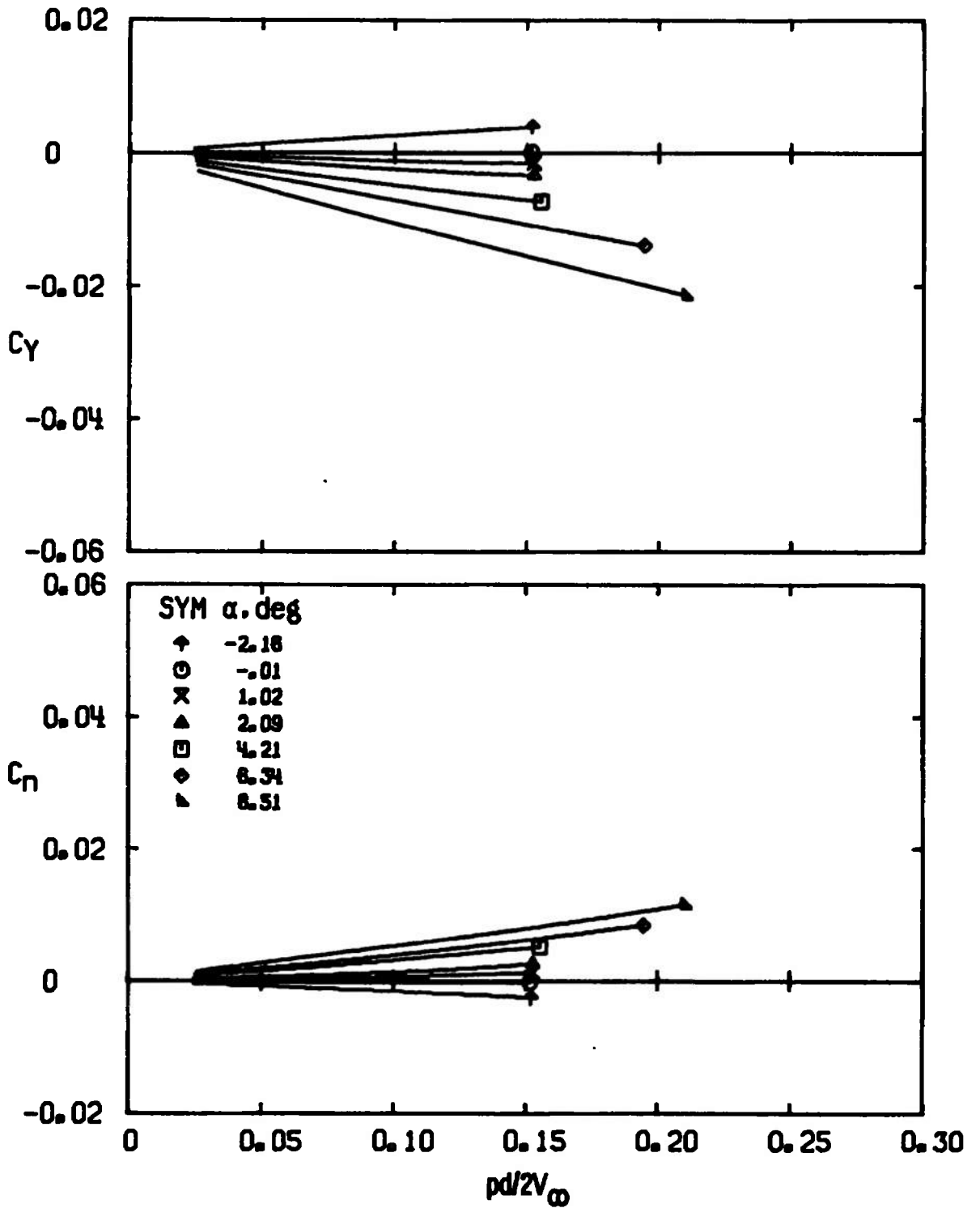
c. $M_\infty = 2.5$
 Figure 15. Concluded.



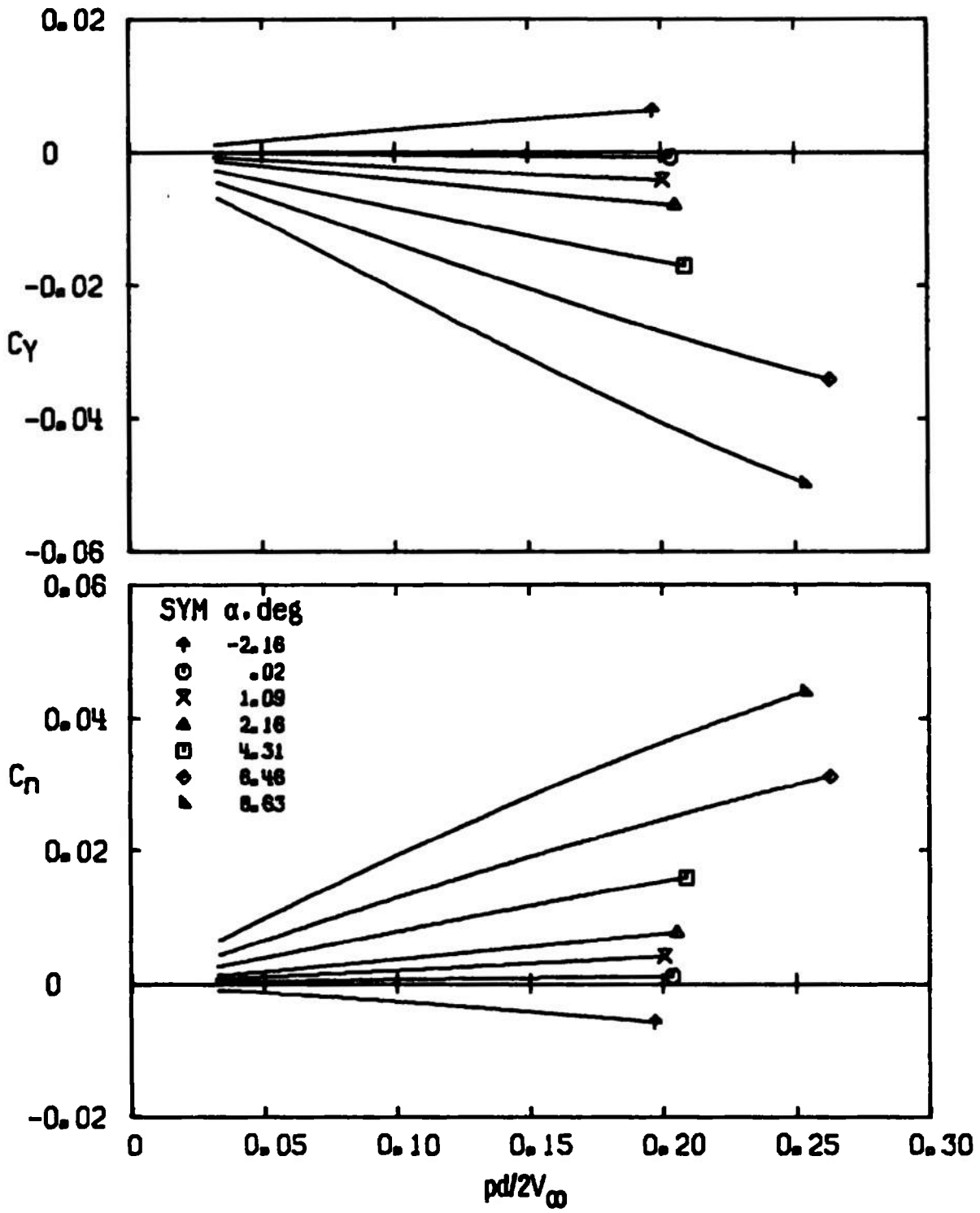
a. $M_\infty = 1.5$
 Figure 16. Variation of C_Y and C_n with $pd/2V_\infty$ for configuration 7, $Re_\rho = 9.6 \times 10^6$.



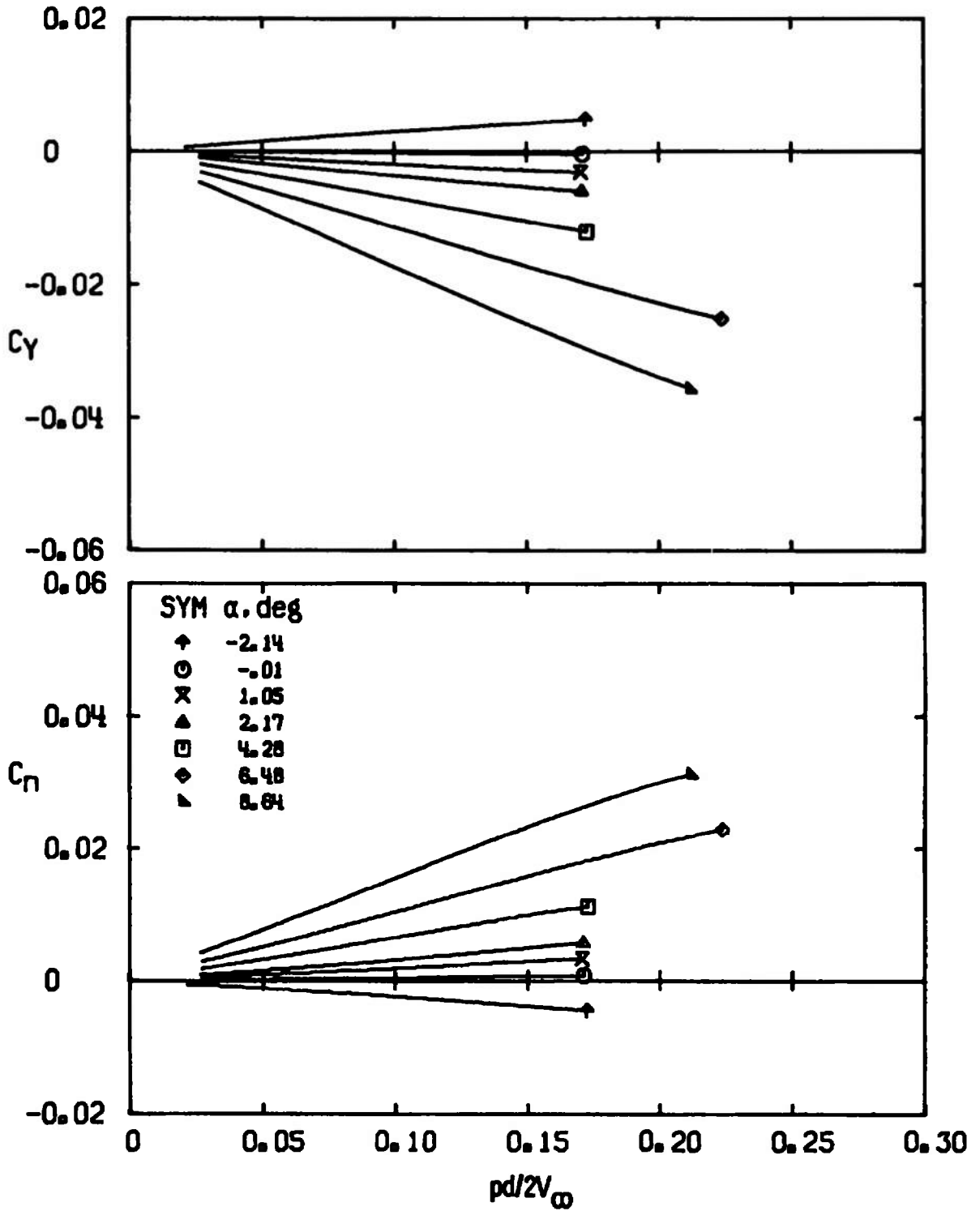
b. $M_{\infty} = 2.0$
 Figure 16. Continued.



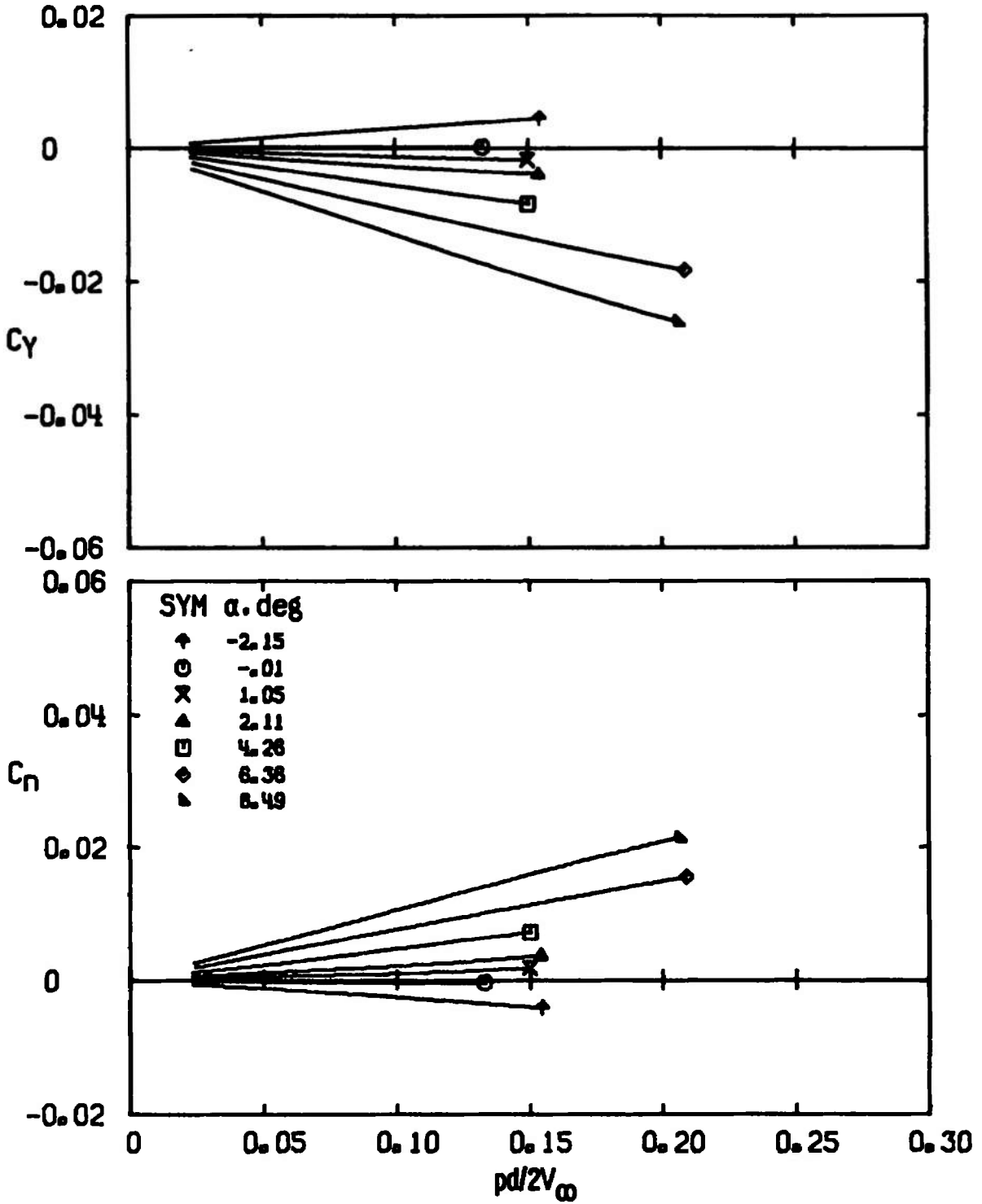
c. $M_{\infty} = 2.5$
 Figure 16. Concluded.



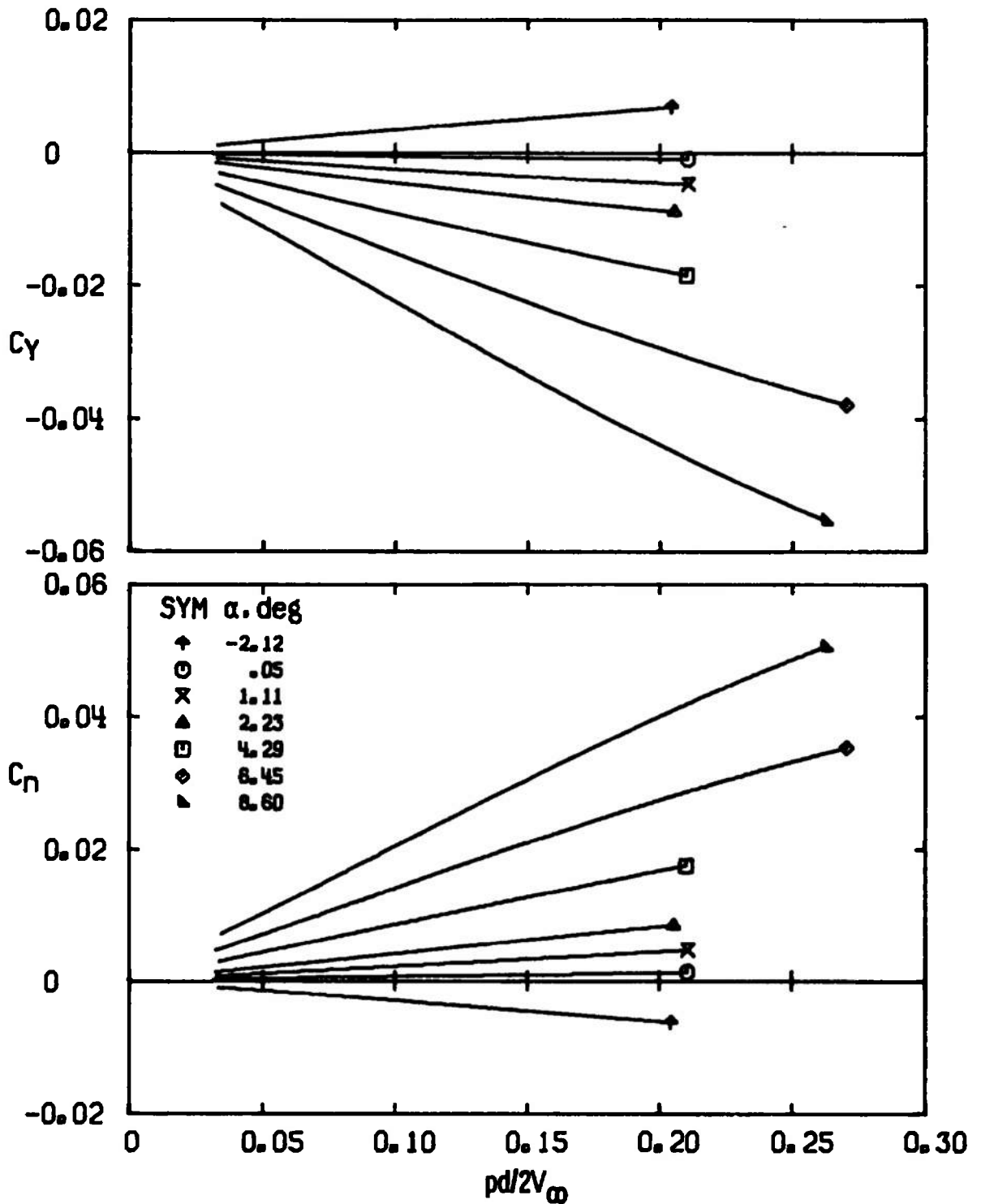
a. $M_\infty = 1.5$
 Figure 17. Variation of C_y and C_n with $pd/2V_\infty$ for configuration 8, $Re_\rho = 9.6 \times 10^6$.



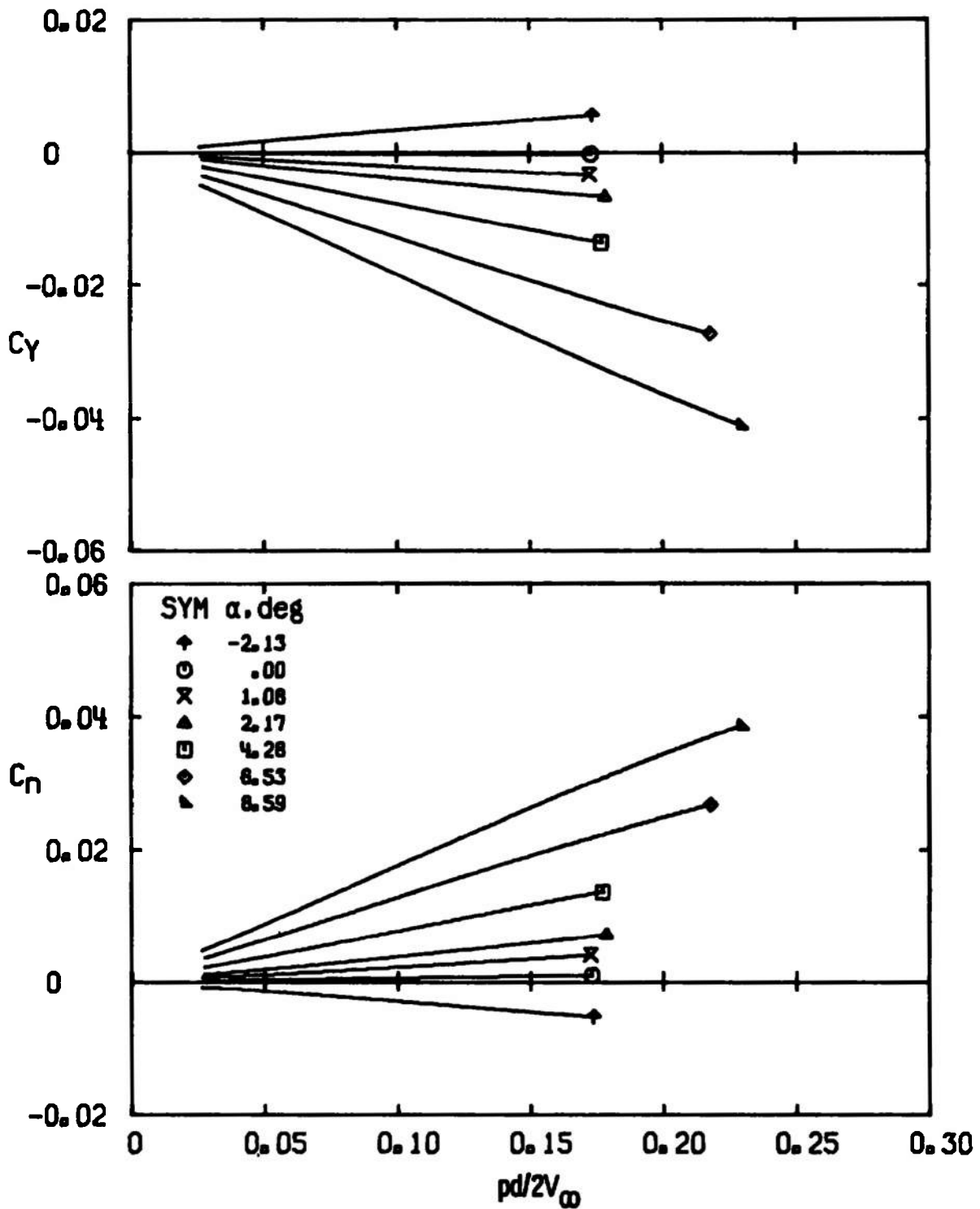
b. $M_\infty = 2.0$
 Figure 17. Continued.



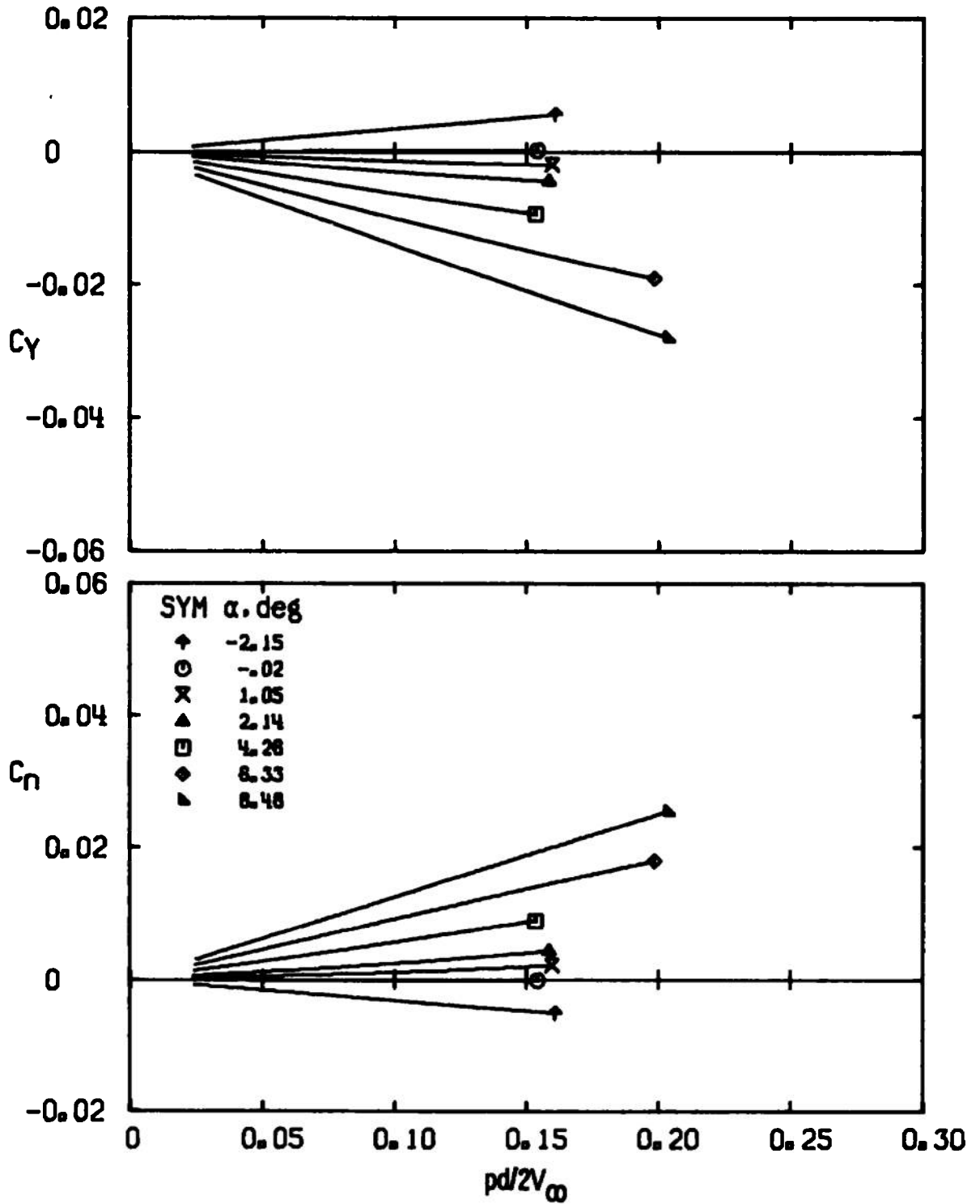
c. $M_\infty = 2.5$
 Figure 17. Concluded.



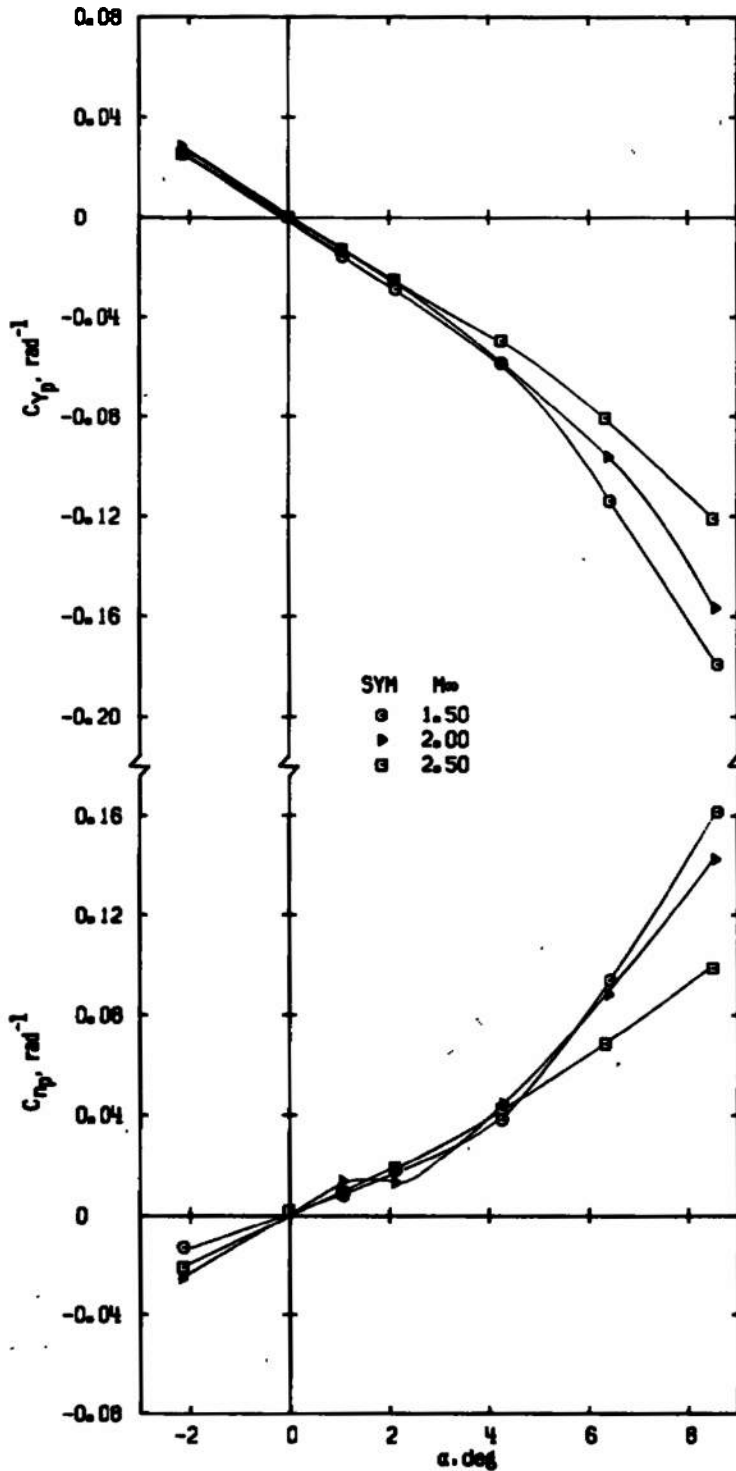
a. $M_\infty = 1.5$
 Figure 18. Variation of C_Y and C_n with $pd/2V_\infty$ for configuration 9,
 $Re_\rho = 9.6 \times 10^6$.



b. $M_\infty = 2.0$
 Figure 18. Continued.

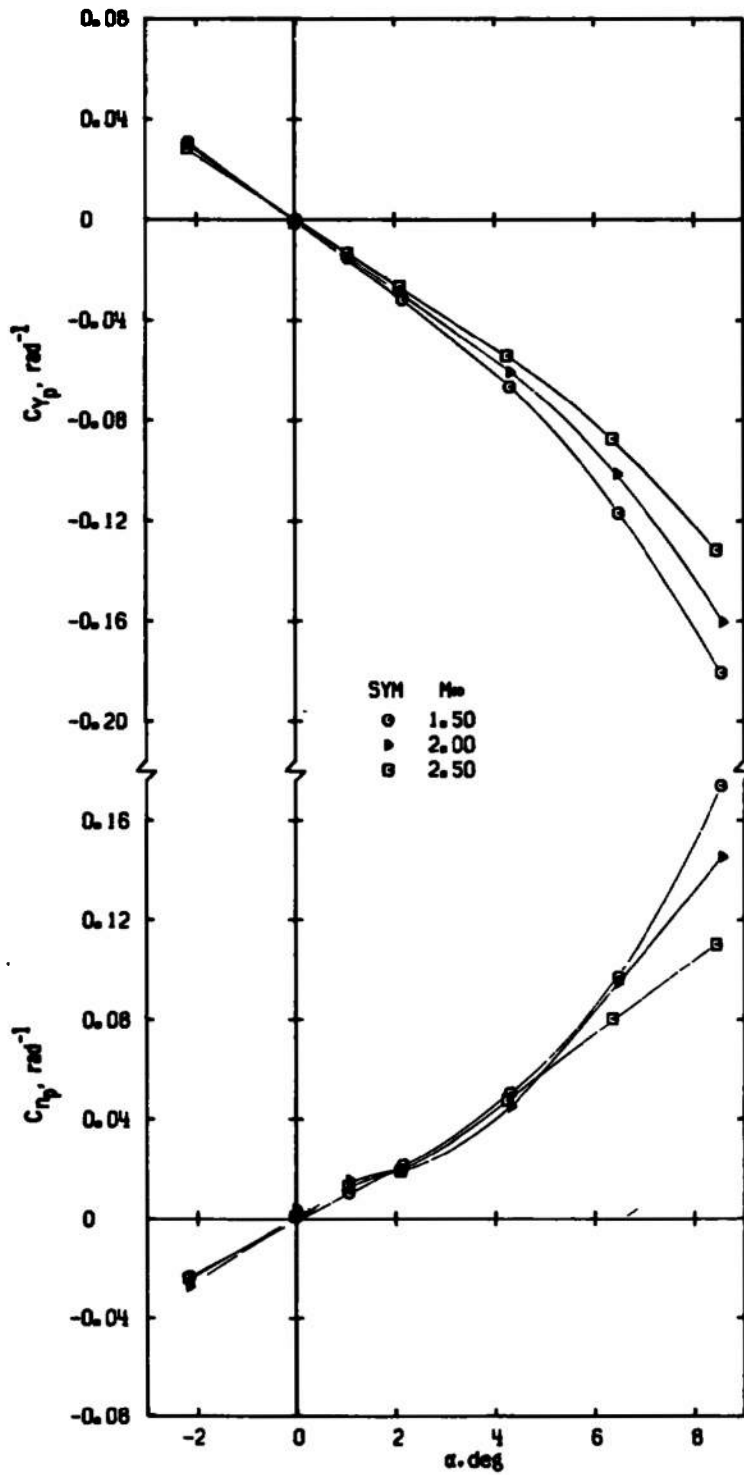


c. $M_\infty = 2.5$
 Figure 18. Concluded.

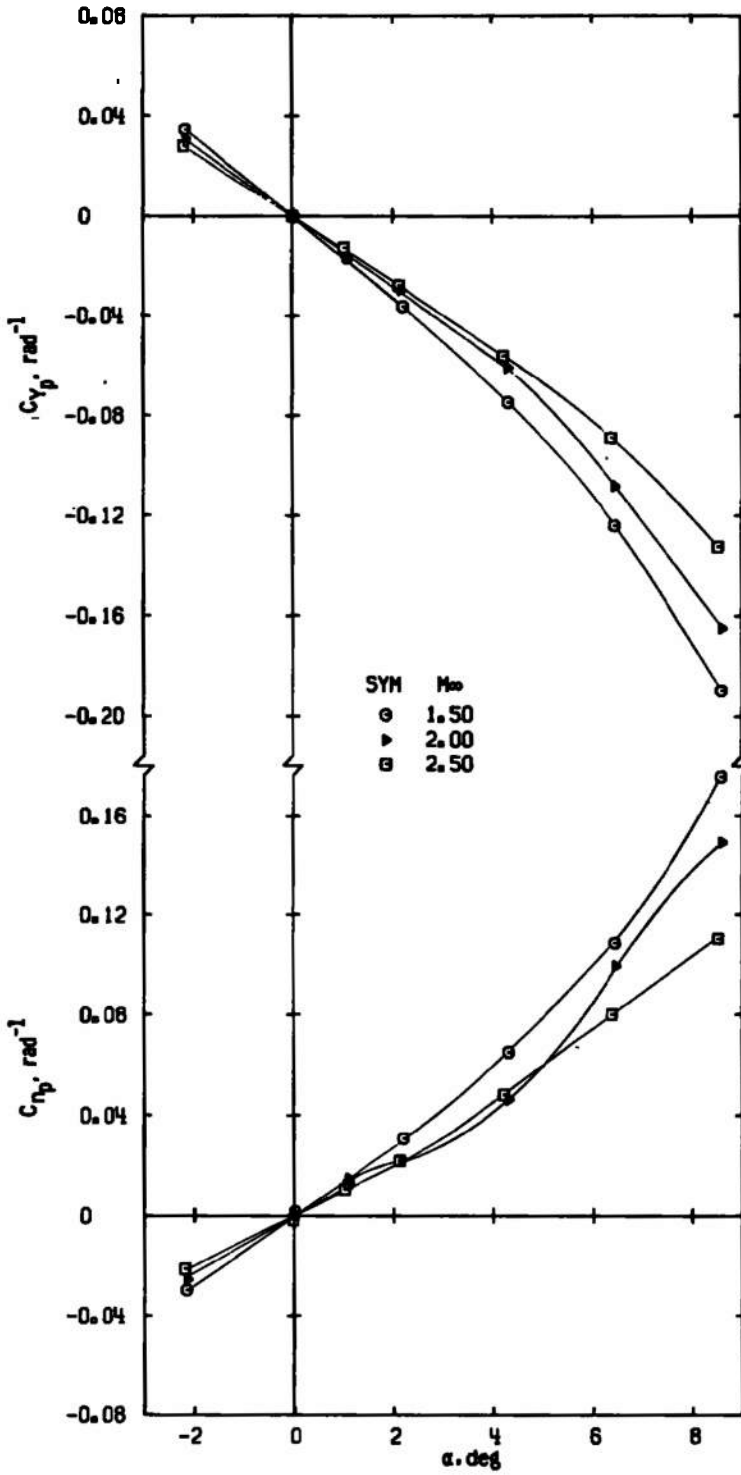


a. Configuration 0

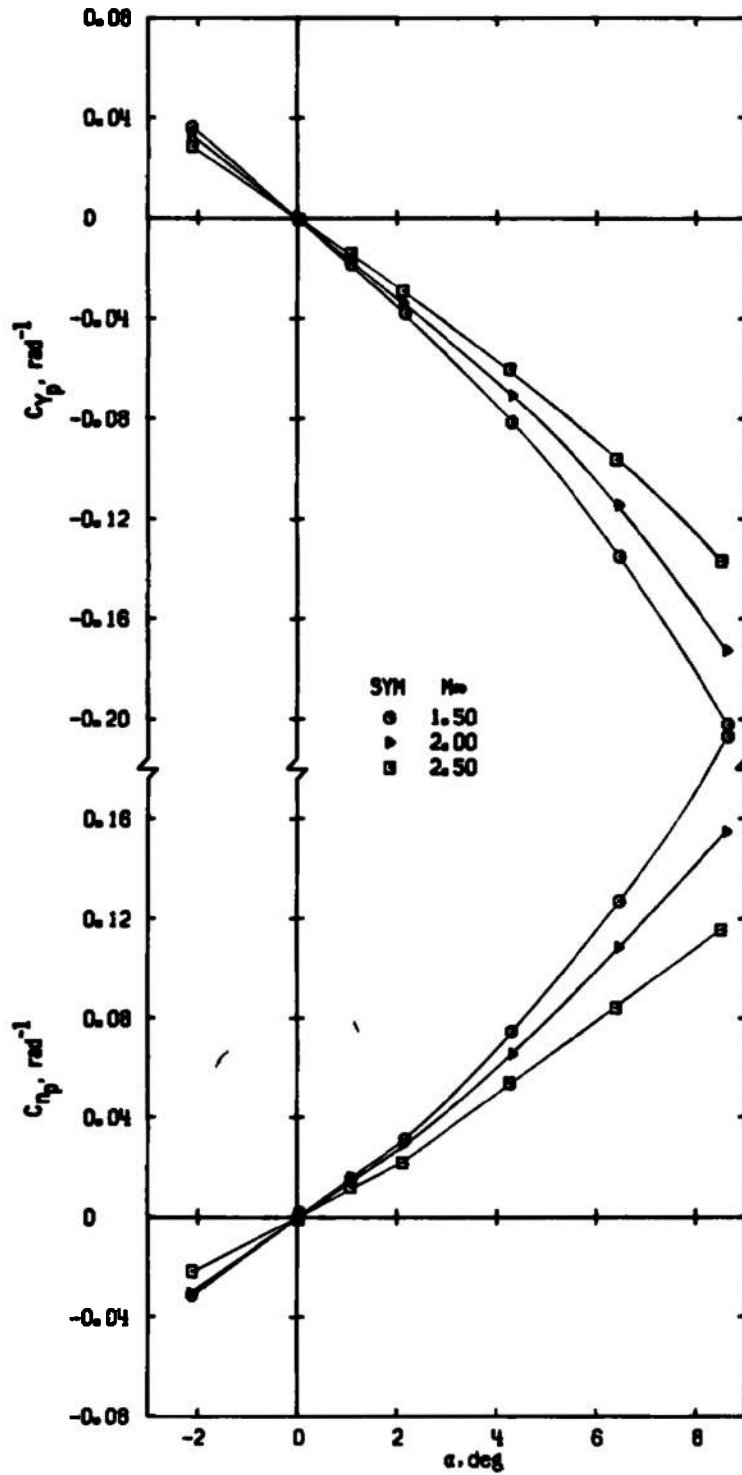
Figure 19. Variation of C_{Y_p} and C_{N_p} with angle of attack, $Re = 9.6 \times 10^6$.



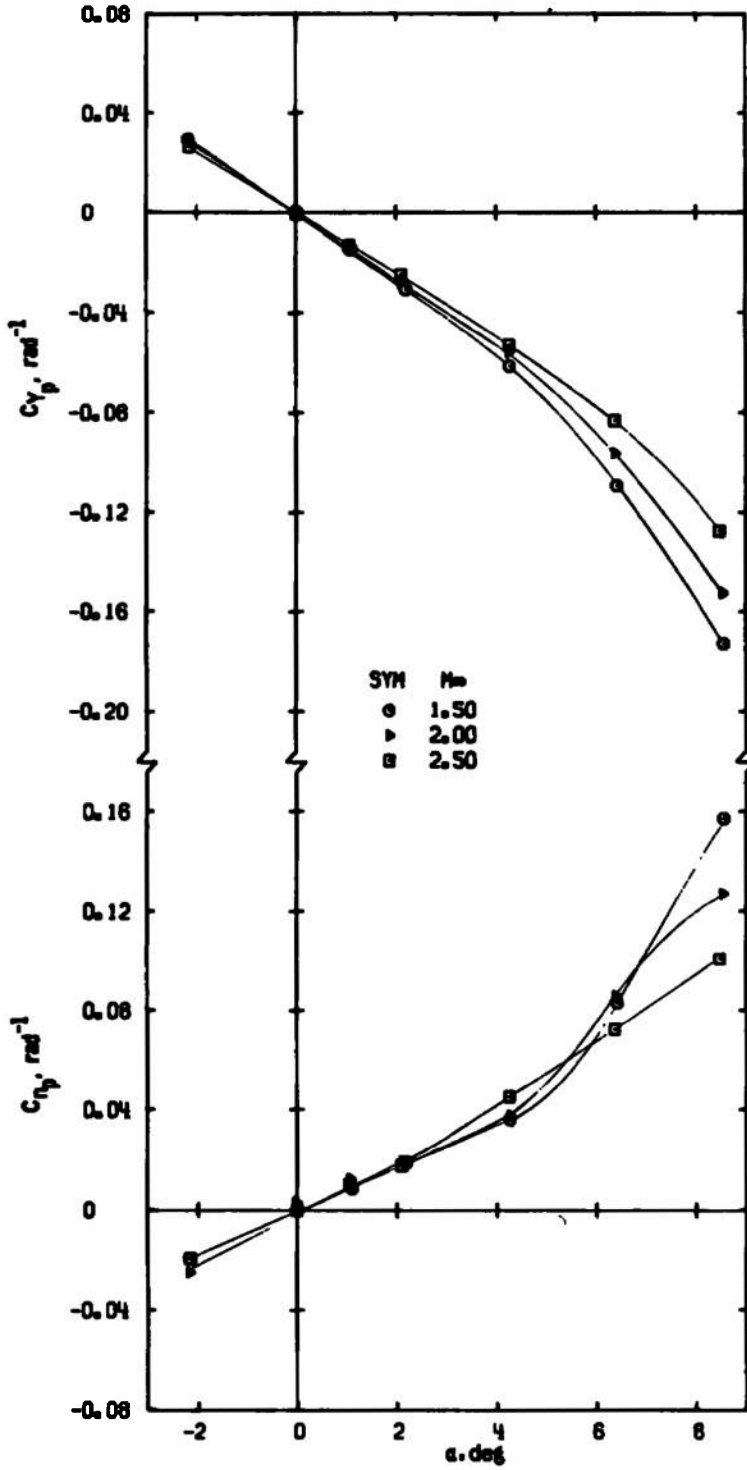
b. Configuration 1
Figure 19. Continued.



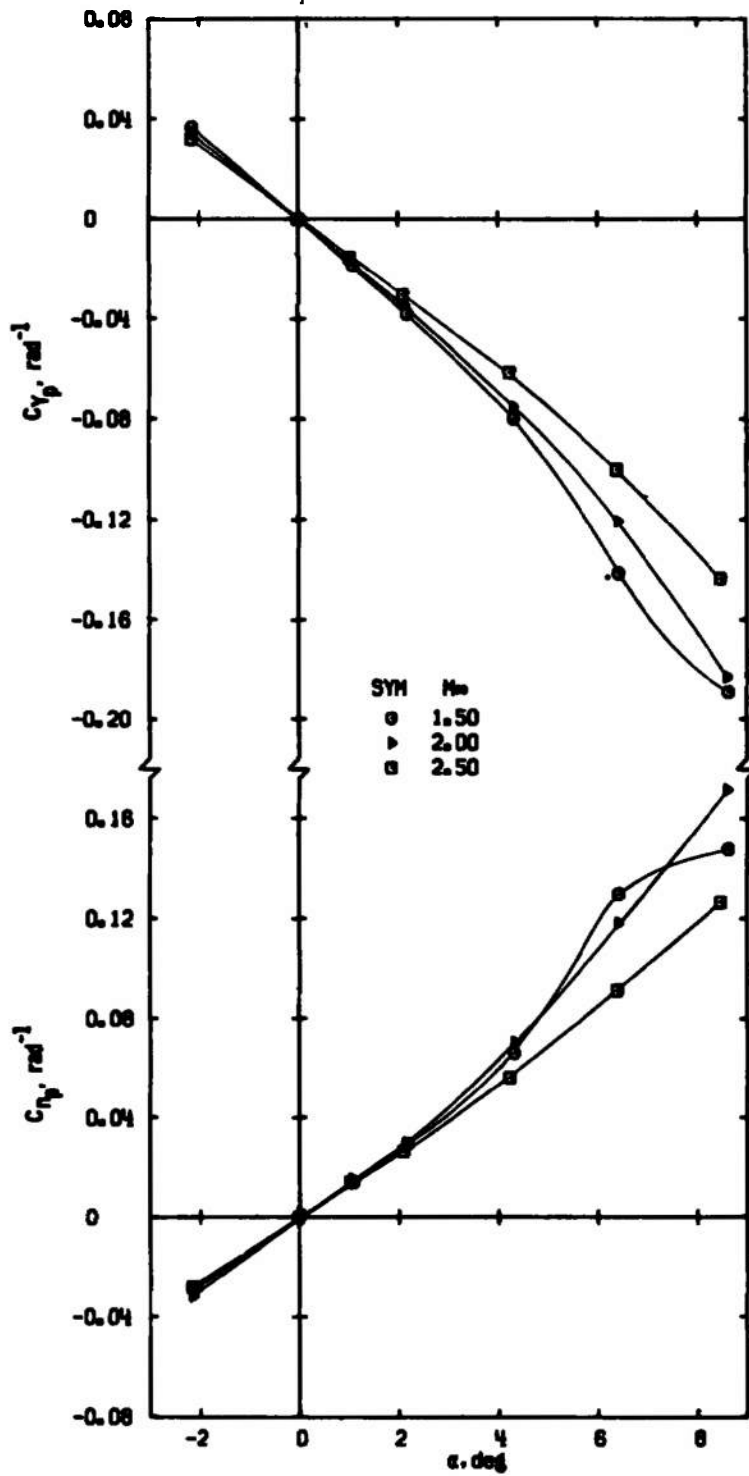
c. Configuration 2
Figure 19. Continued.



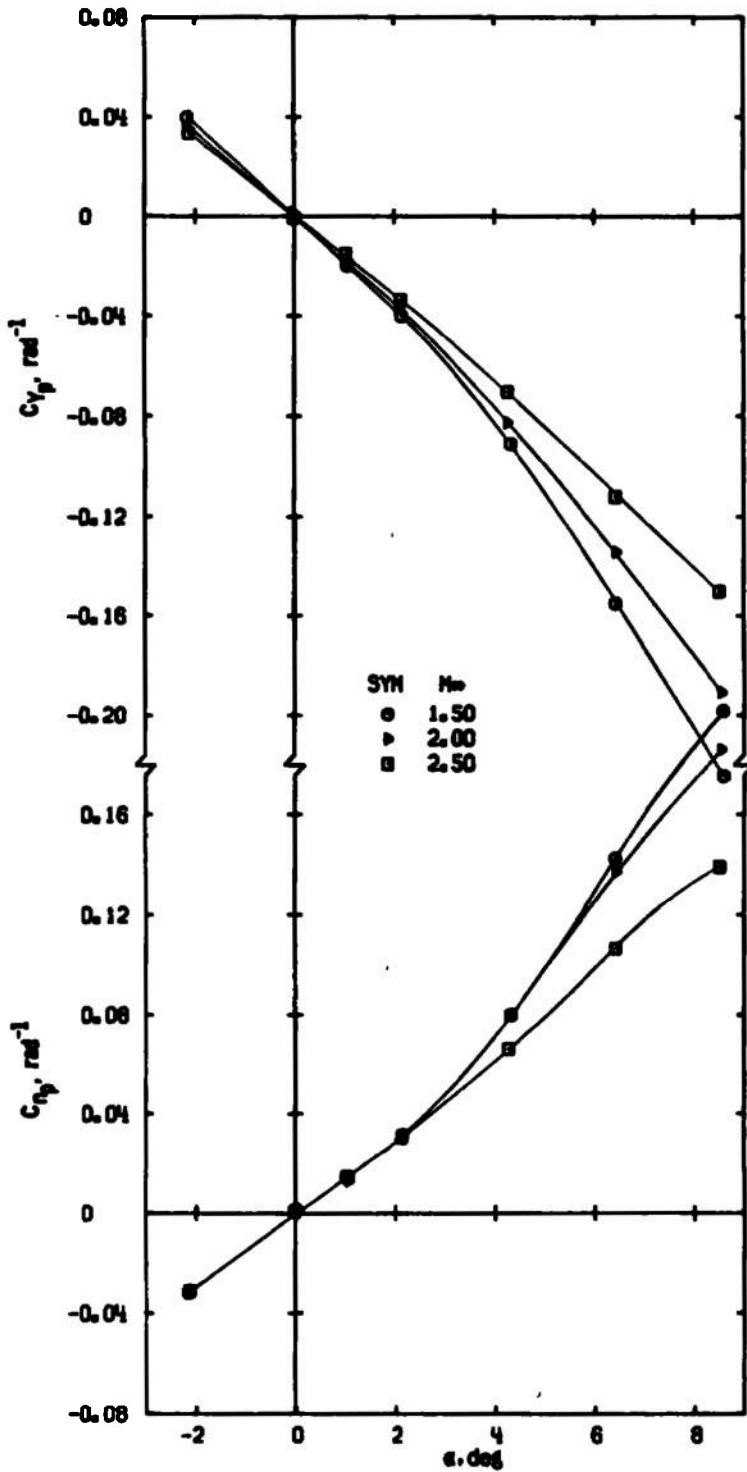
d. Configuration 3
Figure 19. Continued.



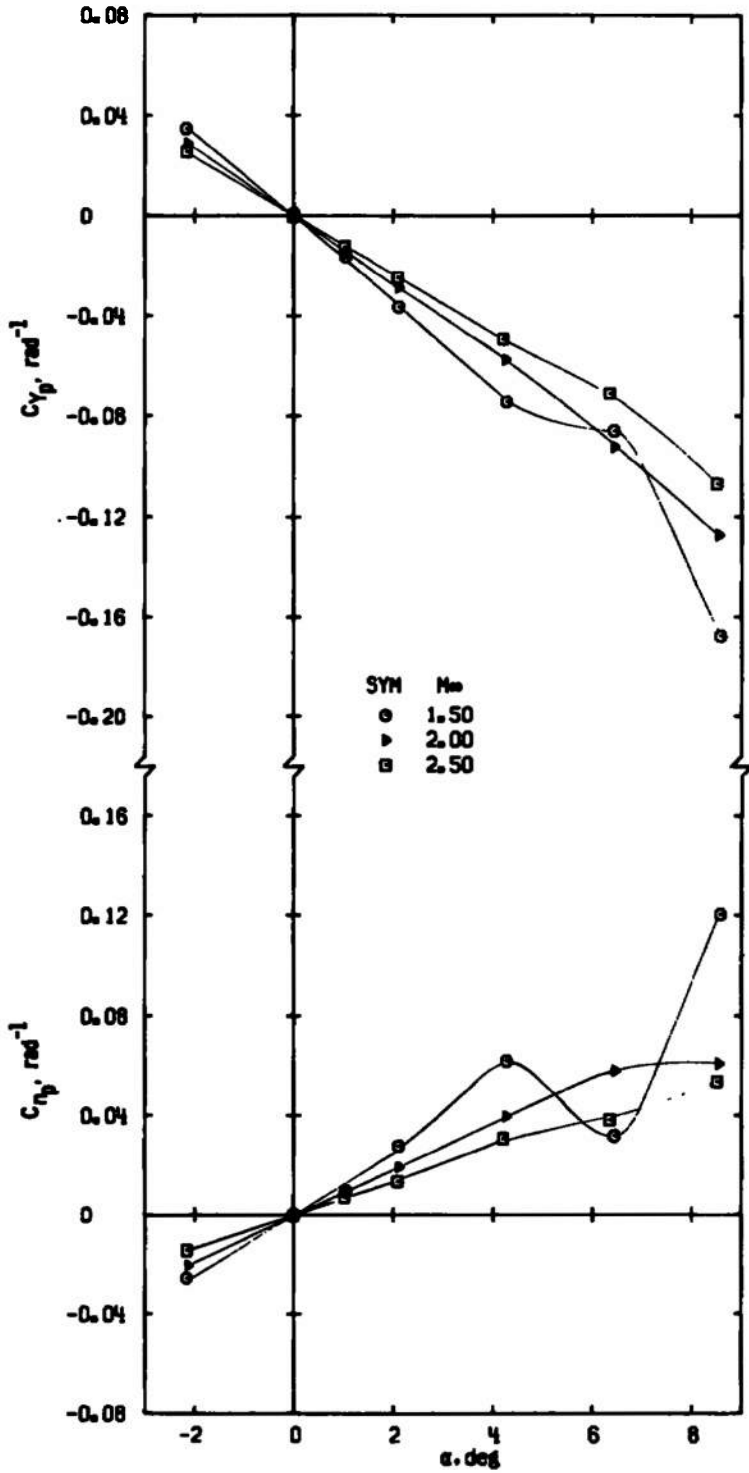
e. Configuration 4
Figure 19. Continued.



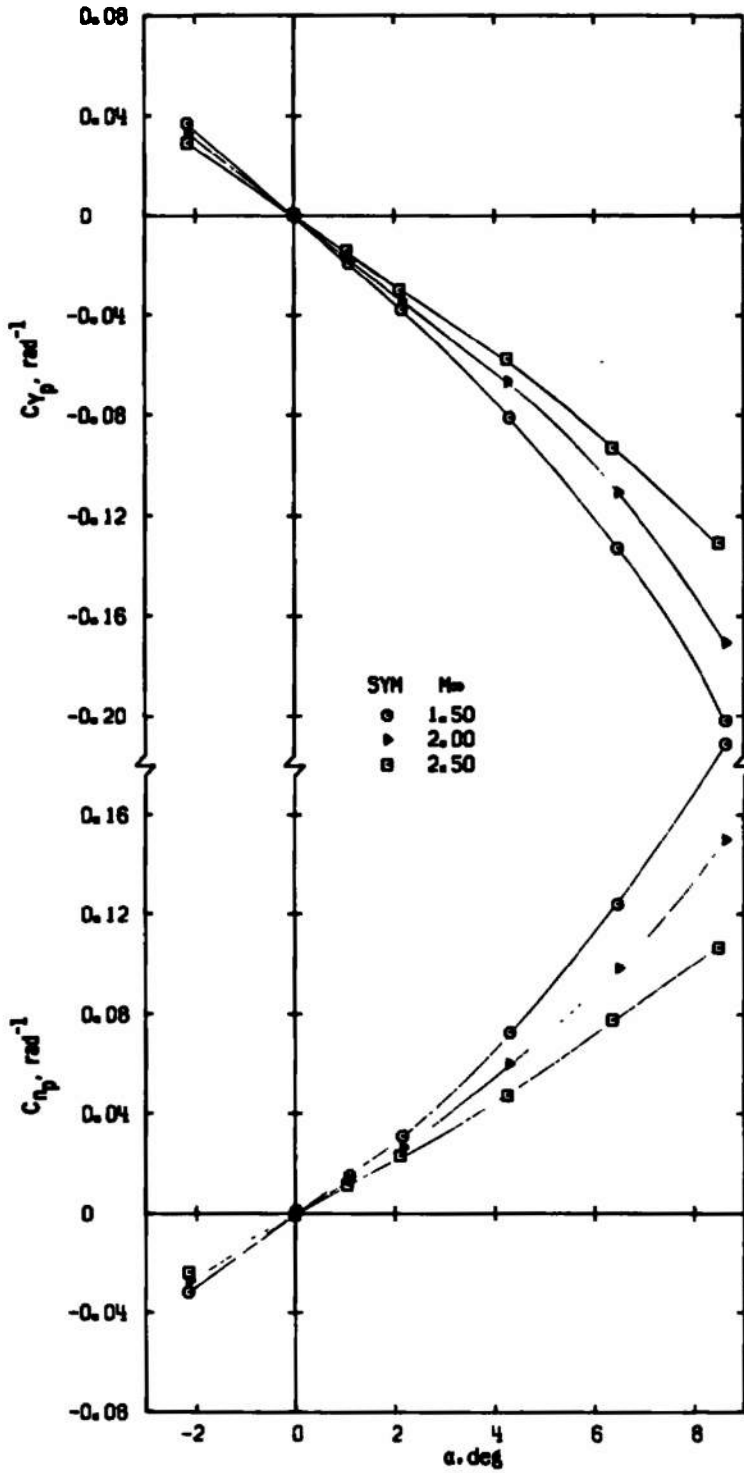
f. Configuration 5
Figure 19. Continued.



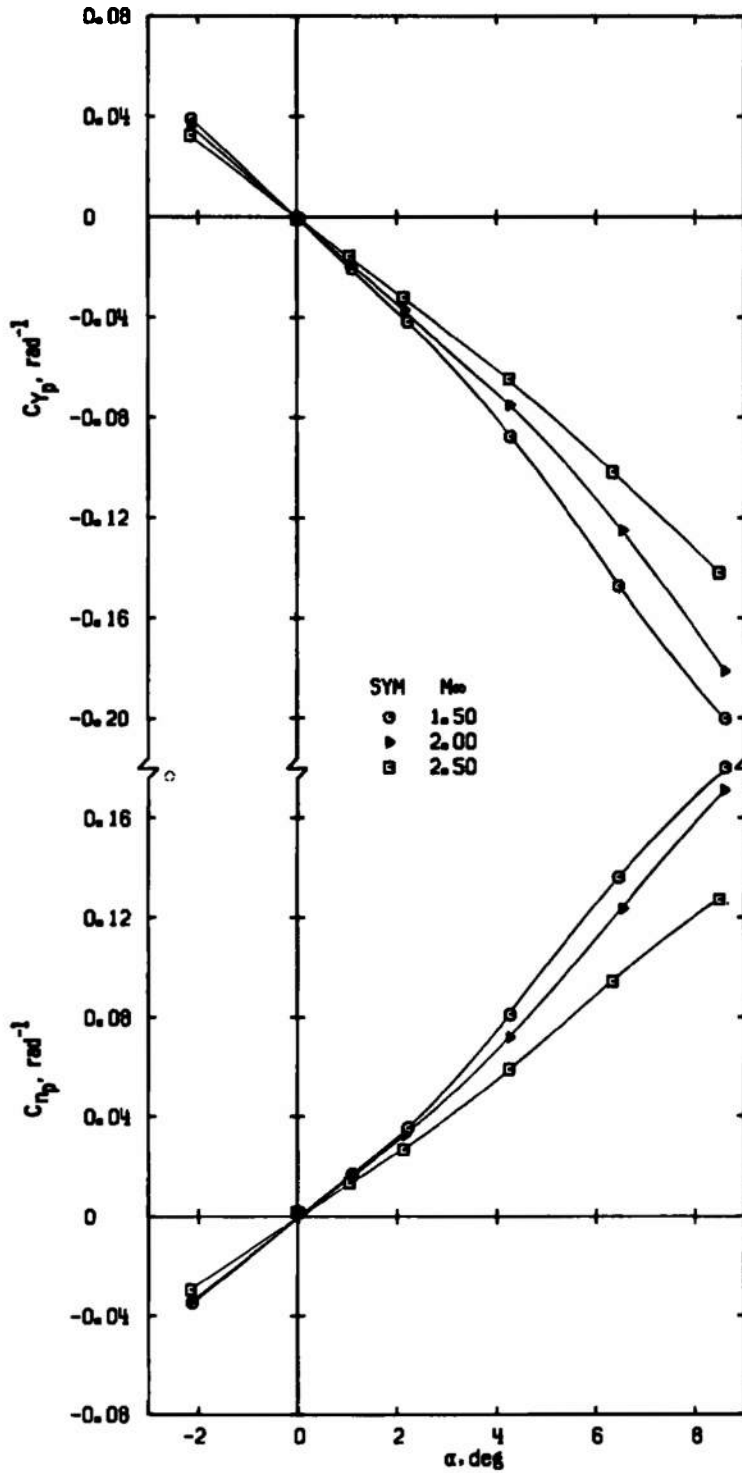
g. Configuration 6
Figure 19. Continued.



h. Configuration 7
Figure 19. Continued.



i. Configuration 8
Figure 19. Continued.



j. Configuration 9
Figure 19. Concluded.

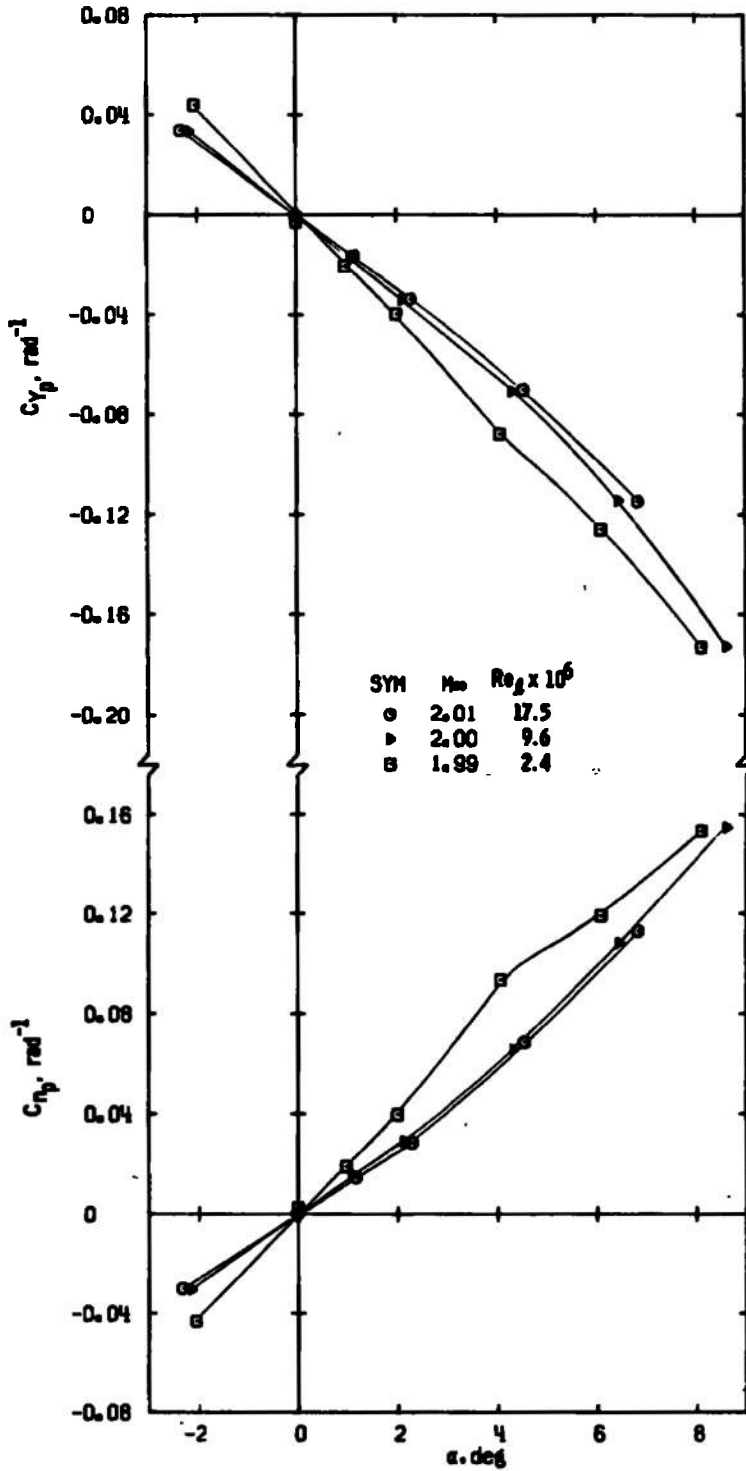
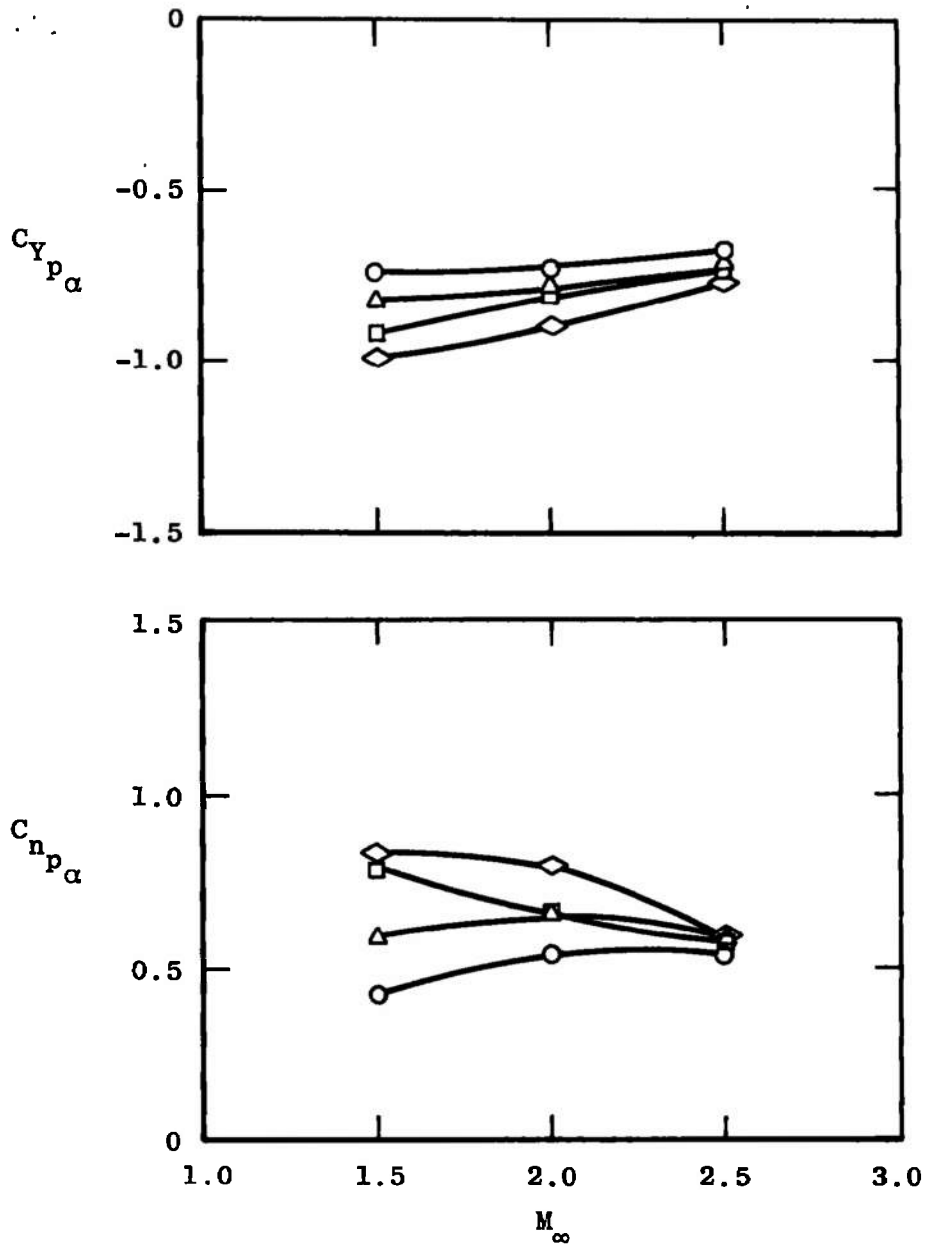


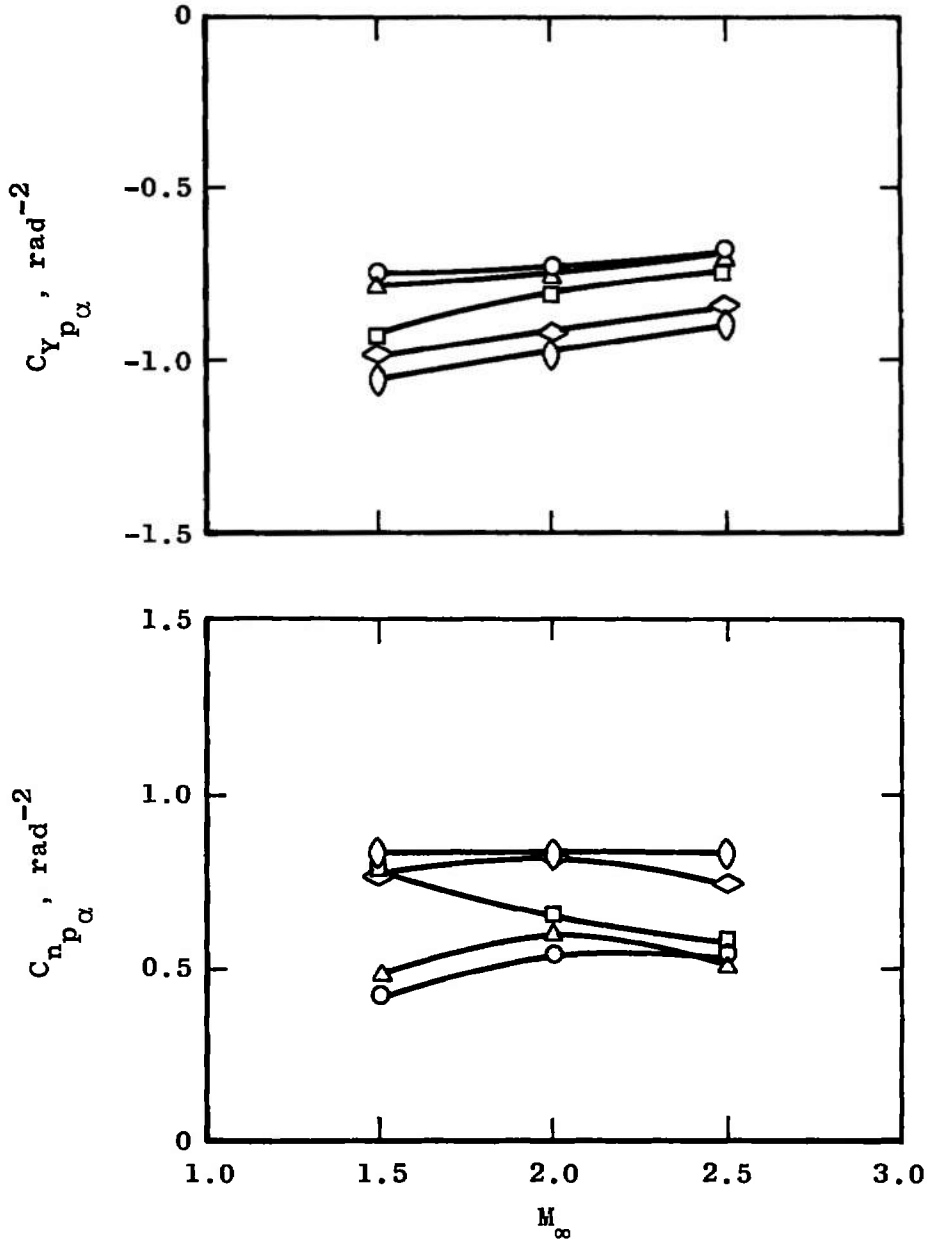
Figure 20. Effect of Reynolds number variation on C_{Y_p} and C_{n_p} , at $M_\infty = 2$, configuration 3.

<u>Sym</u>	<u>Configuration</u>	δ_{BT} , <u>deg</u>	l_{BT} , <u>caliber</u>	d_B , <u>caliber</u>
○	0	0	0	1.00
△	1	2.5	1.0	0.91
□	2	5.0	↓	0.83
◇	3	7.5	↓	0.74



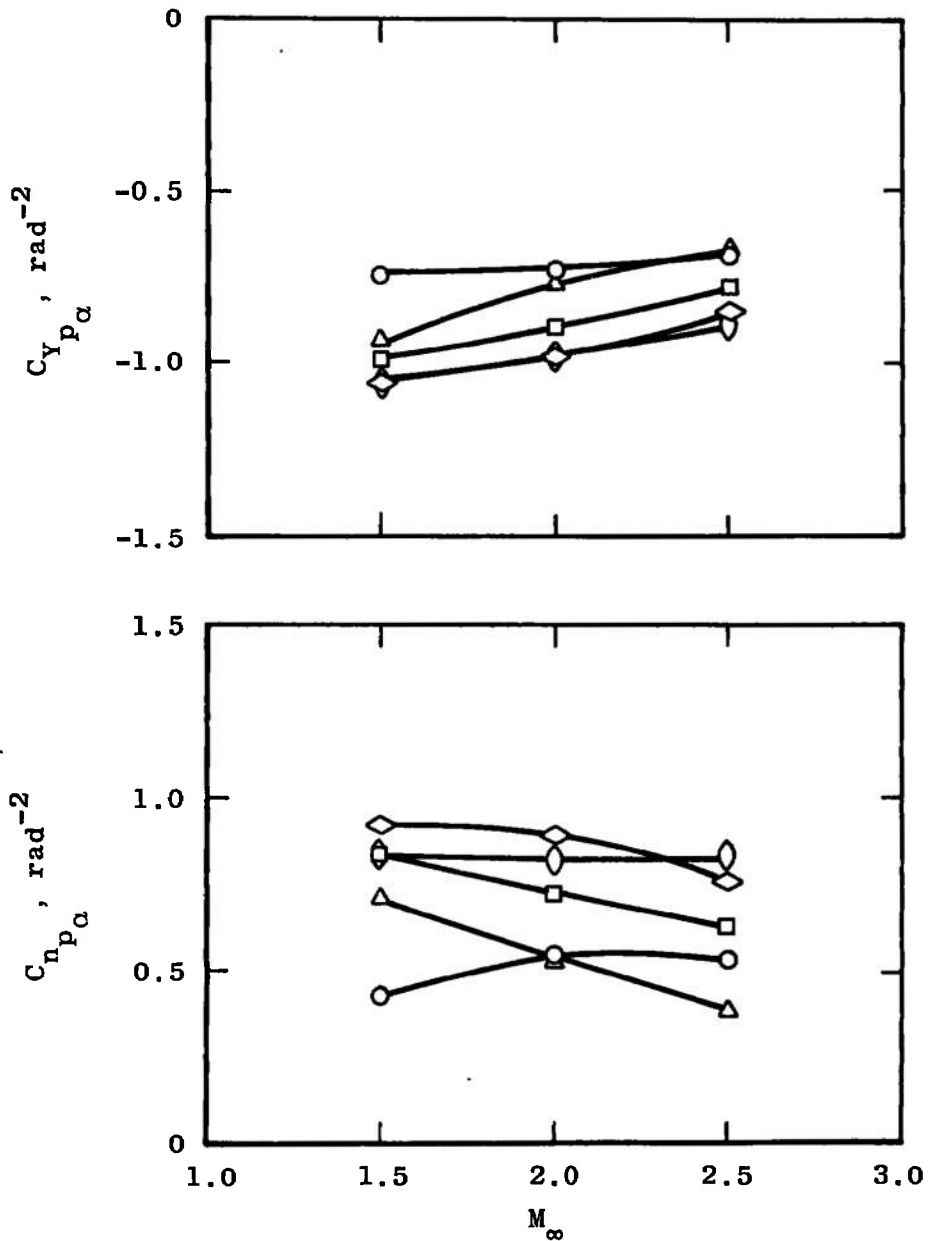
a. Effect of boattail angle with a constant boattail length
 Figure 21. Variation of $C_{Yp\alpha}$ and $C_{Np\alpha}$ with Mach number,
 $Re_\alpha = 9.6 \times 10^6$.

Sym	Configuration	l_{BT} , caliber	δ_{BT} , deg	d_B , caliber
○	0	0	0	1.00
△	4	0.50	5	0.91
□	2	1.00	↓	0.83
◇	5	1.35	↓	0.76
◊	6	1.70	↓	0.70



b. Effect of boattail length with a constant boattail angle
Figure 21. Continued.

Sym	Configuration	l_{BT} , caliber	d_B , caliber	δ_{BT} , deg
○	0	0	1.0	0
△	7	0.45	0.7	18.4
□	8	0.85	↓	10.0
◇	9	1.25	↓	6.9
◊	6	1.70	↓	5.0



c. Effect of boattail length with a constant base diameter
Figure 21. Concluded.

Table 1. Balance Uncertainty

Balance Component	Design Load	Range of Static Loads	Measurement Uncertainty
Normal force, lb	500	±150	±0.05
Pitching moment*, in. -lb	2500	±240	±0.30
Side force, lb	25	± 14	±0.03
Yawing moment*, in. -lb	125	± 70	±0.08

*About balance forward moment bridge

Table 2. Test Summary

Configuration	Boattail Length (l_{BT}), calibers	Boattail Angle (δ_{BT}), deg	Base Diameter (d_B), calibers	M_∞ ($Re = 4 \times 10^6$ /ft)		
				1.5	2.0	2.5
0	0	0	1.0000	x	x	x
1	1.00	2.5	0.9126	x	x	x
2	1.00	5.0	0.8249	x	x	x
3	1.00	7.5	0.7366	x	x*	x
4	0.50	5.0	0.9124	x	x	x
5	1.35	5.0	0.7637	x	x	x
6	1.70	5.0	0.7024	x	x	x
7	0.45	18.4	0.7000	x	x	x
8	0.85	10.0	0.7000	x	x	x
9	1.25	6.9	0.7000	x	x	x

*Also tested at $Re = 1 \times 10^6$ /ft and 7.3×10^6 /ft

Table 3. Wind Tunnel Test Parameters

M_∞	P_{O_2} , psia	T_{O_2} , °R	q_∞ , psia	V_∞ , ft/sec	$Re \times 10^{-6}$, ft ⁻¹
1.50	13.6	560	5.84	1444	3.95
1.99	4.2	564	1.51	1731	1.02
2.00	16.5	560	5.91	1729	4.02
2.01	30.8	567	10.95	1745	7.34
2.50	21.0	560	5.38	1933	4.02

Table 4. Wind Tunnel Parameter Precision

M_∞	Uncertainty, percent					
	M_∞	P_o	T_o	q_∞	V_∞	Re
1.5	± 0.7	± 0.50	± 0.36	± 0.52	± 0.51	± 0.73
2.0	± 0.5	± 0.50	± 0.36	± 0.75	± 0.33	± 0.83
2.5	± 0.3	± 0.50	± 0.36	± 0.78	± 0.23	± 0.83

Table 5. Coefficient Precision

M_∞	α , deg	Uncertainty						
		C_N	C_m	C_Y	C_n	C_{Y_p} , rad ⁻¹	C_{n_p} , rad ⁻¹	pd/2V _∞ [*]
1.5	0	± 0.00036	± 0.00040	± 0.00021	± 0.00011	---	---	± 0.51
	2	± 0.00052	± 0.00094	± 0.00022	± 0.00012	± 0.0015	± 0.0007	
	4	± 0.00085	± 0.00176	± 0.00024	± 0.00014	± 0.0017	± 0.0010	
	8	± 0.00230	± 0.00340	± 0.00037	± 0.00030	± 0.0022	± 0.0018	
2.0	0	± 0.00036	± 0.00039	± 0.00021	± 0.00010	---	---	± 0.33
	2	± 0.00072	± 0.00119	± 0.00022	± 0.00012	± 0.0017	± 0.0008	
	4	± 0.00136	± 0.00225	± 0.00024	± 0.00015	± 0.0020	± 0.0012	
	8	± 0.00380	± 0.00428	± 0.00039	± 0.00033	± 0.0025	± 0.0022	
2.5	0	± 0.00039	± 0.00043	± 0.00023	± 0.00011	---	---	± 0.23
	2	± 0.00079	± 0.00114	± 0.00024	± 0.00012	± 0.0025	± 0.0011	
	4	± 0.00148	± 0.00212	± 0.00025	± 0.00014	± 0.0024	± 0.0013	
	8	± 0.00388	± 0.00390	± 0.00034	± 0.00026	± 0.0022	± 0.0017	

Table 6. Derivative Coefficient Precision

M_∞	Uncertainty			
	C_{N_α} , deg ⁻¹	C_{m_α} , deg ⁻¹	$C_{Y_{p_\alpha}}$, rad ⁻²	$C_{n_{p_\alpha}}$, rad ⁻²
1.5	± 0.00061	± 0.00140	± 0.034	± 0.030
2.0	± 0.00073	± 0.00133	± 0.036	± 0.031
2.5	± 0.00080	± 0.00122	± 0.049	± 0.036

NOMENCLATURE

A	Reference area, model maximum cross-sectional area, 23.715 in. ²
C_m	Pitching-moment coefficient, pitching moment/ $q_\infty Ad$
$C_{m\alpha}$	Pitching-moment coefficient derivative at $\alpha = 0$, $\partial C_m / \partial \alpha$, per deg
C_N	Normal-force coefficient, normal force/ $q_\infty A$
$C_{N\alpha}$	Normal-force coefficient derivative at $\alpha = 0$, $\partial C_N / \partial \alpha$, per deg
C_n	Yawing (Magnus)-moment coefficient, yawing moment/ $q_\infty Ad$ (see Fig. 2)
C_{np}	Magnus-moment spin derivative coefficient for $(pd/2V_\infty) < 0.1$, $\partial C_n / \partial (pd/2V_\infty)$, per radian
$C_{np\alpha}$	Magnus-moment coefficient derivative at $\alpha = 0$, $\partial^2 C_n / \partial (pd/2V_\infty) \partial \alpha$, per radian ²
C_Y	Side (Magnus)-force coefficient, side force/ $q_\infty A$ (see Fig. 2)
C_{Yp}	Magnus-force spin derivative coefficient for $(pd/2V_\infty) < 0.1$, $\partial C_Y / \partial (pd/2V_\infty)$, per radian
$C_{Yp\alpha}$	Magnus-force coefficient derivative at $\alpha = 0$, $\partial^2 C_Y / \partial (pd/2V_\infty) \partial \alpha$, per radian ²
d	Reference diameter, model maximum diameter, 5.495 in.
d_B	Base diameter, calibers (note: one caliber = 5.495 in.)
l	Model length, 28.662 in.
l_{BT}	Boattail length, calibers (note: one caliber = 5.495 in.)
l_c	Length of cylindrical section, calibers (note: one caliber = 5.495 in.)
M_∞	Free-stream Mach number
p	Model spin rate (positive, clockwise viewing from the base), radians/sec
p_0	Tunnel stilling chamber pressure, psia

$pd/2V_\infty$	Spin parameter, radians
q_∞	Free-stream dynamic pressure, psia
Re	Free-stream unit Reynolds number, ft^{-1}
Re_l	Free-stream Reynolds number based on model length
T_0	Tunnel stilling chamber temperature, °R
V_∞	Free-stream velocity, ft/sec
α	Angle of attack, deg
δ_{BT}	Boattail angle, deg